Long-term potentiation and neural network activity in the neonatal rat cerebral cortex *in vivo*

Dissertation

Zur Erlangung des Grades

Doktor der Naturwissenschaften

Am Fachbereich Biologie

Der Johannes Gutenberg-Universität Mainz

vorgelegt von

Shuming An

geb. am 10.09.1982 in Jiangsu China

Mainz, 2013

Tag der mündlichen Prüfung: 20 . June .2013

Table of Contents

List of figures

Abbreviations

5-HTT	serotonin transporter
AChE	acetylcholinesterase
AMPA	α-amino-3-hydroxy-5-methyl-4-isoxazolepropionic acid
ANOVA	Analysis of variance
CP	cortical plate
CSD	current source density
DC	direct current
DiI	1,1'-dioctadecyl-3,3,3',3'-tetramethyl indocarbocyanine
FFT	fast fourier transformation
FP	field potential
IZ	intermediate zone
LTP	Long-term potentiation
M1	primary motor cortex
MEA	multi-electrode array
MUA	multiple unit activity
MZ	marginal zone
NMDA	N-methyl-D-aspartic acid
(P) 0-14	postnatal day 0 to 14
PoM	posterior medial (nucleus)
S1	primary somatosensory cortex
SD	standard deviation
SP	subplate
SVZ/VZ	subventricular zone/ventricular zone
TCA	thalamocortical afferents
TTL	transistor-transistor logic
TW	time-bandwidth product
VPM	ventral posterior medial nucleus
VSDI	voltage sensitive dye image
WM	white matter

1 Summary

1.1 Project 1

Long-term potentiation in the neonatal rat barrel cortex *in vivo*

"Long-term potentiation (LTP) is important for the activity-dependent formation of early cortical circuits. In the neonatal rodent barrel cortex LTP has been so far only studied *in vitro*. I combined voltage-sensitive dye imaging with extracellular multi-electrode recordings to study whisker stimulation-induced LTP for both the slope of field potential and the number of multi-unit activity in the whisker-to-barrel cortex pathway of the neonatal rat barrel cortex *in vivo*. Single whisker stimulation at 2 Hz for 10 min induced an age-dependent expression of LTP in postnatal day (P) 0 to P14 rats with the strongest expression of LTP at P3-P5. The magnitude of LTP was largest in the stimulated barrel-related column, smaller in the surrounding septal region and no LTP could be observed in the neighboring barrel. Current source density analyses revealed an LTP-associated increase of synaptic current sinks in layer IV / lower layer II/III at P3-P5 and in the cortical plate / upper layer V at P0-P1. This study demonstrates for the first time an age-dependent and spatially confined LTP in the barrel cortex of the newborn rat *in vivo*. These activity-dependent modifications during the critical period may play an important role in the development and refinement of the topographic map in the barrel cortex." (An et al., 2012)

1.2 Project 2

Early motor activity triggered by gamma and spindle bursts in neonatal rat motor cortex

Self-generated neuronal activity generated in subcortical regions drives early spontaneous motor activity, which is a hallmark of the developing sensorimotor system. However, the neuronal activity patterns and functions of neonatal primary motor cortex (M1) in the early movements are still unknown. I combined voltage-sensitive dye imaging with simultaneous extracellular multi-electrode recordings in the neonatal rat S1 and M1 *in vivo*. At P3-P5, gamma and spindle bursts observed in M1 could trigger early paw movements. Furthermore, the paw movements could be also elicited by the focal electrical stimulation of M1 at layer V. Local inactivation of M1 could significantly attenuate paw movements, suggesting that the neonatal M1 operates in motor mode. In contrast, the neonatal M1 can also operate in sensory mode. Early spontaneous movements and sensory stimulations of paw trigger gamma and spindle bursts in M1. Blockade of peripheral sensory input from the paw completely abolished sensory evoked gamma and spindle bursts. Moreover, both sensory evoked and spontaneously occurring gamma and spindle bursts mediated interactions between S1 and M1. Accordingly, local inactivation of the S1 profoundly reduced paw stimulation-induced and spontaneously occurring gamma and spindle bursts in M1, indicating that S1 plays a critical role in generation of the activity patterns in M1. This study proposes that both self-generated and sensory evoked gamma and spindle bursts in M1 may contribute to the refinement and maturation of corticospinal and sensorimotor networks required for sensorimotor coordination.

2 Introduction

2.1 Project 1

2.1.1 Sensory pathways from whiskers to barrel cortex

The lemniscal and paralemniscal pathways transfer the sensory information from the whiskers to the barrel cortex **(Fig. 1)**. In the brain stem, the lemniscal pathway begins at the principal trigeminal (PrV) nucleus and sends fibers to the ventral posteromedial (VPM) nucleus in the thalamus. While the paralemniscal pathway starts in the spinal trigeminal nucleus (SpVi) of the brain stem and projects to the posterior (POm) nucleus in the thalamus. Then, the lemniscal pathway projects the thalamoscortical fibers from VPM to the layer IV barrels in the barrel cortex. Comparatively, the paralemniscal pathway targets the layer IV septa through the thalamocortical projections from POm (for review   Lubke and Feldmeyer, 2007;Alloway, 2008).

The lemniscal pathway has a precise topographic organization and each whisker has a well-defined columnar organization. The PrV and VPm nuclei contain "barrelettes" and "barreloids", respectively, which correspond to the spatial distribution of the cortical barrels. Those organizations can maintain the spatial relationships for the neighbouring barrels (Vanderloos, 1976;Jacquin and Rhoades, 1983;Killackey and Fleming, 1985). In the newborn rat, a single whisker deflection activates the corresponding cortical barrel and produces weak neuronal responses in the neighboring septal regions (Yang et al., 2012). The lemniscal system has the specific single-whisker distribution. It can encode spatial and temporal information, such as identification of orientation, shape, distance and other spatial features (Krupa et al., 2001;Harvey et al., 2001;Shuler et al., 2002). However, the paralemniscal pathway has multi-whisker distribution. Neurons in POm and in the cortical septa receive multiple whiskers inputs (Diamond et al., 1992). Furthermore, the paralemniscal system is much poorer in encoding the spatial and temporal encoding information, but more effective in encoding the rate of passive whisker movements than those in the lemniscal system (Melzer et al., 2006a;Melzer et al., 2006b).

Hence, the lemniscal pathway processes spatiotemporal information by whisker contact with external objects, while the paralemniscal pathway encodes the frequency and other kinetic features of active whisker movements. Both pathways work cooperatively with each other to identify the external environment by passive or active whisker movements.
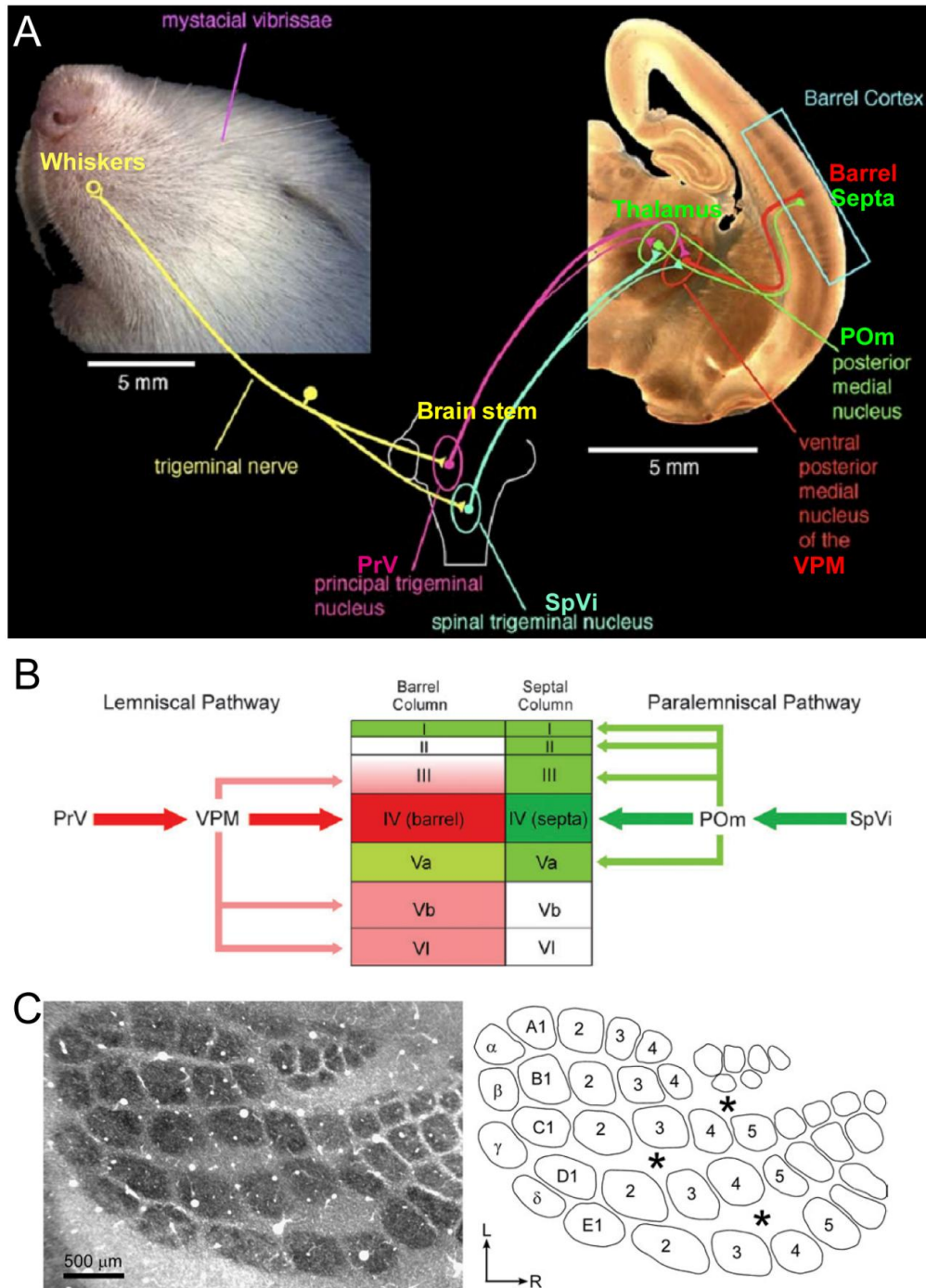
Fig. 1 From whisker to barrel cortex pathway.

A. The periphery sensory input originates in the mechanoreceptors at the base of the whisker. When whiskers are actively or passively deflected, the trigeminal nerves transfer and separate the sensory

information in to the nucleus in the brain stem. One stream goes through the spinal nucleus, then it arrives at the VPM (pink), while the other goes through the principal nucleus, then reaches at the PoM (light blue). Finally, thalamic afferents arising either from neurons in the VPM (red line) or POm (green line) project to different cortical laminae in the somatosensory barrel field (framed area) of the neocortex (modified from Lubke and Feldmeyer, 2007). **B.** Schematic diagram illustrating the lemniscal (red) and paralemniscal pathway (green) from brain stem to the barrel cortex. **C.** The left diagram, photomicrograph of tangential section through layer IV of the barrel field after processing the tissue by cytochrome oxidase staining. The right diagram, which is based on the photomicrograph, designates each barrel according to its arc position (1-5) within a specific row *(A-E)*. Although many septal zones are no more than 70-80 μm in width, the septal regions indicated by the asterisks are more than 200μm wide, R, rostral; L, lateral (modified from Alloway, 2008).

2.1.2 The development of sensory pathways in the barrel cortex

During the last embryonic and first postnatal week, the rat barrel cortex undergoes dramatic developments **(Fig. 2)**. As early as E13, thalamocortical axons and early corticofugal axons arrive in the ventral region of the telencephalon synchronously and are thought to interact. By E17, both lemniscal and paralemniscal pathways have crossed the pallial-subpallial border (PSPB) and have reached the cortex, where they extend tangentially in the intermediate zone (IZ). At the same time, the development of the laminar structure begins, the marginal zone (MZ) and subplate (SP) generate from the cortical plate (CP). Immediately after birth at P0, both lemniscal and paralemniscal pathways have already arrived at the CP and layer V, respectively. Two days later, barrel patterns generate in layer IV by the axons from the lemniscal pathways. At P7, these patterns become more mature. Surprisingly, the paralemniscal pathways reach the superficial layer MZ through layer II/III (for review Price et al., 2006; Galazo et al., 2008).
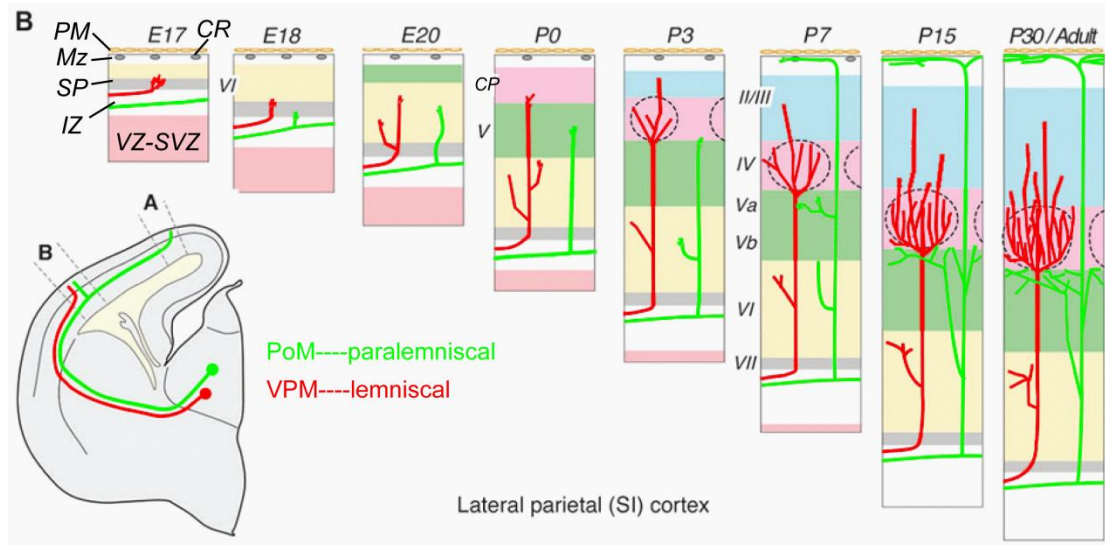
Fig. 2 Schematic diagram illustrating the development of thalamocortical afferents from embryonic day 17 (E17) to postnatal day 30 (P30) in rodents.

In the upper panel, different colors stand for the relative layers of the cortex. The superficial layer is the pia mater (PM) represented by a row of planar brown cells. Marginal zone (MZ) locates at lower layer. Note the expansion of MZ during the postnatal periods. Cajal-Retzius cells (CR) are also depicted (gray dots). Note that these transient cells only exist for about a week in layer I. Subplate (SP) Subplate (SP) is a transient layer and will disappear during the late postnatal period. ''barrel'' domains in layer IV (dashed line circles) generated at P3. There are two pathways from thalamus nucleus (left down panel). Lemniscal pathway (red line) is from the ventroposterior medial nucleus (VPM), while paralemniscal pathway (green line) has projections from the posterior medial nucleus (PoM) (modified from Galazo et al., 2008).

Furthermore, previous studies showed different ways to label the thalamocortical afferents (TCA). In 1990, Erzurumlu and Jhaveri used anterograde DiI histochemistry and found that the TCA didn't show any barrel-related pattern at 25 hours after birth (Erzurumlu and Jhaveri, 1990). It just showed some row-related pattern until the third postnatal day. However, in 1994, Schlaggar and O'Leary applied acetylcholinesterase (AChE) histochemistry to the tangential barrel cortex slices of neonatal rats (Schlaggar and Oleary, 1994). Surprisingly, as early as 4 hours after birth, barrel rows could be identified in slices. Then, 5 rows were clearly shown in slices **(Fig. 3)**. After that, there was a transition from row predominance to barrel

formation which appears by 24 hours after birth. Finally, the barrel-related patches pattern became more mature at 72 hours. Therefore, these suggest that the thalamic afferents show a somatotopic pattern in cortex as early as the time of birth.
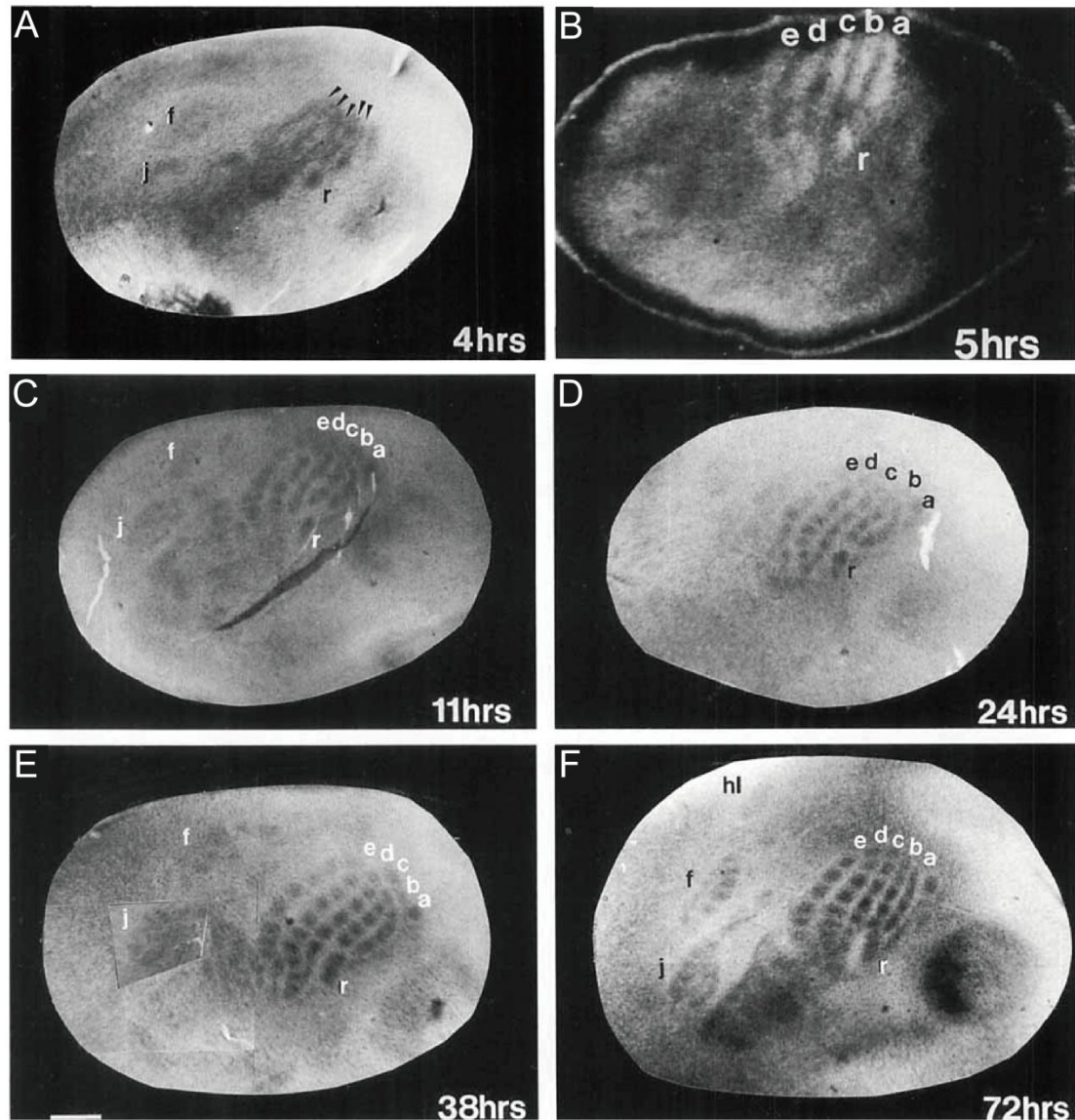
Fig. 3 Anatomical study shows the development of barrels in neonatal rats.

Tangential distribution of AChE-reactive afferents from the flattened cortices of four littermates. *A*, As early as 4 hours after birth, there are five separate rows (AChE-reactive afferents) can be observed in the tangential sections. *B*, One hour later, the five rows are more clearly separated (represented by a-e). *C-D,* the jaw (j), forelimb (f) and hindlimb (hl)representations are less clear than the whisker representation during the 1st postnatal day. *E-F*, after about 38 hours, clear and precise isomorphic map of whiskers in barrel cortex can be identified. r, rhinal vibrissae Scale bar = 675 μm (modified from Schlaggar and Oleary, 1994).

14

2.1.3 The introduction of LTP

As early as 1973, two well known papers published in Journal of Physiology (Bliss and Lomo, 1973;Bliss and GARDNERM.AR, 1973), became a great milestone in neuroscience. Bliss and Lomo first studied LTP in anaesthetized animals (Bliss and Lomo, 1973). Then, Bliss and Gardner-Medwin further studied it using stimulation techniques that triggered activity in hundreds, or perhaps thousands of neurons in awake animals (Bliss and GARDNERM.AR, 1973). Afterwards, there were several thousands of publications about the mechanisms and functions of LTP in the last decades (Malenka, 2003).

In LTP, the strength of synapses between neurons in the central nervous system is enhanced for a long period (Lynch, 2003). LTP consists of three phases: induction, expression and persistence. During the induction phase, both NMDA and GABA receptor mediate the induction of LTP (Collingridge, 2003;Nugent et al., 2009). However, the induction of LTP in some synapses depends on the kainate receptor rather than the NMDA receptors (Bear, 2003). In order to enhance the synapse strength, synapses either increase the release of presynaptic transmitter or increase the number of postsynaptic receptors such as AMPA receptor. In hippocampal slices, previous studies suggested silent synapse ("unfunctional" AMPA receptors) on CA1 cells might contribute the expression of LTP (Nicoll, 2003;Kullmann, 2003). In some cases, LTP continues for several weeks or even months. How does LTP persist? Harris and colleagues found that the protein synthesis contributes to the persistence of LTP in dendritic spines (Harris et al., 2003). E. R. Kandel focused on the abdominal ganglion of Aplysia, suggesting that genetic mechanisms maybe the reasons for the long-lasting synaptic change (Pittenger and Kandel, 2003).

The possible function of LTP has been discussed for nearly 40 years. Most people believed that LTP may serve as a potential mechanism underlying memory traces in the brain (Morris, 2003). Barnes believed that the temporal persistence of LTP was persistent with the expression of memory (Barnes, 2003). Rowan and colleagues proposed that LTP might be affected in Alzheimer's disease (Rowan et al.,

2003). However, more and more scientists found that long-term potentiation (LTP) is important for activity-dependent neuronal development in rodent neocortex (Feldman et al., 1999;Daw et al., 2007;Inan and Crair, 2007).

2.1.4 LTP at thalamocortical synapses

Previous studies suggested that LTP is a likely candidate as the synaptic mechanism underlying certain forms of learning and memory (Morris, 2003). However, there is another considerable evidence showed that the NMDA-dependent LTP serves for the correct formation and refinement of receptive fields in the barrel cortex (Crair and Malenka, 1995;Daw et al., 2007). Chronic application of the NMDA receptor antagonist (AP5) in the barrel cortex during the first postnatal week could disturb the precise topographical map and exhibit deficient experience-dependent receptive field plasticity (Schlaggar et al., 1993;Fox et al., 1996). Furthermore, in neonatal rat barrel cortex, LTP can also be induced *in vitro* by a pairing protocol from postnatal day (P) 3 to 7 **(Fig. 4)** (Crair and Malenka, 1995;Isaac et al., 1997;Barth and Malenka, 2001), the time period that coincides with barrel map formation (Fox, 1992;Fox et al., 1996;Foeller and Feldman, 2004). The magnitude of LTP in the barrel cortex gradually decreases between P3 and P8 (Crair and Malenka, 1995). Similarly, synaptic plasticity (ocular dominance plasticity, ODP and LTP) is important for the development of the visual cortex (Malenka and Bear, 2004). For example, a long time period in the dark for animals could result in a longer critical period for ODP and LTP in the visual cortex (Kirkwood et al., 1995). Tetrodotoxin application in the open eye abolished the ODP (Antonini and Stryker, 1993). Again postsynaptic NMDA receptor antagonists also abolish ODP and LTP (Bear et al., 1990;Daw et al., 1999). All these studies suggest that NMDA receptor-dependent synaptic plasticity is involved in the formation and refinement of receptive fields in the primary sensory systems.
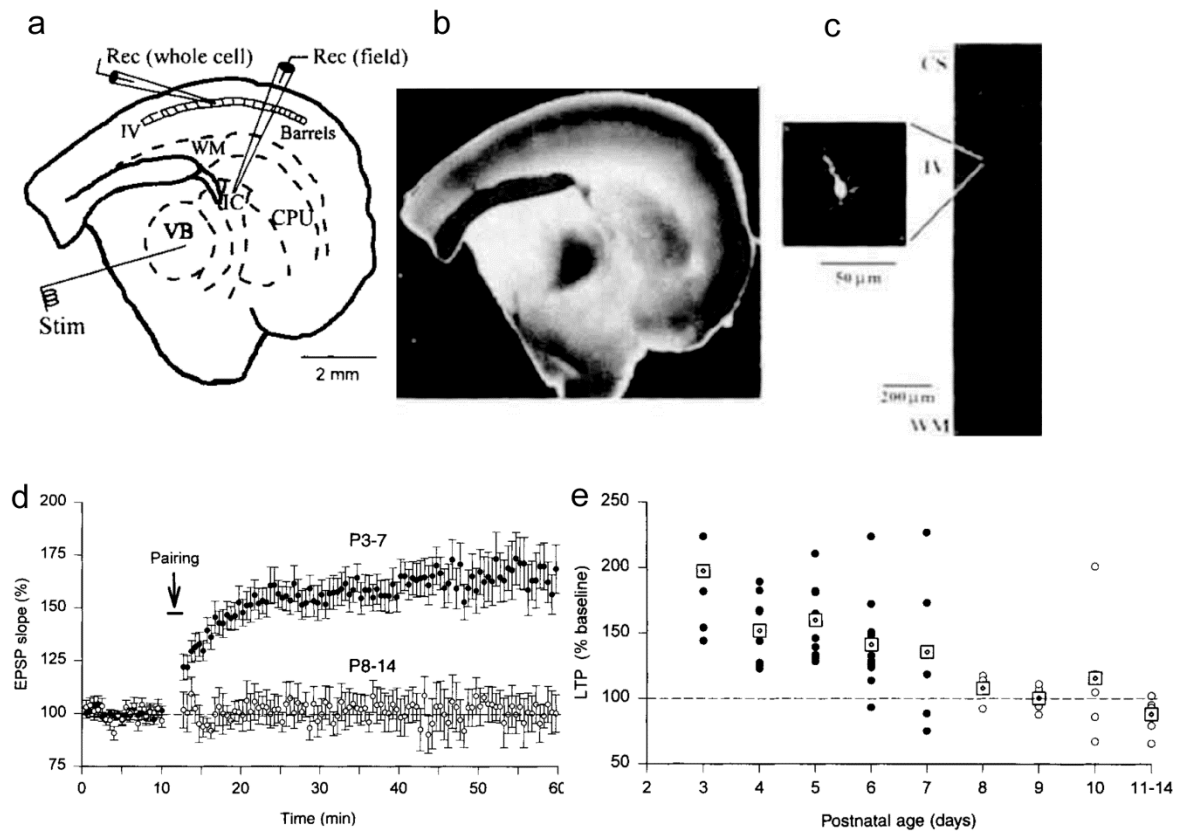
Fig. 4 Age-dependent expression of LTP at thalamocortical synapse in P3 to P14 rats.

a. Schematic diagram of the stimulation protocol. Stimulating electrodes (stim) are placed into the ventrobasal nucleus of the thalamus (VB) and whole cell (Rec) and field potential recordings are performed in layer IV and internal capsule (IC). CPU, caudate/putamen; WM, white matter. *b-c,* histology of a thalamocortical slice and a lucifer yellow filled layer IV cell. *d.* Age-dependent expression of LTP. Relative FP slopes recorded in different age groups. Pairing stimulation is applied with 100 stimuli at 1 Hz, meanwhile the cell is depolarized at -10 to 0 mV. *e.* Scatter diagram of EPSP slopes in the groups of different ages. Note the gradual decreases of the LTP magnitude during the critical period (modified from Crair and Malenka, 1995).

2.1.5 Silent synapses may contribute to thalamocortical LTP

Previous studies showed different mechanisms for LTP at thalamocortical synapses (Feldman et al., 1999;Daw et al., 2007). Nevertheless, an increase in the number or conductance of AMPA receptors may result in the potentiation of synaptic strength. In the immature somatosensory cortex, thalamocortical synapses have been found to contain NMDARs, but not functional AMPARs (Isaac et al., 1997). These

17

synapses do not have detectable EPSCs at resting membrane potential (-70mV) and keep "silent" because of the voltage-dependent Mg^{2+} block of NMDARs. NMDARs rather than AMPARs contribute to the synaptic responses at resting membrane potential (Isaac et al., 1997). At P2-P3, about 30% of thalamocortical synapses keep "silent", based on comparison of failure rates at hyperpolarized and depolarized potentials **(Fig. 5)**. Interestingly, in P4-P5 animals, the proportion of silent synapses increases to 40%. However, after P5, the proportion of silent synapses decreases dramatically. At P8-P9, there is no silent synapses at all **(Fig. 5)** (Isaac et al., 1997). These observations are in good agreement with previous reports on the age-dependent expression of LTP in thalamocortical slice preparation of the newborn rat (Crair and Malenka, 1995). As show in **Fig. 4e**, the strongest LTP can be induced at P3-P5 indicating that the large amount of the silent synapses reveals the highest capability for activity-dependent change. After P5, the proportion of silent synapses falls sharply which may result in the weak LTP during these ages. The pairing stimulation may cause the rapid appearance of AMPA currents which converts silent synapses to functional ones. All above observations suggest that thalamocortical synapses are initially born with silent (post)synaptic elements which become functional by LTP (Feldman et al., 1999).
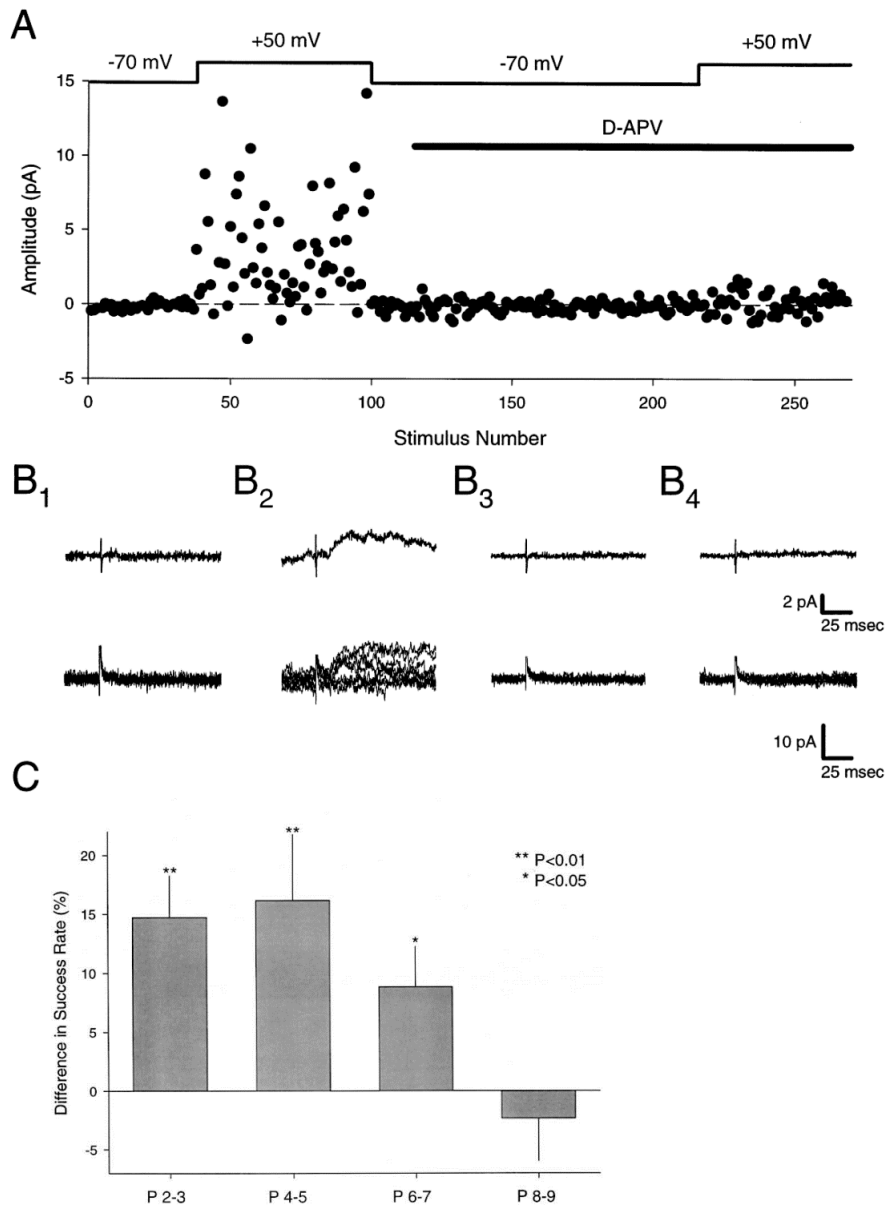
Fig. 5 Silent thalamocortical synapses.

A. Voltage-clamp recording in a layer IV cell. Note no AMPAR-mediated EPSCs holding at -70 mV, but robust EPSCs exist when depolarizing to +50 mV. D-APV (25 μM) blocked the EPSCs observed at +50 mV. Each point represents the amplitude of an individual EPSC. *B.* Average of 40 responses (top) and eight superimposed consecutive responses (bottom) for the following epochs of the experiment shown in *A*, respectively. *C.* Bar diagram of success rates at depolarized versus hyperpolarized potentials for thalamocortical EPSCs in minimal stimulation experiments at different ages. Note that the silent synapses exist during the critical period. Data are expressed as mean ± s.e.m. (modified from Isaac et al., 1997).

2.2 Project 2

2.2.1 Central pattern generators (CPGs) generate early motor activity

Brainstem activity in young infants and during active sleep were firstly suggested to induce ascending activation of the cortex and descending activation of the musculature **(Fig. 6)** (Roffwarg et al., 1966). The hypothesis has been elaborated that brainstem-initiated twitching of the paws generates sensory feedback and then activates the cortex (for review, see Blumberg, 2010b). However, in mammals, including humans, the spinal cord has been suggested as CPG for locomotion (MacKay-Lyons, 2002;Dietz, 2003;Ijspeert, 2008;Guertin, 2009;Minlebaev et al., 2011). In sleeping newborn rats, spontaneous muscle twitches send the tactile feedback to the spinal cord and guide the organization of spinal sensorimotor circuits (Petersson et al., 2003). In adult animals, forelimb representation in M1 has been suggested to pertain to three different categories of movement, for example, stereotyped repetitive behaviors, complex voluntary movements and fine motor manipulation skills (for review, see Levine et al., 2012).
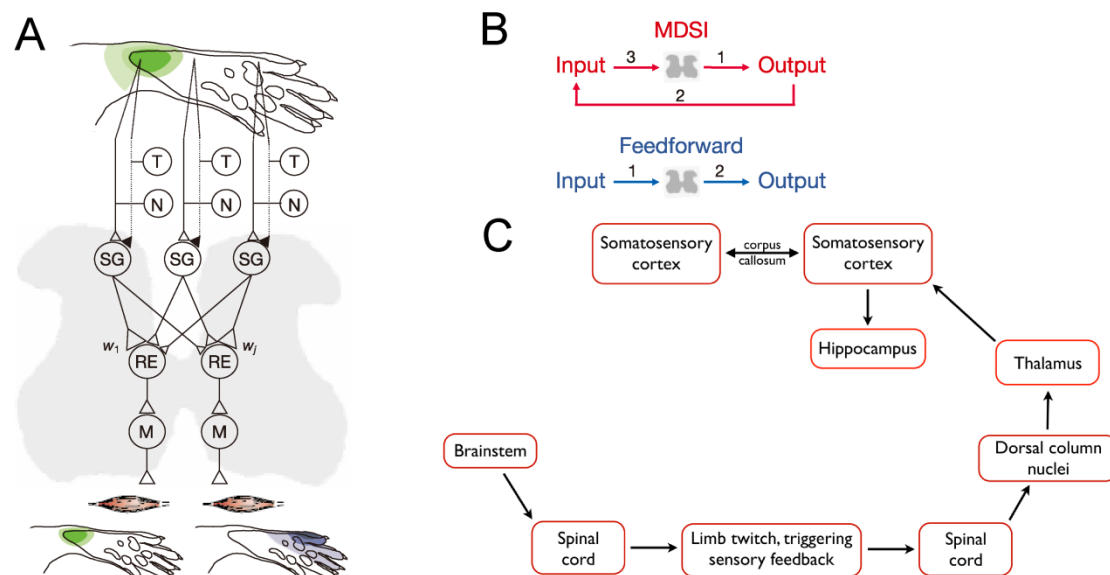
Fig. 6 Spinal cord and brainstem generate movements.

A. Schematic illustrations of organization of spinalcord and paw reflex module. The primary sensory afferents send the tactile information through monosynaptical and oligosynaptical circuits. Then the

tactile (T) and nociceptive (N) projections converge in substantia gelatinosa (SG); next all the projections arrive at the reflex-encoding neurons (REs) located in the deep dorsal horn. Finally, the REs have synaptic inputs to the motor neurons (M) which can cause the movement of paw. ***B.*** There are two hypotheses of stimulated learning principles. Red indicates motor-directed somatosensory imprinting (MDSI). Blue indicates the feedforward learning. Number stands for the sequence of events. ***C.*** The CPG triggering pathway from the triggering of a twitch to the processing of sensory peripheral feedback in the forebrain. CPG located in the brainstem can trigger activity in spinal cord. Then activity in M1 causes the limb twitch. After that, the sensory feedback returns to spinal cord again. Next, sensory information go up to the dorsal column nuclei, thalamus, and somatosensory cortex. Finally information arrives at the hippocampus or goes to the other hemisphere through the corpus callosum. Black arrows stand for the stream of sensory information flow (Petersson et al., 2003;modify from Blumberg, 2010b).

2.2.2 The development of the early motor activity

Sensorimotor coordination emerges in the early development of humans (de Vries et al., 1982;Cioni and Prechtl, 1990) and rodents (Gramsbergen et al., 1970;Clarac et al., 2004). Sixteen distinct movement patterns have been observed in fetuses during the first 20 weeks of gestation (de Vries et al., 1982) and preterm infants (Cioni and Prechtl, 1990). Neonatal rats can perform crawling, swimming and air stepping behaviors with four legs during the 1st postnatal week (Clarac et al., 2004). As early as P0 (**Fig. 7**), a rat can not support its whole body with four limbs. It can drag along the body with the forepaws. Two days later, the pup can move its head and perform slow crawling behavior. At P5, the pup can elevate its shoulder and head and accomplish plantigrade walking (Clarac et al., 2004). In P3–P9 rats, motivational locomotion could be induced by olfactory stimuli (Jamon and Clarac, 1998). During the 2nd postnatal week, the pup begins to walk with four limbs, but with poor control of the trunk. After P15, the rat receives visual and auditory information after eye and ear opening. In this way, complex motor behaviors can be completed more efficiently. For example, it can perform adult swimming and walking pattern behaviors (Clarac et al., 2004).

The adult rat possesses more skilled, flexible and motivational locomotion with gait using (walk, trot, gallop), direction following (forward, backward) and medium traversing (terrestrial, aquatic, aerial), such as stepping and swimming (Clarac et al.,

2004). Central pattern generators (CPGs) synaptic connections have been suggested to be critical for these behaviors (Clarac et al., 2004). Moreover, different electromyography (EMG) patterns and duration were observed in various behaviors, i.e. characteristic asymmetric EMG waveform with double bursts contributes to the stepping; the bell-shaped EMG curve with only single burst is necessary for the swimming (Gruner and Altman, 1980;Deleon et al., 1994).
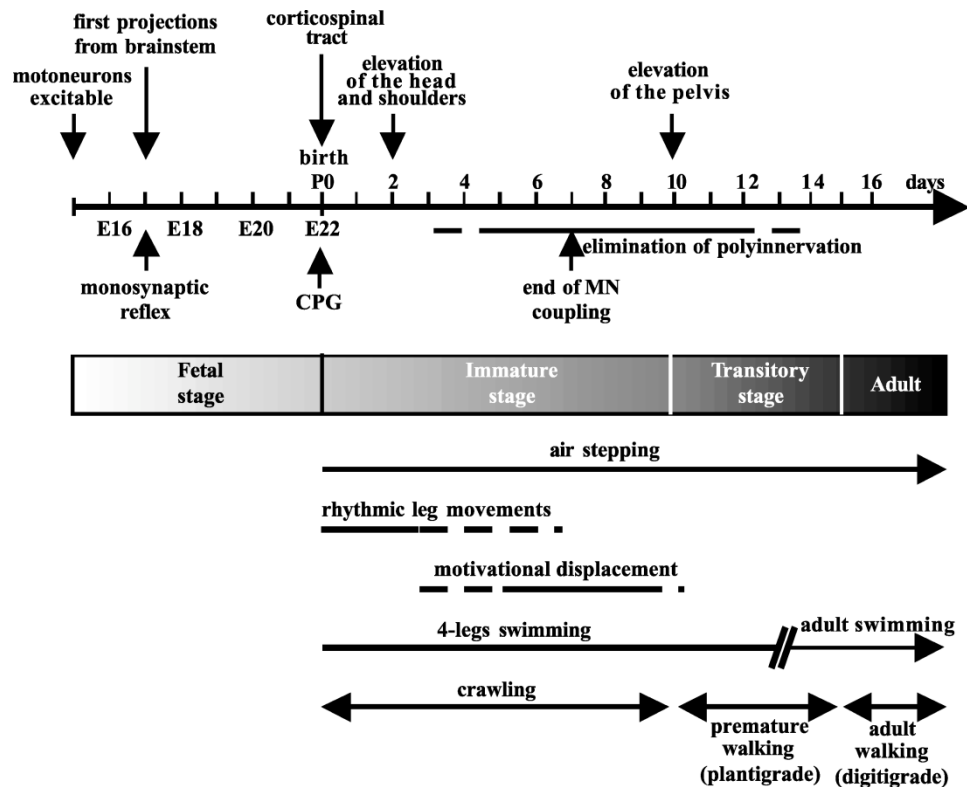
Fig. 7 The development of the locomotion behaviors in the rat.

The development of locomotion can be divivded into fetal, immature, transitory and adult stages. Motor neurons and central pattern generators have already operated during the fetal stage. The immature stage starts at P0 and ends at P10. During this period, the corticospinal tract has already connected the motor cortex to the spinal cord. Meanwhile, some basic and simple behaviors can be oberserved. From P10 to P15 is the period for the transitory stage. During this stage, the rat eye and ear are opening, meanwhile they can perform whisking. Fanally, in the adult stage, they can perform adult swimming and walking with high motivation (modified from Clarac et al., 2004).

2.2.3 Early neuronal activity patterns triggered by sensory feedback modify the

functional topography map

Although genetically determined molecular factors considerably contribute to functional sensorimotor connectivity (for review, see Polleux, 2005), early synchronized oscillatory network activities are also believed to be essential for the formation of the functional neuronal circuits (for review, see Khazipov and Luhmann, 2006) and maintenance of tonotopic maps in neonatal cortex (Tritsch et al., 2007;Colonnese et al., 2010;Minlebaev et al., 2011;Yang et al., 2012). These early activity patterns control axon growth and synaptogenesis (for review, see Allene and Cossart, 2010). As show in **Fig. 8,** sensory periphery input could also trigger early activity patterns, for example, early movements drive spindle bursts in the neonatal primary somatosensory cortex (S1) (Khazipov et al., 2004). In the early whisker system, spontaneous whisker twitches (Tiriac et al., 2012) and whisker sensory stimulation elicit both gamma and spindle bursts which synchronize developing thalamus and barrel cortex (Yang et al., 2009;Minlebaev et al., 2011;Yang et al., 2012). In visual system, retinal waves trigger spindle bursts in the neonatal visual cortex (Hanganu et al., 2006;Colonnese et al., 2010). In the developing auditory system, supporting cells in the cochlea spontaneously release ATP and process the bursts of action potentials in auditory nerve fibres before the onset of hearing (Tritsch et al., 2007;Tritsch and Bergles, 2010). Conversely, these early patterns of electrical activity drive motor output, e.g. the self-generated bursts in spinal cord (Gramsbergen et al., 1970;Petersson et al., 2003;Clarac et al., 2004) and brain stem (Blumberg, 2010b;Tiriac et al., 2012) triggers spontaneous movements. Even muscles can twitch spontaneously during sleep (Petersson et al., 2003;Mcvea et al., 2012).
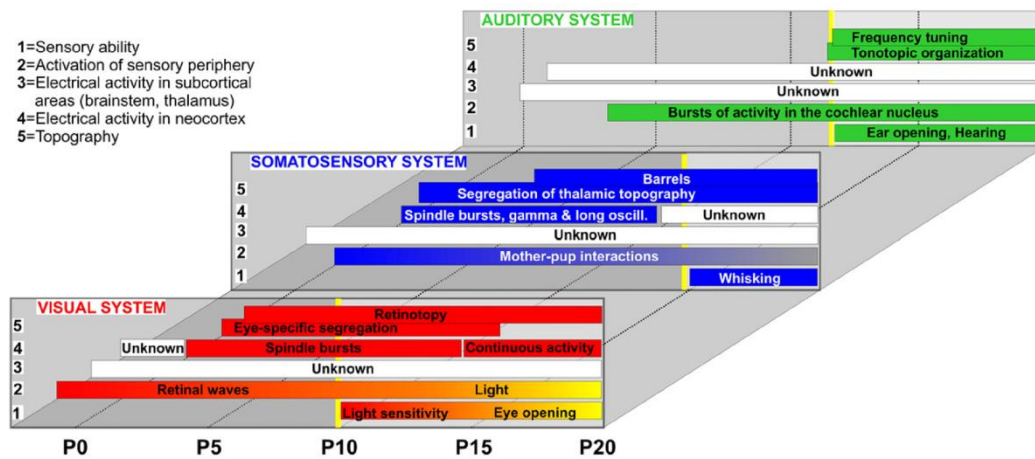
Fig. 8 The development of sensory systems in rats.

During the initial phases of development, genetically determined molecular factors contribute considerably to the functional senorimotor connectivity. Then, sensory periphery input triggers early activity patterns. The patterned activities are critical for the barrel, retinotopic, tonotopic map refinement and muturation (Hanganu-Opatz, 2010).

The maturation of somatotopic sensory cortical map has been suggested to require the spindle bursts in S1 driven by the spontaneous paw twitches (Khazipov et al., 2004). The precise barrel map needs the localized gamma and spindle bursts in neonatal vibrissal S1 (Yang et al., 2012) induced by the spontaneous whisker movements (Tiriac et al., 2012). In the visual system, the patterned spontaneous retinal waves are both critical for the retinotopic map refinement in the superior colliculus (McLaughlin et al., 2003;Chandrasekaran et al., 2005),and trigger spindle bursts (Hanganu et al., 2006) required for the development of precise maps in V1 (Cang et al., 2005). In the auditory system, spontaneous activity in auditory nerve fibers before the onset of hearing is essential for the refinement and maintenance of tonotopic maps in the developing auditory system (Gabriele et al., 2000;Rubel and Fritzsch, 2002a;Kandler, 2004;Leake et al., 2006;Leao et al., 2006;Tritsch et al., 2007;Tritsch and Bergles, 2010).

2.2.4 The development of corticospinal tract

Anatomical tracer studies in newborn mice at P0 have demonstrated that, corticospinal motor neurons located at layer V in motor cortex have already sent the axons to spinal cords **(Fig. 9)** (Arlotta et al., 2005;Molyneaux et al., 2007). Different

molecular mechanisms contribute to the specification and development of corticospinal motor neurons. e.g., a small number of corticospinal motor neurons genes (such as, Diap3, Igfbp4 and Crim1) seem to be restricted to the sensorimotor cortex. Other genes are expressed across the full extent of layer V (e.g., Ctip2, encephalopsin, Fezf2, Clim1, Pcp4 and S100a10) (for review, see Molyneaux et al., 2007). All these genes have been proven to be important for the development of the corticospinal tract. In the absence of the Ctip2 gene, defects in fasciculation, outgrowth and pathfinding were observed in subcerebral projection neuron axons. At the same time, dramatically less axons reach the brainstem. Furthermore, reduction of Ctip2 expression in Ctip2-heterozygous mice results in abnormal developmental pruning of corticospinal axons. All these results suggest that Ctip2 is a crucial regulator of subcerebral axon extension and of the refinement of collaterals as these neurons mature (Arlotta et al., 2005). In addition, after knocking out the Fezf2 gen in null mutant mice, neither subcerebral projection neurons nor corticospinal tract to the spinal cord or the brainstem could be found (Molyneaux et al., 2005). However, it is still unknown that the patterns of activity expressed in primary motor cortex (M1) and whether these activities can transfers through cortical spinal tract during the early developmental stages.
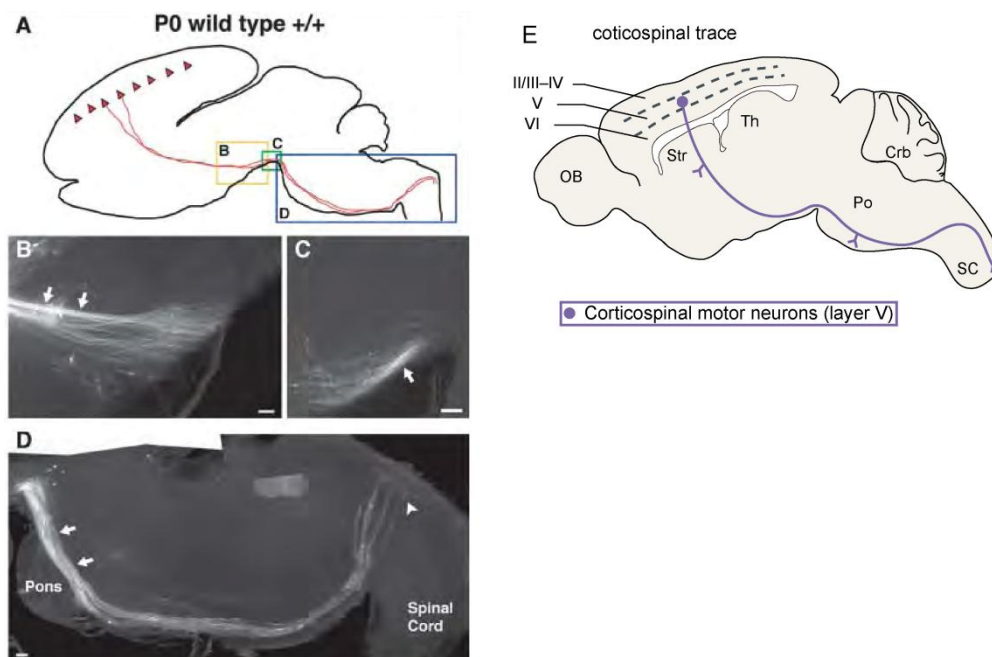
Fig. 9 Corticospinal tracts in P0 mice.

A. Schematic representations of sagittal views of the brain and proximal spinal cord in a P0 mice, cortical spinal motor neuron somas in the cortex (red triangles) and their axonal projections toward the spinal cord (red lines). *B-D.* Representative parts of positions are shown at an expanded scale (right). Note the corticospinal tract stained by Dil from cortex to the spinal cord. *E.* Schematic diagram of a sagittal section of a mouse brain. Note that the corticospinal motor neurons (purple dot) located at layer V of the cortex project to the spinal cord (modify from Arlotta et al., 2005;Molyneaux et al., 2007).

2.2.5 The development of corpus callosum projections

In newborn rodents, the callosal projection neurons have already crossed the corpus callosum (CC) **(Fig. 10)** (Tritsch et al., 2007;Molyneaux et al., 2007;Rouaux and Arlotta, 2012). Genetically determined molecular factors control the specification and development of callosal neurons. The Lmo4 gene expressed in callosal neurons of layers II/III and V has been suggested to be important for the development of callosal projection (Arlotta et al., 2005;Molyneaux et al., 2007). However, the neural activity patterns have also been demonstrated to be critical for the development of corpus callosum circuits. In neonatal S1, the weak evoked responses in the ipsilateral hemisphere were observed with EEG (Marcano-Reik and Blumberg, 2008) and VSDI (Mcvea et al., 2012) recordings. Moreover, the weak ipsilateral On-response could be also elicited in V1 by optic nerve stimulation from P3 onwards (Hanganu et al., 2006). Surprisingly, in the whisker system, the whisker stimulation failed to evoke a detectable response in the ipsilateral barrel cortex in the same age of newborn rats (Yang et al., 2009). Nevertheless, in adult mice, the tactile whisker stimulation could induce the reliable VSDI evoked response in bilateral sensorimotor cortices (Ferezou et al., 2007).
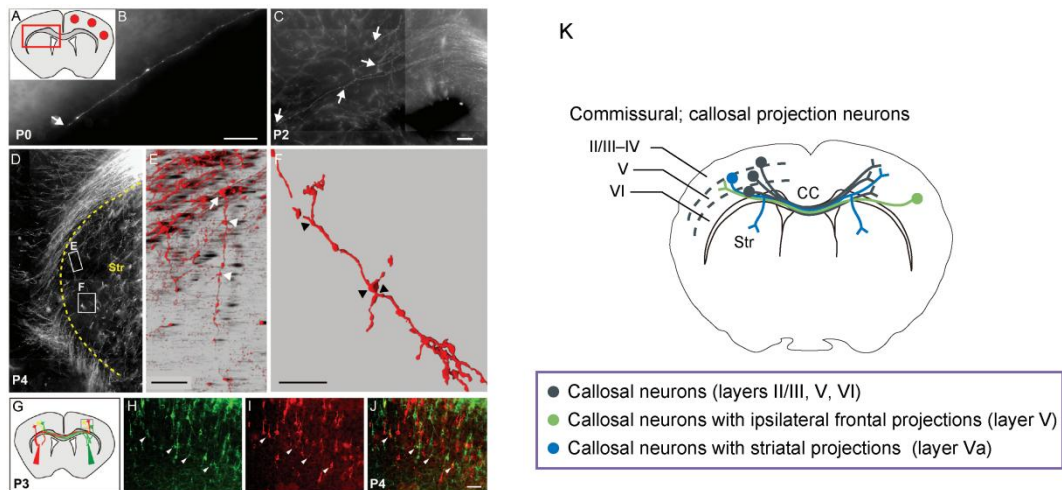
Fig. 10 The development of the callosal projection neurons.

A. Schematic representations of a coronal section of the brain in newborn mice. Note the injection position of the DiI crystals (red dots). *B.* At P0, rare pioneering axons are seen (arrow), prior to entry into the contralateral striatum. *C.* Increase in the number of axons in the contralateral corpus callosum (arrows) at P2. *D-J.* At P3-P4, the number of axons in the contralateral corpus callosum increase dramatically. *K.* Callosal projection neurons. Callosal neurons located at layers II/III, V and VI extend an axon across the CC to the other hemisphere. There are three kinds of callosal neuron: *(1)* the callosal neurons have single projections to the contralateral cortex (black); *(2)* the callosal neurons have triple projections to the contralateral cortex and bilateral striatums (blue); *(3)* the callosal neurons have double projections to the contralateral cortex and ipsilateral frontal cortex (green) (modified from Molyneaux et al., 2007;Sohur et al., 2012).

2.11 Aims of the thesis

2.11.1 Project 1

Whether LTP can be induced by whisker stimulation in the adult barrel cortex *in vivo* is a matter of debate. Multi-whisker stimulation by air puffs at 5 Hz for 30 s did not induce LTP in adolescent mice (Takata et al., 2011), while multi-whisker stimulation at 2 or 8 Hz for 10 min induced a stable LTP in layers II/III and IV of the barrel cortex of mature mice (Megevand et al., 2009). Whether LTP can be elicited in the neocortex *in vivo* before the onset of the critical period has not been investigated yet. Therefore, we asked whether single-whisker stimulation may elicit LTP in the neonatal (P0-P7) rat barrel cortex *in vivo*. In addition, we addressed the questions (i) whether the expression of LTP reveals any age-dependence during the first two postnatal weeks, (ii) if the LTP is restricted to the stimulated barrel-related column and (iii) which cortical layers reveal LTP. To address these questions, we performed multi-channel extracellular electrophysiological recordings from barrels and barrel-related columns that were functionally identified by voltage-sensitive dye responses following single whisker stimulation.

2.11.2 Project 2

Anatomical tracer studies in newborn mice at P0 have demonstrated that, corticospinal motor neurons located at layer V in motor cortex have already sent the axons to spinal cords (Arlotta et al., 2005;Molyneaux et al., 2007). Spindle bursts have been found to be the only patterns of activity in paws S1 (Khazipov et al., 2004). However, what the patterns of activity expressed in M1 and their relation to spontaneous movements during the early developmental stages are unknown. It is also not clear what the interactions between S1 and M1 and what the functional roles of S1 neuronal activity in M1. To address these questions, we simultaneously performed multichannel extracellular electrophysiological recordings in S1 and M1 that were functionally identified by voltage-sensitive dye responses following paw touch stimulation.

2.12 Statement

This thesis contains some parts, which have already been published or will be published: Long-term potentiation in the neonatal rat barrel cortex *in vivo* (An et al., 2012). Gamma and spindle bursts in neonatal rat motor cortex drive and are triggered by early motor activity (An et al. in preparation).

3 Materials and methods

3.1 Project 1

All experiments were carried out in accordance with the national laws for the use of animals in research and approved by the local ethical committee (#23177-07/G10-1-010). Voltage-sensitive dye imaging (VSDI), field potential (FP) and multiple-unit activity (MUA) recordings were made in the barrel cortex of head restrained neonatal Wistar rats P0 to P14.

3.1.1 Surgical preparation

The surgical procedure was performed according to the methods as described previously (Hanganu et al., 2006;Hanganu et al., 2007;Yang et al., 2009). P0 to P7 rats were put under deep ice-cooling anesthesia alone and injected with light intraperitoneal (0.5-1 g/kg, Sigma-Aldrich, Taufkirchen, Germany). The skill and the soft tissue over the skull were carefully removed. Then, the exposed skull was dry (**Fig. 11**). Next, barrel cortex is marked with the red dots (barrel cortex, P0-P1,0-2 mm posterior to bregma and 2-4 mm from the midline; P3-P5,0-2 mm posterior to bregma and 2.5-4.5 mm from the midline; P6-P7,1-3 mm posterior to bregma and 3-5 mm from the midline). After that, the head was fixed into the stereotaxic apparatus using one holder fixed with dental cement occipital bones. The bone, but not the dura mater, over S1 was carefully removed by drilling a 2 x 2 mm^2 craniotomy (**Fig 12A1**). Afterwards, the body of the animals was surrounded by cotton and kept at a constant temperature of 37° C by placing it on a heating blanket. During recordings, milk was fed to reduce the distress when the pups showed any sign of thirsty.
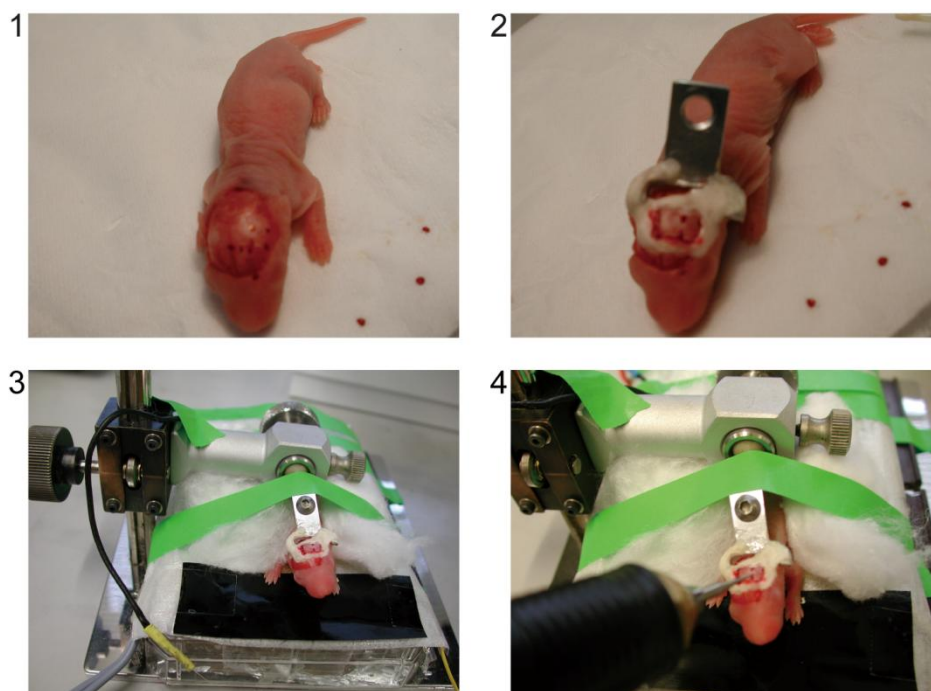
Fig. 11 Surgery preparation.

(1) The skin on the skull was carefully removed. The skull was dry and marked with the red dots for the craniotomy of S1. *(2)* Dental cement was used to fix a head holder on the ipsilateral and occipital bones. *(3)* The pup's head was fixed into the stereotaxic apparatus with screw. *(4)* The bone, but not the dura mater, over S1 was carefully removed by drilling a square of 2×2 mm^2.

3.1.2 Whisker stimulation

All whiskers except B2, C2 and D2 were trimmed under anaesthesia following the surgical preparation. A single whisker (usually C2) was stimulated approximately 1 mm from the snout using a miniature solenoid actuator (modify from Krupa et al., 2001) that generated for 32 ms a deflection in the rostral-to-caudal direction at 136 mm/s (4 °/ms). Recording sessions consisted of a 30 min baseline recording period, followed by a 10 min 2 Hz stimulation period for the induction of LTP and a 60 min post-stimulation period (**Fig.14D**). During the baseline recording and post-stimulation period, two stimuli with 60 s interval were applied every 5 min.

3.1.3 Voltage-sensitive dye imaging

The voltage-sensitive dye RH1691 (Optical Imaging, Rehovot, Israel) was dissolved at 1 mg/ml in a saline solution containing (in mM): 125 NaCl, 2.5 KCl, 10

HEPES (pH 7.3 with NaOH). The voltage-sensitive dye was topically applied to the surface of the barrel cortex and allowed to diffuse into the cortex for 15 to 30 min (**Fig 12A2**). Subsequently, unbound dye was carefully washed away with saline solution. This procedure resulted in a complete staining of all cortical layers from the subplate to the marginal zone / layer I in P0-P1 rats and in a more superficial staining pattern in P6-P7 animals , similar as described previously for adult rodent cerebral cortex (Berger et al., 2007;Ferezou et al., 2007). The cortex was covered with 1% low-melting agarose and a cover slip was placed on top to stabilize the tissue. Excitation light from a red LED (MRLED 625 nm, Thorlabs GmbH, Dachau, Germany) was band pass filtered (630/30 nm) and reflected towards the sample by a 650 nm dichroic mirror (**Fig 12A3, 4**). The excitation light was focused onto the cortical surface with a 25 mm Navitar video lens (Stemmer Imaging, Puchheim, Germany). Emitted fluorescence was collected via the same optical pathway, but without reflection of the dichroic mirror, long pass filtered (660 nm) and focused via another 25 mm Navitar lens onto the chip of a MiCam Ultima L high speed camera (Scimedia, Costa Mesa, CA, USA). This tandem-type macroscope design (Ratzlaff and Grinvald, 1991) resulted in a 1x magnification. As the high speed camera has a detector with 100x100 pixels and a chip size of 10x10 mm^2, the field of view was 10x10 mm^2. Using a C-mount extension tube we reduced the field of view to 2.6x2.6 mm^2 and thereby reduced in addition the vignetting. Every pixel collected light from a cortical region of 26x26 μm^2 (**Fig. 12B1**). The tandem-type macroscope comprising the LED, the filter cube and the two video optics were built in the mechanical workshop of our institute. Fluorescence measurements were synchronized to electrophysiological recordings through TTL pulses.

Spontaneously ongoing activity was detected during 16 s long imaging sessions while evoked activity following whisker stimulation was imaged in 2 s long sessions, both with an unbinned whole frame sampling frequency of 500 Hz. For both sets of experiments, data were not averaged.

After VSDI recording, VSDI evoked response image (**Fig. 12B2**) and photo of craniotomy with clear blood vessel (**Fig. 12B3**) merged together, which can provide the precise position for multi-channel recording.

3.1.4 Evaluation of voltage-sensitive dye imaging data

Images were analyzed offline using custom-made routines in MATLAB software version 7.7 (Mathworks, Natick, MA). In order to improve the signal to noise ratio, the image data were first processed using 5x5 pixel spatial binning followed by 60 Hz low pass filtering. Bleaching of fluorescence was corrected by subtraction of a best-fit double-exponential or 5th degree polynomial (curve fitting tool in MATLAB). The normalized change of fluorescence intensity($\Delta F / F0$) was calculated as the change of fluorescence intensity (ΔF) in each pixel divided by the initial fluorescence intensity (F0) in the same pixel.

Only fluorescent changes with a maximal $\Delta F / F0$ of at least 0.2% were considered as evoked responses or spontaneous events. To evaluate their onset, 3x3 pixels were taken around a pixel with a signal at least 7 times higher than the baseline standard deviation, which represented the point of earliest activity as determined by the experimenter. The duration of the events was determined as the time in which the signal was above the half-maximal $\Delta F / F0$ amplitude. The area of the evoked response or spontaneous event was defined as the contour plot of the VSDI response with reference to the half-maximal $\Delta F / F0$ amplitude. The spatial representation of VSDI responses were displayed according to this threshold. The diameter of the VSDI responses were calculated from the area of VSDI responses under the assumption of a circular response ($d=2(a/\pi)1/2$).

Voltage-sensitive dye imaging (VSDI) recording
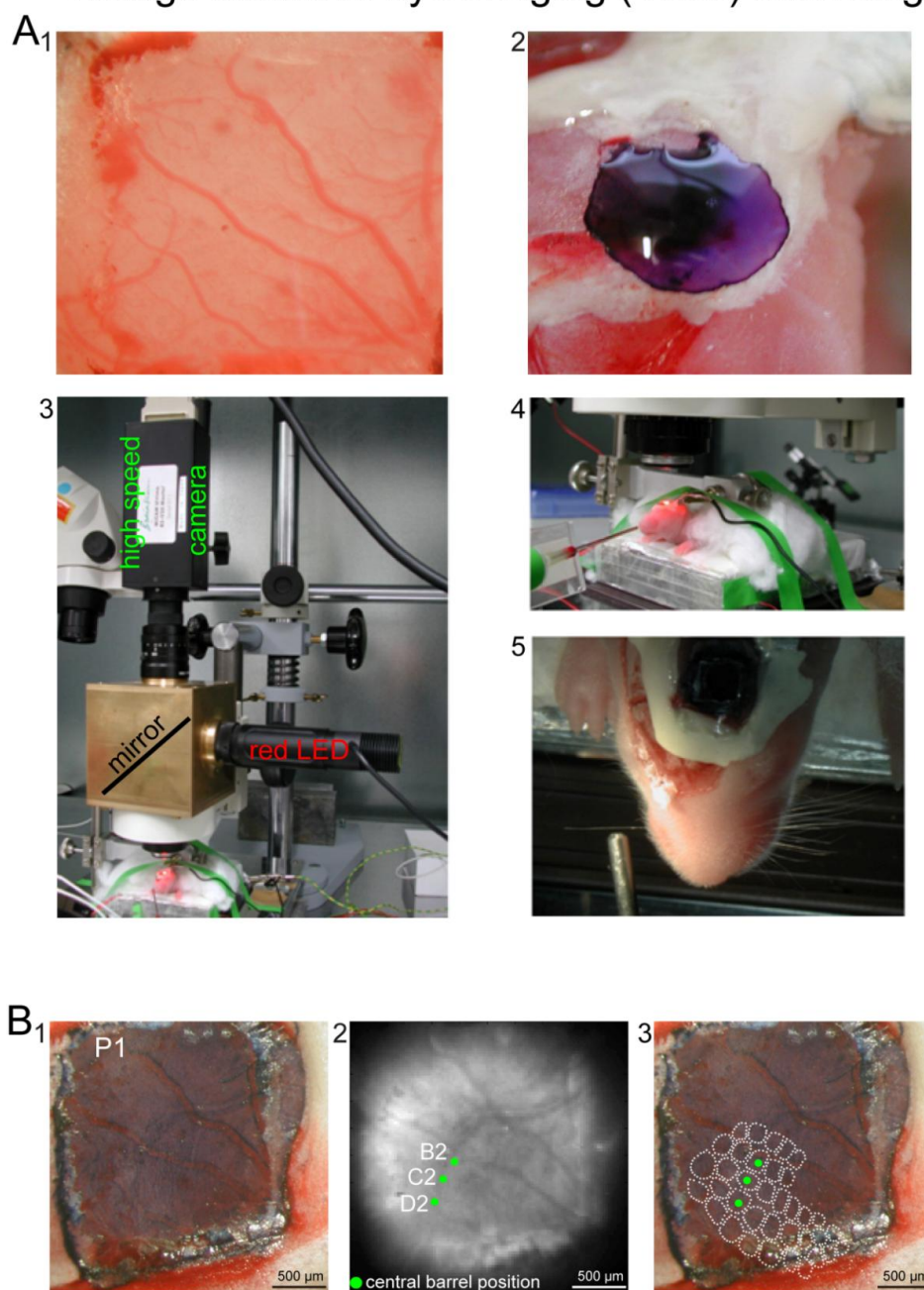
Fig. 12 Voltage-sensitive dye imaging recording.

A: (1) Exposed barrel cortex. (2) Staining barrel cortex with VSD. Schematic illustration (3) and photograph (4,5) of experimental set-up combining selective single whisker stimulation and VSDI recording. B: (1) Photograph of barrel cortex at P1 after VSDI recording. (2) Image for B2, C2 and D2 barrel by single whisker stimulation. The green points are central barrel position. (3) Merged picture by B1 and B2. Barrel field map was generated on the basis of a cytochrome oxidase stained horizontal section and superimposed according to the evoked responses.

3.1.5 Multi-electrode recording protocols

Protocols were similar to those described previously (Yang et al., 2009). According the positions of blood vessel and central positions of principle barrels in the last merged picture (**Fig. 12B3**), we could perform multi-channel recording.

Field potential (FP) and multiple unit activity (MUA) were recorded by a four-shank (**Fig. 17A1**) or a one-shank (**Fig. 20A**) 16-channel Michigan electrode (1-2 MΩ, NeuroNexus Technologies, Ann Arbor, MI) into one barrel column according to VSD response. The recording sites were separated by 125 μm in horizontal direction and 50 in vertical direction for the four-shank electrode (**Fig. 17A1**). Moreover, the recording sites in one-shank electrode were separated by 100 μm at P3-P5 (**Fig. 20B**) and 50 μm at P0-P1 (**Fig. 20C**). Both two kinds of electrodes were labelled with DiI (1,1'-dioctadecyl-3,3,3',3'-tetramethyl indocarbocyanine, Molecular Probes, Eugene, OR, USA). DiI stained tracks could help to reconstruct electrodes array position on Nissl-stained coronal section (**Fig. 20A**). FP and MUA were recorded at least for 2 hours at a sampling rate of 20 kHz using a multi-channel extracellular amplifier and the MC_RACK software (Multi Channel Systems).

3.1.6 Introcortical current source-density (CSD) analysis

Current source density (CSD) profiles were calculated from the FP profiles according to a three point formula described by Nicholson and Freeman (Freeman and Nicholson, 1975). The CSD values Im were derived from the second spatial deviation of the extracellular field potentials Φ and calculated by the finite-difference formula

$$I_m = -(1/kh^2) \sum_{m=-n}^{n} a_m \Phi(X + mh)$$

in which h gives the distance between two successive recording points and X is the coordinate perpendicular to the cortical layer. The remaining constants are as follows: n = 1, k = 1, a_0 = -2 and a±l = 1.

3.1.7 Calculate the slope of FP

The efficacy of synaptic transmission was calculated from the slope of the initial negativation of the evoked FP response (**Fig. 13A**). Evoked FP responses were visually inspected to exclude artifacts or contaminations with spontaneous activity (**Fig. 13B, C**). The slope was determined between 20 and 80% of maximal FP amplitude and was normalized to the average slope recorded during a 30 min baseline interval. The largest FP slopes located in layer IV at P3-P7 and cortical plate at P0-P1 were chosen for comparing among different ages (**Fig. 15B**), spatial locations (**Fig. 17-18**) and layers groups (also in layer II/III at P3-P5 and deep layer at P0-P1, **Fig. 21**). For statistical analyses slope values were averaged for a 5-30 min and 35-60 min poststimulus intervals. Data analysis was performed with MATLAB software versions R2008B.
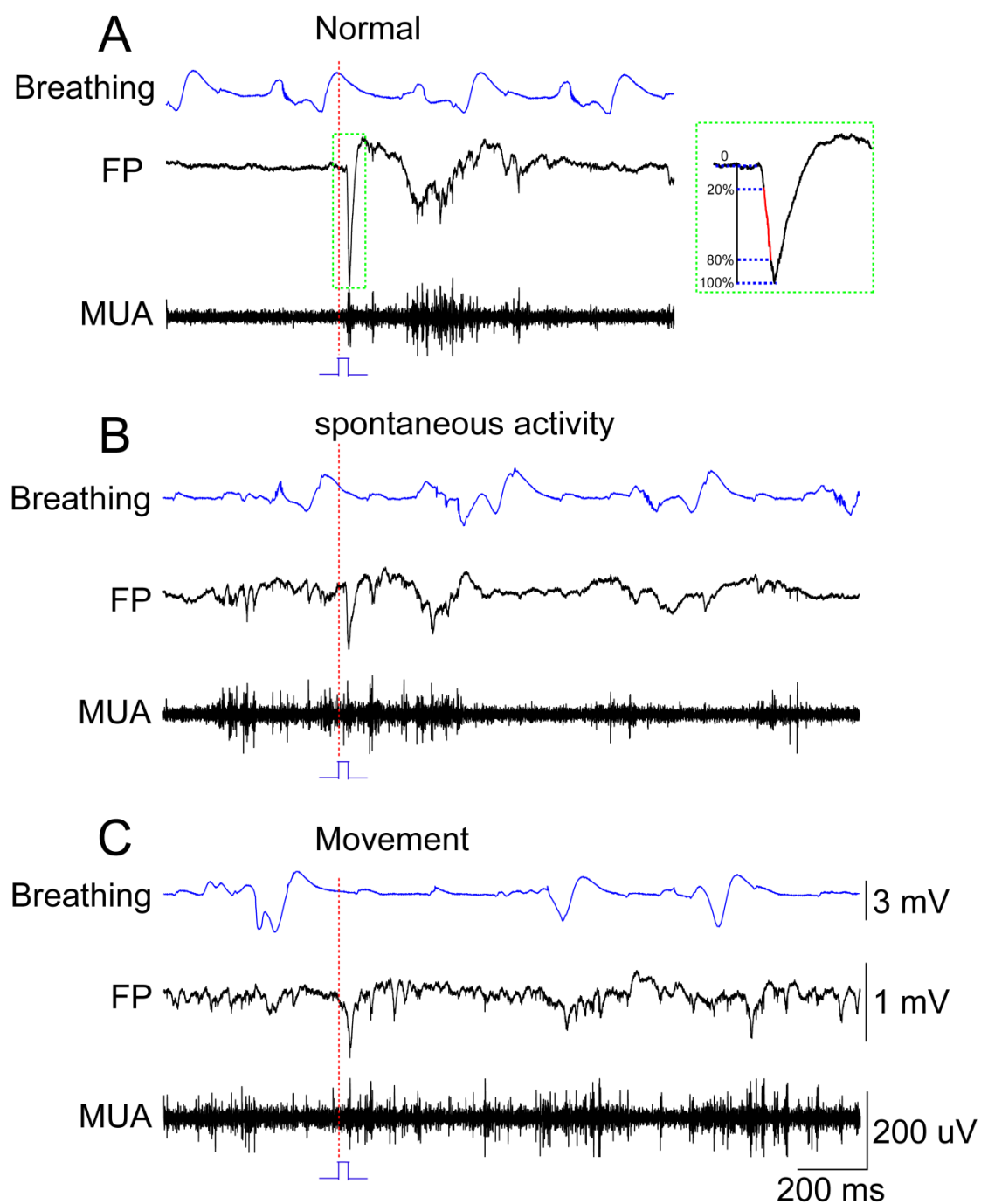
Fig. 13 Cortical response by single whisker deflection recorded at different situations.

A. Normal evoked response by single whisker deflection. Right, FP slope is calculated as the slope of the 20 – 80% amplitude interval of the initial negative deflection (indicated in red). Red dash line indicate the time point of single whisker stimulation. *B.* Evoked response is considerably attenuated by previous spontaneous activity. *C.* Evoked response is considerably attenuated by body movement.

3.1.8 Frozen slices:

After electrophysiological recordings, animals were deeply anesthetized by hypothermia and decapitated. The skull was removed and a section including the cortical barrel field was cut tangential to the cortical surface. The section was fixed in 4% paraformaldehyde for 24 h and washed in 0.01 M PBS. After cryoprotecting in PB (0.1M; pH 7.5) with 30% sucrose for 20 until 90 hours coronal sections of the brains or tangential sections were cut to 200 μm thick sections on a freezing microtome, collected in a multiculture plate filled with PB buffer and immunostained after making the DiI- fotos.

3.1.9 Serotonin Transporter (5-HTT) staining

Serial 200 μm thick tangential slices of flattened barrel cortex were cut on a cryotome and stained for serotonin transporter using a modification of a previously published protocol (Pinon et al., 2009). Slices were washed with PBS, followed by blocking and permeabilisation with 7% normal goat serum and 0.8% triton in PBS (2 h, RT) and incubated overnight at RT in rabbit anti-serotonin transporter polyclonal antibody (1:1000, AB9726, Chemicon, Germany). Antibody staining was visualized using a fluorescent antibody (Streptavidin Alexa-Cy3, 1:400, S-6402; Sigma, Deisenhofen, Germany). Slices were washed in PBS, mounted and coverslipped.

3.1.10 Statistics

Data in the text are presented as mean ± s.e.m. In the bar diagrams, data are shown as box plots giving the median, 25th and 75th percentiles, whiskers (10th and 90th percentiles), and outliers using SigmaPlot 10.0 software. Statistical analyses were performed with SPSS software version 13.0 using Mann-Whitney-Wilcoxon, repeated-measures ANOVA and one way ANOVA tests. Mann-Whitney-Wilcoxon test were used in two groups in which data sets without normal distribution. Repeated measurements in the same animals were analyzed by repeated-measures ANOVA test.

One way ANOVA test which followed by multiple comparisons with Bonferroni correction was performed to compare more than two groups at 35-60 min after 2 Hz stimulation.

3.2 Project 2

3.2.1 Animals and surgical preparation

All experiments were performed on neonatal Wistar rats (either sex) aged P0-P5 in accordance with the national laws for the use of animals in research and approved by the local ethical committee (#23177-07/G10-1-010). Surgical preparation was similar as described previously (Yang et al., 2012;An et al., 2012). Briefly, anesthesia was induced by initial hypothermia and intraperitoneal urethane injection (0.2 g/kg, Sigma-Aldrich, Steinheim, Germany). The head of the pup was fixed into the stereotaxic apparatus. A 3×3 mm^2 craniotomy was made over the left hemisphere by removing the skull and leaving the dura mater intact (**Fig. 22A**). The craniotomy included the forepaw and hindpaw representations in S1and M1 cortices. During recording the body was kept at a constant temperature of 37 ℃ by a heating blanket and cotton.

3.2.2 Forepaw or hindpaw touch stimulations and movement detections

The forepaw or hindpaw were stimulated approximately 1 mm away from the dorsal aspect using a miniature solenoid actuator (modified from Krupa et al., 2001) that generated for 30 ms a pressure on the skin. The inter-stimulus interval was 1 min.

Movements of the forepaw and hindpaw were recorded using piezoelectric transducer attached to them (**Fig. 23A**).

3.2.3 Voltage-sensitive dye imaging (VSDI)

Functional forepaw and hindpaw representations in S1 and M1 were identified by VSDI similar as described previously (Yang et al., 2012). The voltage-sensitive dye RH1691 (Optical Imaging, Rehovot, Israel) was dissolved in Ringer's solution containing (in mM): 125 NaCl, 2.5 KCl, 10 HEPES (pH 7.3 with NaOH) and was topically applied to the exposed cortical surface for 20 min. Excitation light from a

red LED (MRLED 625 nm, Thorlabs GmbH, Dachau, Germany) was band pass filtered (630/30 nm), reflected towards the sample by a 650 nm dichroic mirror, and focussed by a 25 mm Navitar video lens (Stemmer Imaging, Puchheim, Germany). Emitted fluorescence was collected via the same optical pathway, long pass filtered (660 nm) and focused via another 25 mm Navitar lens and a C-mount extension tube onto the chip of a MiCam Ultima L high speed camera (Scimedia, Costa Mesa, CA, USA). Every pixel of this camera collected light from a cortical region of 26x26 μm^2.

3.2.4 Analysis of VSDI Data

The analysis methods was similar as described previously (Yang et al., 2012). Ten trials of forepaw or hindpaw sensory evoked VSDI response from one pup were collected to obtain an average response. The averaged data were then processed using a 5 × 5-pixel spatial binning followed by 60-Hz low-pass filtering to improve the signal-to-noise ratio. Bleaching of the fluorescence signal was corrected by subtraction of a best-fit fifth-degree polynomial using the curve-fitting tool in MATLAB (Mathworks, Natick, MA, USA). We calculated the normalized change of fluorescence intensity ($\Delta F/F0$) as the change of fluorescence intensity (ΔF) in each pixel divided by the initial fluorescence intensity (F0) from the same pixel.

When the fluorescent changes in a maximal $\Delta F/F0$ were more than 0.3%, we considered them as evoked responses. The onset time of response was determined at the time point when VSDI signals were 5 times higher than the baseline standard deviation. The spatial representation of VSDI responses was defined at half-maximal $\Delta F/F0$ amplitude.

3.2.5 Multi-electrode recordings

As described previously (Yang et al., 2012), field potentials (FPs) and multiple-unit activity (MUA) were recorded with two 4-shank 16-channel Michigan electrode (1-2 MΩ, NeuroNexus Technologies, Ann Arbor, MI). On the four-shank electrode the recording sites were separated by 125 μm in horizontal direction and 50

μm in vertical direction (**Fig. 22A4**). One silver wire was placed just on the surface of the cerebellum as a ground electrode. Two recordings electrodes were positioned perpendicular to the cortical layers in S1 and M1 cortices respectively. At least one shank of each electrode was inserted into the center of the forepaw representations in S1 and M1 as identified with VSDI (**Fig. 22A, B**). FPs and MUA were recorded for at least 2 h at a sampling rate of 20 kHz using a multi-channel extracellular amplifier and MC_RACK software (Multi Channel Systems, Reutlingen, Germany).

3.2.6 Intracortical microstimulation in M1

After identification of the forepaw representation in M1 by VSDI, we inserted one four-shank 16-channel Michigan electrode perpendicular to the cortical layers with at least one shank inserted into the center of the M1 representation. On the four-shank electrode the electrode sites were separated by 200 μm in both horizontal and vertical directions. Electrodes were labelled with DiI (1,1'-dioctadecyl-3,3,3',3'-tetramethyl indocarbocyanine, Molecular Probes, Eugene, OR, USA) for subsequent histological reconstruction of the electrode tracks in Nissl-stained coronal sections through M1 (**Fig. 24A**). By current source density (CSD) analysis of forepaw sensory evoked reponses, we selected 2 channels located in layer V at a depth of 500-600 μm for bipolar electrical stimulation. A single pulse (150 μA, 100 μs duration) and twenty biphasic current pulses at 10 or 40 Hz were delivered separately through the 2 channels by a modified MEA1060-Inv-BC preamplifier (Multi Channel Systems,) and a stimulus generator (STG 2004, Multi Channel Systems,).

3.2.7 Local blockade of M1, S1 and forepaw

Pharmacologic inactivation of forepaw M1 or S1 was performed by local application of lidocaine via a glass pipette (tip diameter of 30–40 μm) filled with lidocaine (1% in Ringer's solution) hydrochloride monohydrate (Sigma-Aldrich) and attached to a syringe. The tip of the glass pipette was positioned on the M1 or S1

surface close to the multi-channel recording electrode. After a 30 min baseline recording, 2–4 μl lidocaine was applied. Blockade of M1 or S1 lasted approximately for 30 min.

Local inactivation of neuronal activity from the forepaw to M1 was achieved by application of lidocaine (3% in saline). After a 30 min baseline recording, 40 μl of lidocaine was injected into forepaw. Blockade of M1 or S1 lasted approximately for 1 hour.

3.2.8 Analysis of multi-electrode recordings data

As described previously (Yang et al., 2012), the FP signals from each channel were analyzed using the unfiltered data. MUA was detected using 200 Hz high-pass filtered signals with a threshold at 5 times the baseline SD and a bin of 1 ms. The post-stimulus time histograms (PSTH) were analyzed by summing up the activity in ~20 trials and normalized to number of spikes per second per trial. Sliding window method with 10 ms window and 1 ms step was applied for the PSTH calculation.

Gamma and spindle bursts were detected as follows. FPs contained at least 3 cycles with a duration less than 120 ms (the frequency more than 25 Hz), we defined them as gamma busts.. Similarly, FPs contained at least 3 cycles with a duration more than 150 ms (the frequency less than 20 Hz), we defined them as spindle busts. Furthermore, both gamma and spindle bursts should be accompanied by MUA.

The time–frequency spectrogram, power spectra, and coherence were analyzed using unfiltered raw data. Matlab spectrogram function with a time window of 100 ms and an overlapping of 99 ms (Matlab 7.7, Math works) was used for the time–frequency spectrogram analyses. Chronux toolbox (www.chronux.org) was used for spectrum and coherence analyses. Furthermore, Jackknife method provided in the Chronux toolbox was used to calculate 95% confidence intervals (CIs). Both spectrum and coherence analyses were performed using a time–bandwidth product of TW= 1 with K = 1 taper, and the padding factor for the fast fourier transformation (FFT) was 2.

3.2.9 Statistical tests

Data are presented as mean $\pm$ s.e.m. Statistics were tested with paired t-test (for comparing subsequent measurements in the same group of animals) and one way ANOVA (for comparing more than two different groups) tests followed by multiple comparisons with Bonferroni correction using SPSS software version 13.0 or Mann–Whitney–Wilcoxon test for the data sets recording in two sites but from one animal using GraphPad Prism (GraphPad Software, Inc.).

4 Results

4.1 Project 1

4.1.1 10 min whisker stimulation at 2 Hz induces age-dependent expression of LTP in the neonatal rat barrel cortex

The FP responses to single whisker stimulation recorded in newborn rat barrel cortex *in vivo* consisted of an early gamma activity followed by spindle bursts as described previously (Minlebaev et al., 2007;Yang et al., 2009;Minlebaev et al., 2011;Yang et al., 2012). To analyze activity-dependent modifications of the evoked responses, we quantified the slope of the initial negative going FP response, which reflects the early activation of the cortex via the thalamocortical pathway.

In P3-P5 rats (n=16 pups) repetitive single whisker stimulation at 2 Hz for 10 min (**Fig. 14**) induced a significant ($F(1.44,21.58)=0.77$, $p<0.001$) increase in the slope of the FP that persisted for >60 min. The FP slope increased dramatically ($P<0.001$, $P<0.001$ for 5-30 min, 35-60min against baseline, respectively) to 183.7 $\pm$ 12.4% (n=16) during the 5-30 min interval and to 208.1 $\pm$ 14.0% during the 35-60 min interval after LTP induction (upper traces in **Fig. 15A1**, red symbols in **Fig. 15A2, 3**). No significant changes ($F(2,16)=1.66$, $P=0.22$) in the FP slope (97.60 $\pm$ 2.39, 100.66 $\pm$ 2.83, 105.57 $\pm$ 4.64 at baseline, 5-30 min, 35-60 min, respectively) could be observed in the age-matched control group (n=9 pups), which did not receive repetitive 2 Hz whisker stimulations (lower traces in **Fig. 15A1**, open squares in **Fig. 15A2, 3**). Moreover, the relative FP slope showed the larger potentiation during the post stimulation recording than control group ($P<0.001$, $P<0.001$ for 5-30 min, 35-60 min in the stimulation group against control group respectively). These data demonstrate for the first time that the cerebral cortex of P3-P5 rats shows a prominent LTP to physiological stimulation of the afferent pathway *in vivo*.

Previous *in vitro* studies have documented in thalamocortical slices of newborn rats that the magnitude of LTP in barrel cortex gradually decreases between P3 and P7

and LTP cannot be induced after the first postnatal week (Crair and Malenka, 1995). In order to address the question whether a similar age-dependent expression of LTP can be also observed *in vivo* to physiologically relevant afferent stimulation, we studied the expression of LTP in P0-P1 and P6-P14 rats. In P0-P1 animals (n=12), single whisker stimulation at 2 Hz for 10 min induced a significant $(F(2,22)=79.30, p<0.001)$ and stable LTP ($P<0.001$, $P<0.001$ for 5-30 min, 35-60min against baseline, respectively) during the 5-30 min ($161.7 \pm 6.1\%$) and 35-60 min ($150.7 \pm 3.6\%$) post-induction interval (filled black squares in **Fig. 15B1, B2**). In P6-P7 rats (n=10), single whisker stimulation elicited an increase in the FP slope during the 5-30 min ($146.5 \pm 19.5\%$) and 35-60 min ($149.9 \pm 23.6\%$) post-induction interval, which were, however, not significantly $(F(1.16,10.43)=4.39, p=0.351)$ different from the baseline responses (blue symbols in **Fig. 15B1, B2**). In P8-P14 (n=5) rats no obvious changes in the FP slope (98.68 ± 1.1, 99.30 ± 3.9, 105.3 ± 5.6 at baseline, 5-30 min, 35-60 min, respectively; $F(2,8)=0.98$, $P=0.417$) could be evoked (green symbols in **Fig. 15B1, B2**). Furthermore, the 35-60 min LTP phase was significantly ($p=0.027$, $P=0.037$, for P3-P5 against P0-P1, P6-P7 respectively) smaller in P0-P1 and P6-P7 animals when compared to the P3-P5 group. In summary, these results indicate that LTP is limited to the critical periods with highest magnitude at P3-P5.
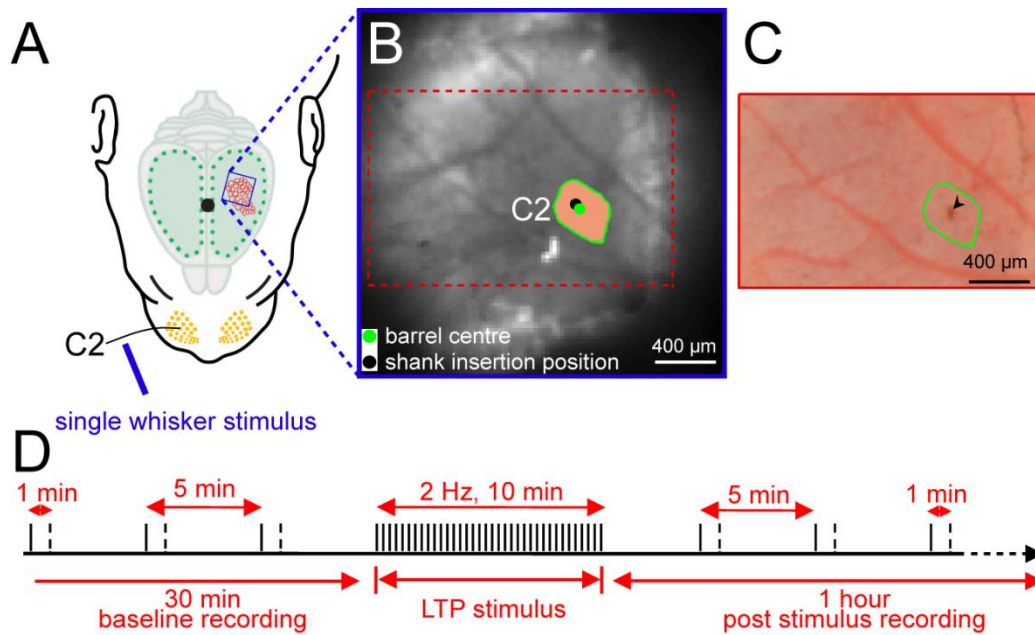
Fig. 14 Schematic diagram of the experimental setup.

Schematic diagram of the experimental setup illustrating selective mechanical stimulation of the C2 whisker *(A)* and simultaneous VSDI in the barrel cortex *(B)*. The exposed barrel cortex was stained with the voltage sensitive dye RH1691. A single whisker deflection of the C2 whisker elicits a local VSDI response in a P3 rat. The green dot indicates the centre of the C2 barrel-related cortical column. The black dot is the electrode insertion position. The orange color represent the region of the C2 whisker stimulation evoked VSDI response. *C.* shows the same area after termination of the electrophysiological recording and retraction of the recording electrode. The red dot shows the electrode insertion point (indicated by *arrowhead*). *D.* Stimulation protocol for induction of LTP. During baseline recording, the whisker was deflected twice per 5 min at 1 min interval for 30 min. For LTP induction the whisker was deflected at a frequency of 2 Hz for 10 min. Afterwards the same 2 stimuli per 5 min were used again for 60 min during the post stimulation recording period.

Fig. 15 Mechanical deflection of a single whisker for 10 min at 2 Hz elicits LTP of FP slope in barrel cortex of newborn rats *in vivo*.

A. Time course of FP responses before and after induction of LTP. *A1.* Representative FP recording during baseline, the 5-30 min and 35-60 min phases after 2 Hz stimulation (red) or without 2 Hz stimulation (black) in a P4 rat. *A2.* Relative FP slopes recorded in P3-P5 control and LTP group. Data are expressed as mean ± s.e.m. *A3.* Box plots of FP slopes in P3-P5 control and LTP group with baseline, 5-30 min and 35-60 min post stimulation. *B1.* Relative FP slopes recorded in different age groups. Data are expressed as mean ± s.e.m. *B2.* Box plots of FP slopes in LTP groups of different ages with baseline, 5-30 min and 35-60 min post stimulation. Significant levels between different intervals were tested with paired t-test, differences to control experiments were tested with Mann–Whitney–Wilcoxon test, and differences among age groups were tested with one-way ANOVA followed by multiple comparisons. Significance levels of p<0.001 (***) and p<0.05 (*) were identified.

Furthermore, we quantified the spike number of single whisker evoked response to analyze activity-dependent modifications, which reflects the early plasticity of the cortex via the neuronal network.

Similarly, in P3-P5 rats (n=16 pups) repetitive single whisker stimulation at 2 Hz for 10 min induced a significant ($F(2,30)=54.547$, p<0.001) increase in the spike number of single evoked response that persisted for >60 min. The the spike number increased dramatically ($P<0.001$, $P<0.001$ for 5-30 min, 35-60min against baseline, respectively) to 163.5 $\pm$ 9.0% (n=16) during the 5-30 min interval and to 194.0 $\pm$ 9.7% during the 35-60 min interval after LTP induction (upper traces in **Fig. 16A1**, red symbols in **Fig. 16A2, 3**). No significant changes ($F(1.3,10.1)=2.373$, $P=0.152$) in the spike number (101.7 $\pm$ 1.1, 107.0 $\pm$ 2.0, 109.6 $\pm$ 5.2 at baseline, 5-30 min, 35-60 min, respectively) could be observed in the age-matched control group (n=9 pups), which did not receive repetitive 2 Hz whisker stimulations (lower traces in **Fig. 16A1**, open squares in **Fig. 16A2, 3**). Moreover, the relative the spike number showed the larger potentiation during the post stimulation recording than control group ($P<0.001$, $P<0.001$ for 5-30 min, 35-60 min in the stimulation group against control group respectively). Again, these data also demonstrate for the first time that the cerebral cortex of P3-P5 rats shows a prominent LTP to physiological stimulation of the afferent pathway *in vivo*.

Similarly, we studied the MUA acitivity of LTP in P0-P1 and P6-P14 rats. In P0-P1 animals (n=12), single whisker stimulation at 2 Hz for 10 min induced a significant ($F(2,22)=35.4$, p<0.001) and stable LTP (P<0.001, P<0.001 for 5-30 min, 35-60min against baseline, respectively) during the 5-30 min (139.7 $\pm$ 6.5%) and 35-60 min (149.2 $\pm$ 5.6%) post-induction interval (filled black squares in **Fig. 16B1, B2**). In P6-P7 rats (n=10), single whisker stimulation elicited an increase in the spike number during the 5-30 min (124.6 $\pm$ 8.9%) and 35-60 min (137.1 $\pm$ 11.8%) post-induction interval, which were significantly ($F(2,18)=7.8$, p=0.004) increase than the baseline responses (blue symbols in **Fig. 16B1, B2**). In P8-P14 (n=5) rats no obvious changes in the spike number (99.3 $\pm$ 2.3, 103.5 $\pm$ 4.6, 97.4 $\pm$ 1.2 at baseline, 5-30 min, 35-60 min, respectively; $F(2,8)=0.8$, $P=0.474$) could be evoked (green symbols in **Fig. 16B1, B2**). Furthermore, the 35-60 min LTP phase was significantly

(p=0.004, P<0.001, for P3-P5 against P0-P1, P6-P7 respectively) smaller in P0-P1 and P6-P7 animals when compared to the P3-P5 group. In summary, these results consistent with FP slope of LTP and again indicate that LTP is limited to the critical periods with highest magnitude at P3-P5.
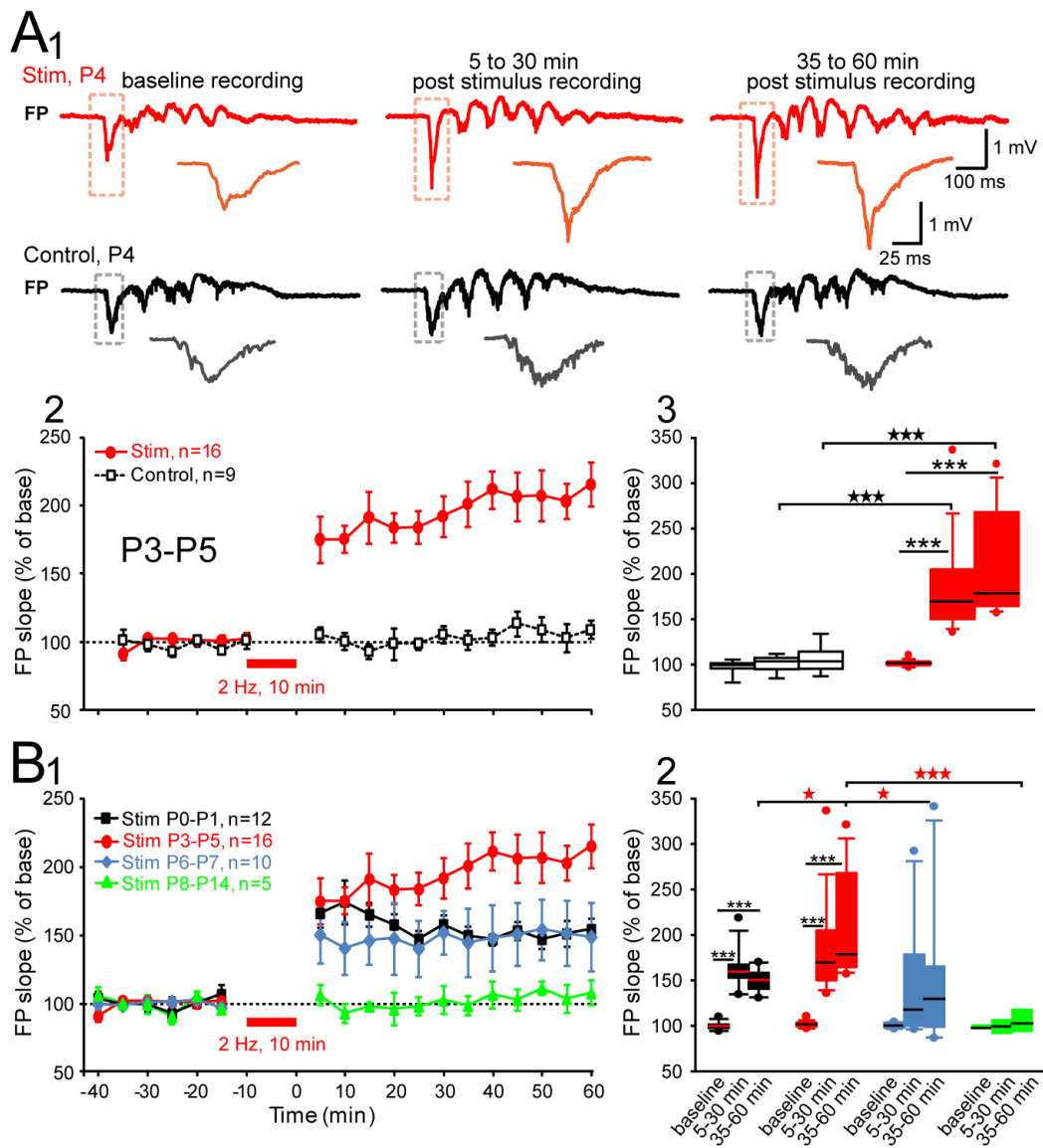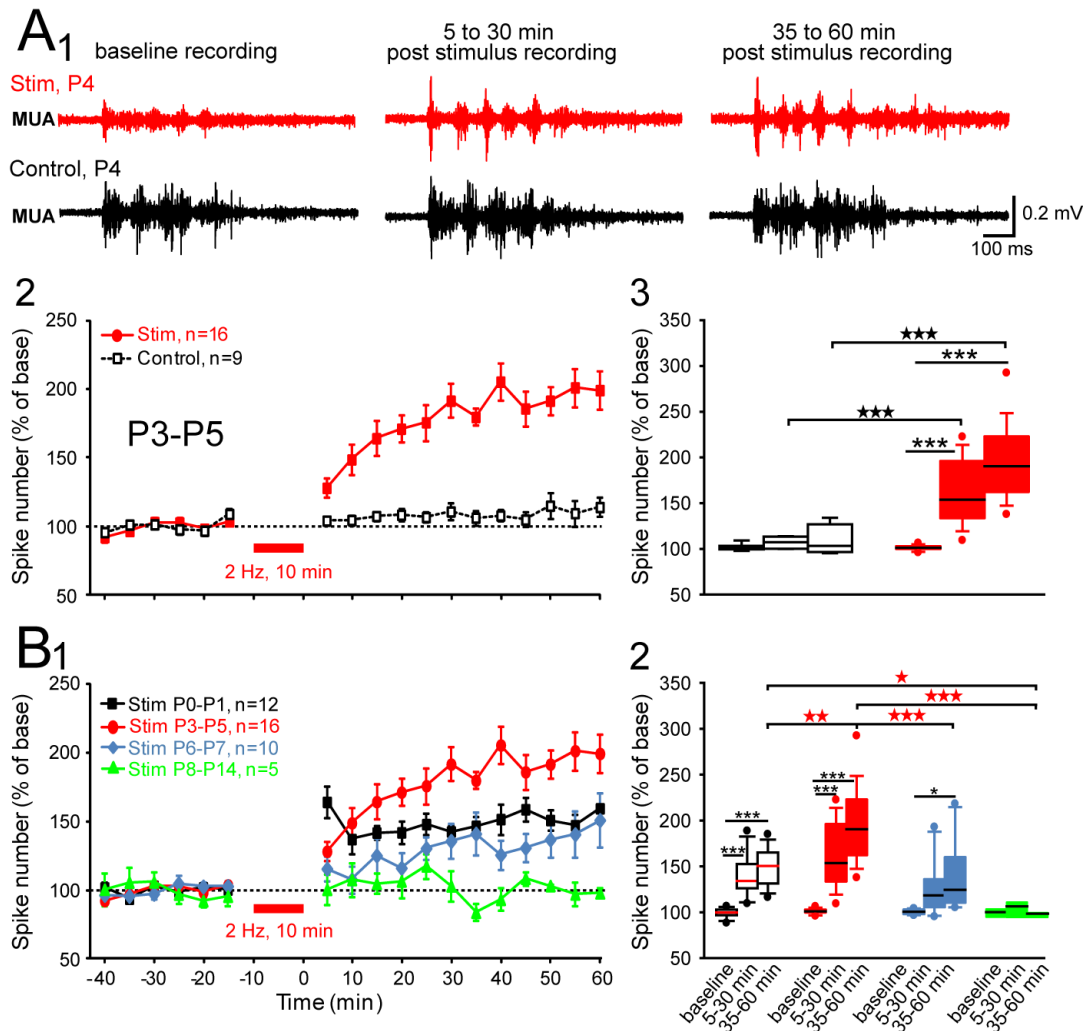

Fig. 16 Mechanical deflection of a single whisker for 10 min at 2 Hz elicits LTP of MUA in barrel cortex of newborn rats *in vivo*.

A. Time course of MUA samples before and after induction of LTP. *A1.* Representative MUA recording during baseline, the 5-30 min and 35-60 min phases after 2 Hz stimulation (red) or without 2 Hz stimulation (black) in a P4 rat. *A2.* Relative spike number recorded in P3-P5 control and LTP group. Data are expressed as mean ± s.e.m. *A3.* Box plots of spike number in P3-P5 control and LTP group with baseline, 5-30 min and 35-60 min post stimulation. *B1.* Relative spike number recorded in different age groups. Data are expressed as mean ± s.e.m. *B2.* Box plots of spike number in LTP groups of different ages with baseline, 5-30 min and 35-60 min post stimulation. Significant levels between different intervals were tested with paired t-test, differences to control experiments were tested with Mann–Whitney–Wilcoxon test, and differences among age groups during 35-60 min phase were tested with one-way ANOVA followed by multiple comparisons. Significance levels of p<0.001 (***), p<0.01 (**) and p<0.05 (*) were identified.

4.1.2 Spatial expression of LTP

Next we studied the question, whether the expression of LTP is restricted to the stimulated whisker-related cortical column or whether neighboring regions, septa and barrels, also show a significant LTP to our stimulation paradigm. To address this question, we used multi-electrode arrays which covered a distance of 375 μm and which allowed the recording of FP responses in the activated barrel-related column and in neighboring regions (**Fig. 17A1**).

We studied the spatial distribution of LTP in P3-P5 and P0-P1 rats, since only these two age groups showed a significant LTP. The stimulated whisker related cortical column was identified by VSDI and the 4×4-channel Michigan-type electrode was inserted perpendicularly into the barrel cortex with one electrode shank located in the centre of the whisker-related column (**Fig. 17A2, 3**). The time-course and magnitude of LTP was analyzed for various distances from this central position (green dot in **Fig. 17A2**). The magnitude of LTP was largest at a distance of <100 μm from the centre of the barrel and reached an average value of $180.7 \pm 8.9\%$ and $202.2 \pm 10.3\%$ during the 5-30 and 35-60 min LTP phase, respectively ($F(1.42,31.31)=86.75$, $P<0.001$, n=23 channels in 19 pups) (**Fig. 17B1, B2**). At a distance of 100-200 μm from the centre of the barrel (n=8 channels in 7 pups), a significant ($F(2,14)=62.12$, $P<0.001$) and stable LTP during the first ($149.4 \pm 6.0\%$) and second LTP phase ($154.5 \pm 6.0\%$) could be observed (**Fig. 17B1, B2**), but the second LTP phase was significantly ($p<0.05$) smaller at this location as compared to the barrel centre. At 200-300 μm from the centre of the barrel (n=12 channels in 9 pups), a significant ($F(2,22)=7.993$, $P=0.02$) LTP could be only observed during the 5-30 min ($121.6 \pm 5.9\%$), but not during the 35-60 min phase after LTP induction ($119.3 \pm 6.0\%$) (**Fig. 17B1, B2**). Furthermore, the magnitude of the 35-60 min LTP phase was significantly ($p<0.001$) smaller when compared to the LTP measured at a distance of <100 μm from the barrel centre. Similar results could be obtained for the P0-P1 age group (**Fig. 17C1, C2**), a stable expression of LTP at electrode positions located <100 μm from the center of the barrel related column ($157.8 \pm 9.1\%$ and $168.3 \pm 9.2\%$ for 5-30 and

35-60 min intervals, respectively; $n=$ 14 channels in 12 pups, **Fig. 17C1, C2**). A lower LTP expression was observed at distances between 100 and 200 μm (125.9 ± 8.6% and 134.8 ± 6.2% respectively, $n=$ 8 channels in 4 pups), while no significant LTP could be observed at electrode distances >200 μm ($n=$ 7 channels in 4 pups, **Fig. 17C1, C2**). These suggest that the expression of LTP in newborn rat barrel cortex is mostly restricted to the activated barrel-related column.
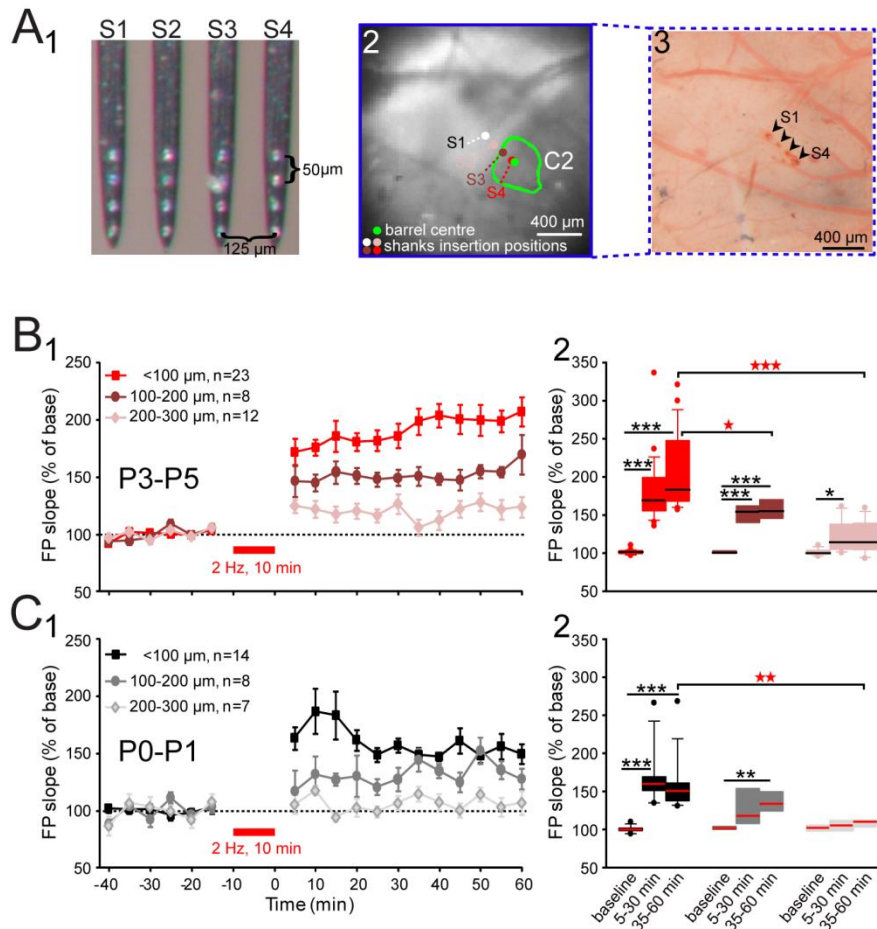
Fig. 17 The magnitude of LTP decreases with distance from the centre of the stimulated barrel.

A. Photograph of the 4×4-channel Michigan electrode array *(1)*. A local VSDI response was elicited by C2 single whisker deflection in a P4 rat *(2)*. The green dot indicates the centre of the C2 barrel-related cortical column. The colored dots are the electrode insertion positions. The green circle represents the region of the C2 whisker stimulation evoked VSDI response. *A3* shows the same area after termination of the electrophysiological recording and retraction of the recording electrode. The black dots show the electrode insertion point (indicated by *arrowheads*). *B-C.* Relative FP slopes recorded in various distances from the centre of the stimulated barrel in P3-P5 *(B1)* and P0-P1 *(C1)*. Data are expressed as mean ± s.e.m. *B3.* Box plots of FP slopes in various distances from the centre of the stimulated barrel in P3-P5 *(B2)* and P0-P1 *(C2)* age groups with baseline, 5-30 min and 35-60 min post LTP-stimulus. In

same distance groups , ***, p < 0.001, **, p < 0.01, *, p < 0.05 for 5-30 and 35-60 min LTP phases against baseline respectively, repeated measures ANOVA followed by multiple comparisons with Bonferroni correction. In three different distances, ★★★, p < 0.001, ★★, p < 0.01，★, p<0.05, for relative FP slope in < 100 μm against 200 - 300 μm,100 - 200 μm during 35-60 min phase respectively, one-way ANOVA followed by multiple comparisons with Bonferroni correction.

4.1.3 Input-specific LTP expression in principal barrel and septa

The spatial expression of LTP and its relationship to the cortical barrel and septa organization was studied in more detail by histological analyses of the recording sites after termination of the *in vivo* experiments. Tangential sections though layer IV of the barrel cortex were stained for the serotonin transporter (5-HTT) and the positions of the four electrode shanks of the multi-channel Michigan probes could be clearly identified (**Fig. 18A1**). In the example shown in **Fig. 18A1**, one shank was located in the barrel of the stimulated whisker C2, one shank was positioned in the septal region between C2 and C3 and two electrode shanks were located in the neighboring C3 whisker-related barrel. Deflection of the C2 whisker induced characteristic FP responses in the whisker-related barrel, the septal region and with a smaller amplitude also in adjacent whisker-related barrels (**Fig. 18A**2). Using the spatial information, the analyses demonstrated that the magnitude of LTP was largest in the barrel of the stimulated whisker (n=6 pups) reaching an average value of 190.8 ±17.5% (**Fig. 18B**). In the septal regions a significantly (p=0.032) smaller LTP of 138.6 ±7.8% (n=5 pups) was observed (**Fig. 18B**). No LTP could be observed in the neighboring non-stimulated barrel-related column (n=4 pups).
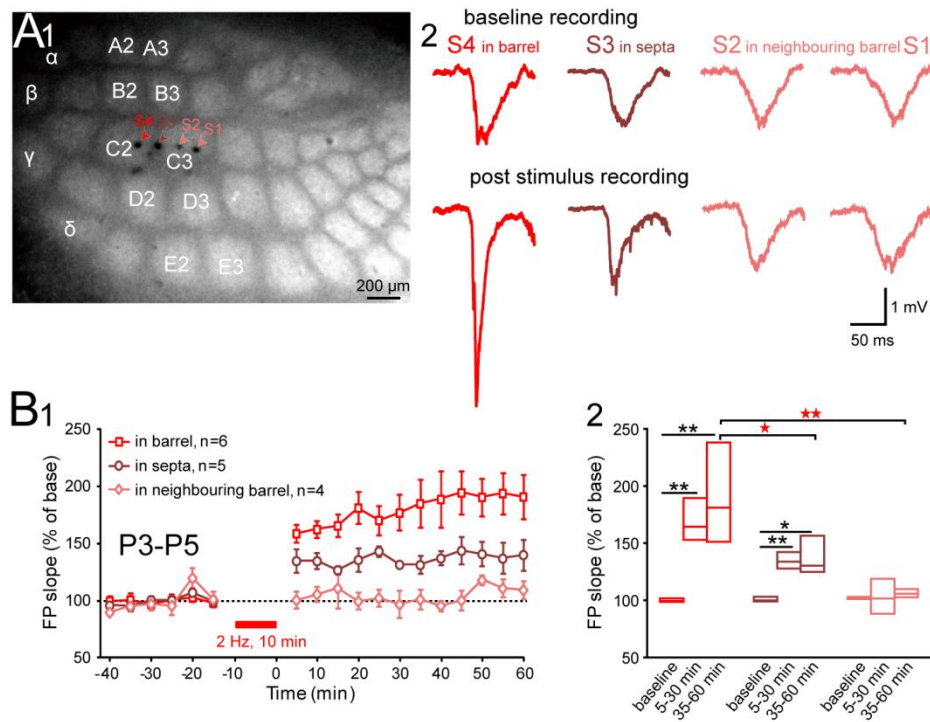
Fig. 18   LTP is expressed in the barrel of the stimulated whisker and to a lesser extent in the surrounding septal region.

A1, Photomicrograph of tangential section through layer IV of the barrel field of a P5 rat after processing the tissue for 5-HTT staining. Colored arrowheads indicate different locations of the four shanks of the 4x4-channel Michigan electrode. *A2,* FP responses recorded in the barrel-related column, in the neighbouring septum and in an adjacent barrel during baseline and post LTP induction periods from the same P5 rat as shown in *B1*. *B1,* mean ± s.e.m of relative FP responses recorded in the stimulated barrel (square), in the surrounding septal region (circle) and in the neighbouring barrel (diamond) of P3-P5 rats. *B2,* box plots of FP slopes recorded in barrel, septa and neighbouring barrel of P3-P5 rats averaged for baseline, 5-30 min and 35-60 min post LTP induction. **, P < 0.01; *, P < 0.05, 5-30 min and 35-60 min post LTP induction vs. pre-stimulation, repeated measures ANOVA followed by multiple comparisons with Bonferroni correction; ★★, P < 0.01,★, P < 0.05 in barrel vs. in neighbouring barrel and in septa during 35-60 min phase respectively,, one-way ANOVA followed by multiple comparisons with Bonferroni correction.

Furthermore, we quantified the spike number of single whisker evoked response to analyze activity-dependent modifications in the spacial distribution (**Fig. 19A**). The magnitude of LTP was largest at a distance of <100 μm from the centre of the barrel and reached an average value of 163.6 ± 8% and 193.7 ± 8.7% during the 5-30 and 35-60 min LTP phase, respectively ($F(2,34)=68.2$, $P<0.001$, n=18) (**Fig. 19B1,2**). At a distance of 100-200 μm from the centre of the barrel (n=7), a significant ($F(2,12)=38.5$, $P<0.001$) and stable LTP during the first (143.2 ± 6.2%) and second LTP phase (147.3 ± 6.1%) could be observed (**Fig. 19B1, 2**), but the second LTP

phase was significantly (p=0.004) smaller at this location as compared to the barrel centre. At 200-300 μm from the centre of the barrel (n=10), no LTP ($F(2,18)=0.274$, $P=0.763$) could be observed after LTP induction (**Fig. 19B1, 2**). Furthermore, the magnitude of the 35-60 min LTP phase was significantly (p<0.001) smaller when compared to the LTP measured at a distance of <100 μm from the barrel centre. Similar results could be obtained for the P0-P1 age group (**Fig. 19C1, 2**), a stable expression of LTP at electrode positions located <100 μm from the center of the barrel related column (141.4 ± 6.2% and 147.9 ± 5.8% for 5-30 and 35-60 min intervals, respectively; n= 14, **Fig. 19C1, 2**). A lower LTP expression was observed at distances between 100 and 200 μm (135.4 ± 14.2% and 135 ± 14.2% respectively, n= 8), while no significant LTP could be observed at electrode distances >200 μm ($F(2,12)=2.057$, $P=0.171$; n= 5, **Fig. 19C1, 2**).
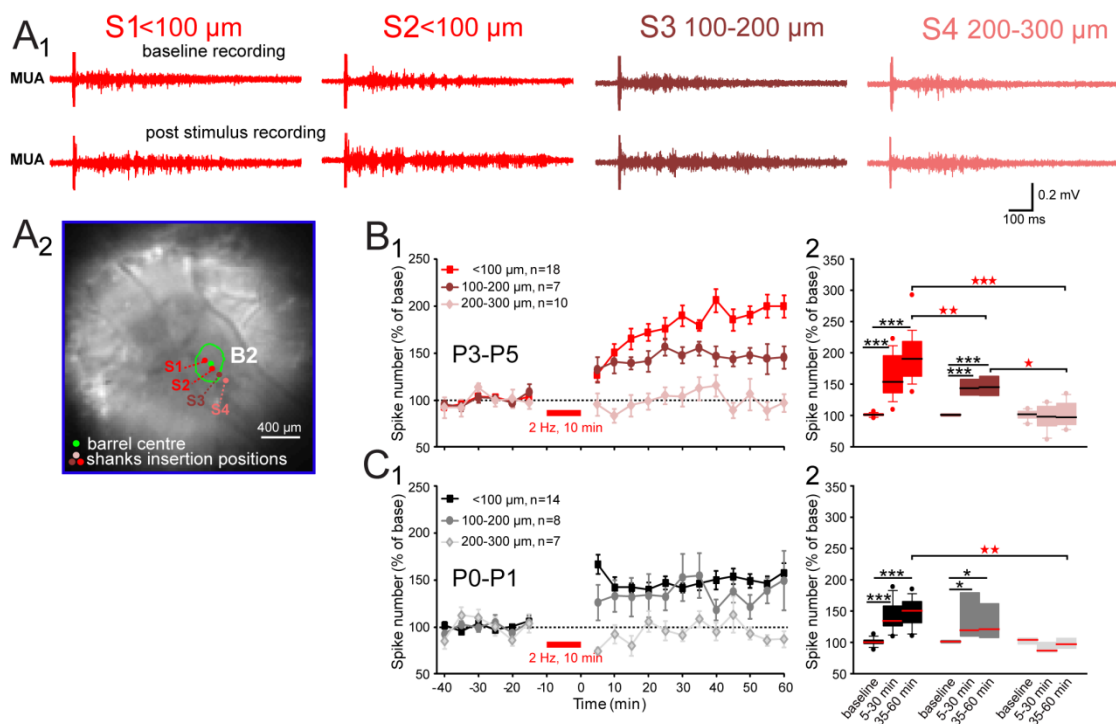
Fig. 19 The magnitude of LTP decreases with distance from the centre of the stimulated barrel.

A1, MUA recorded at distances of <100 μm, 100-200 μm and 200-300 μm from the barrel centre during baseline (up) and post LTP induction periods (down) from a P4 rat. *A2,* A local VSDI response was elicited by B2 single whisker deflection in a P4 rat. The green dot indicates the centre of the B2 barrel-related cortical column. The colored dots are the electrode insertion positions. Different colors stand for the various distances from the centre of the stimulated barrel. The green circle represents the region of the C2 whisker stimulation evoked VSDI response. *B-C,* Relative sipke number recorded in

various distances from the centre of the stimulated barrel in P3-P5 *(B1)* and P0-P1 *(C1)*. Data are expressed as mean ± s.e.m. Box plots of FP slopes in various distances from the centre of the stimulated barrel in P3-P5 *(B2)* and P0-P1 *(C2)* age groups with baseline, 5-30 min and 35-60 min post LTP-stimulus. In same distance groups , ***, $p < 0.001$; *, $p < 0.05$ for 5-30 and 35-60 min LTP phases against baseline respectively, repeated measures ANOVA followed by multiple comparisons with Bonferroni correction. In three different distances, ★★★, $p < 0.001$, ★★, $p < 0.01$，★, $p<0.05$, for relative FP slope in < 100 μm against 200 - 300 μm,100 - 200 μm during 35-60 min phase respectively, one-way ANOVA followed by multiple comparisons with Bonferroni correction.

These data indicate that single whisker stimulation in newborn rats *in vivo* elicits a prominent and spatially confined LTP. Interestingly, a significant and spatially confined LTP could be already observed in P0-P1 rats, but at this early age, structural barrels can be not identified with histological methods and layer IV has not been fully developed yet (Erzurumlu et al., 1990).

4.1.4 Layer-specific expression of LTP

CSD analyses show the laminar location, direction (sink and source) and magnitude of the transmembrane currents, which are responsible for generating the local synaptic activity (Mitzdorf, 1985;Heynen and Bear, 2001;Megevand et al., 2009). To elucidate the laminar localization of the potentiated synapses we performed CSD analyses in P0-P1 and P3-P5 rat barrel cortex *in vivo*. A one-shank 16-channel Michigan probe with an inter-electrode-distance of 100 μm for P3-P5 and 50 μm for P0-P1 was inserted perpendicularly into the stimulated column as identified by VSDI. The electrodes covered all cortical layers from the cortical surface to the white matter (**Fig. 20A**). Field potentials and the corresponding CSD profiles before and after the LTP stimulus were compared in both age groups.

In P3-P5 animals, the baseline CSD profiles were characterized by a prominent current sink in layer IV that extended into the lower part of layer II/III (**Fig. 20B1**). These patterns are consistent with previously reported findings in the neonatal rat barrel cortex *in vivo* (Minlebaev et al., 2007;Yang et al., 2009). After 2 Hz 10 min single whisker stimulation, the synaptic potentiation was confined to this current sink (**Fig. 20B2**), indicating a prominent increase in efficacy of the thalamocortical synaptic input innervating layer IV and lower layer II/III. In P0-P1 animals, in which

layers II/III and partly layer IV have not yet been formed (Molnar et al., 1998), a pronounced synaptic potentiation of the current sink in the cortical plate / upper layer V could be observed (**Fig. 20C**). The corresponding source was located in lower layer V and in layer VI.
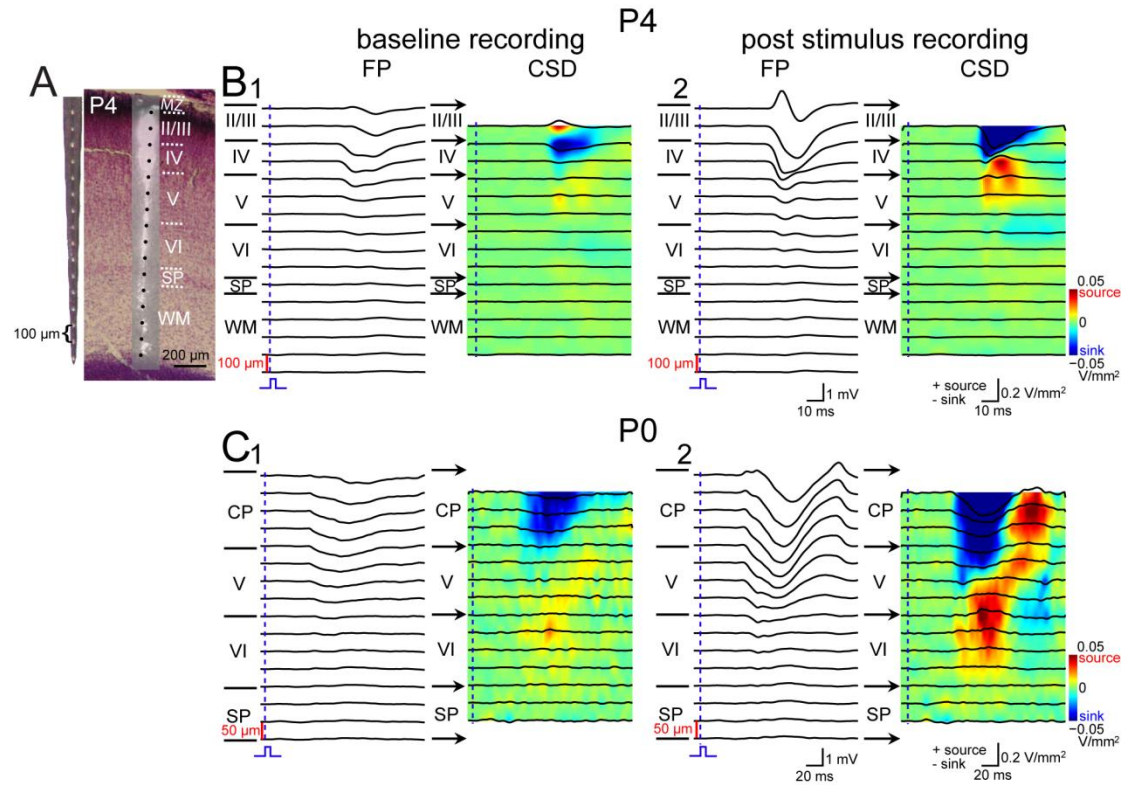
Fig. 20 Representative field potential response depth profiles and corresponding CSD analyses obtained before and after induction of LTP in a P4 (B) and P0 (C) rats.

*A,*Photograph of the 1x16-channel Michigan electrode array (left). Digital photomontage reconstructing the location of the DiI-covered electrode in coronal Nissl-stained section (right). ***B-C,*** Depth profiles of FP responses to single whisker stimulation and corresponding CSD analyses in a P4 and P0 rat. The inter-electrode-distances in the P4 animal was 100 μm, for the P0 rat 50 μm. Left panel *(1)* shows control data obtained during baseline recording. Right panel *(2)* shows data after LTP induction. In CSD analyses, current sinks (blue) are downward and current sources (red) are upward going.

We studied the various layer-specific expression of LTP in P3-P5 and P0-P1 rats, since only these two age groups showed a significant LTP, while not in all P6-P7 pups a prominent LTP could be induced (**Fig. 15B**). The stimulated whisker related cortical column was identified by VSDI and the 1×16-channel Michigan-type electrode was inserted perpendicularly into the centre of the whisker-related column (**Fig. 20A**). The time-course and magnitude of LTP was analyzed for various depths (**Fig. 20A, C**). At

P3-P5, the magnitude of LTP was largest in layer IV and reached an average value of 180.3 $\pm$ 13% and 219.2 $\pm$ 22.2% during the 5-30 and 35-60 min LTP phase, respectively ($F(1.11,6.69)=29.26$, $P=0.001$, n=7 pups) (**Fig. 20B**). In layer II/III (7 pups), a significant ($F(2,12)=13.79$, $P=0.01$) and stable LTP during the first (171.7 $\pm$ 15.9%) and second LTP phase (200.8 $\pm$ 26.6%) could be observed (**Fig. 20B**). In layer V (n=7 pups), a significant ($F(2,12)=34.2$, $P<0.001$) LTP could be both observed during the 5-30 min (167.4 $\pm$ 11.4%) and during the 35-60 min (161.2 $\pm$ 8.9%) phase after LTP induction (**Fig. 20B**). However, no LTP could be found in the layer VI (n=7 $P>0.05$, pups). Furthermore, the magnitude of the 35-60 min LTP phase was significantly ($F(3,24)=3.3,P=0.037$) different among the various layers. Similar results could be obtained for the P0-P1 age group (**Fig. 20C**), a stable expression of LTP could be induced in cortical plate (161.5 $\pm$ 2.2% and 147.5 $\pm$ 3.2% for 5-30 and 35-60 min intervals, respectively; $n=$ 8 pups, **Fig. 20D**). A lower LTP expression was observed in layer V (143.9 $\pm$ 5.0% and 136.6 $\pm$ 7.6% respectively, $n=$ 8 pups), while no LTP could be observed both in layer VI and subplate ($F(2,14)=1.23,P=0.32$; $F(2,14)=1.61,P=0.037$respectively,$n=$ 8 pups, **Fig. 20D**). However, no conclusive evidence for LTP of the thalamus-to-subplate synapse could be observed in this study as well as in thalamocortical slice preparations (unpublished observations). These data indicate that long-term changes in whisker-evoked responses of the barrel cortex after 2 Hz stimulation mainly involved the granular and supragranular layers.
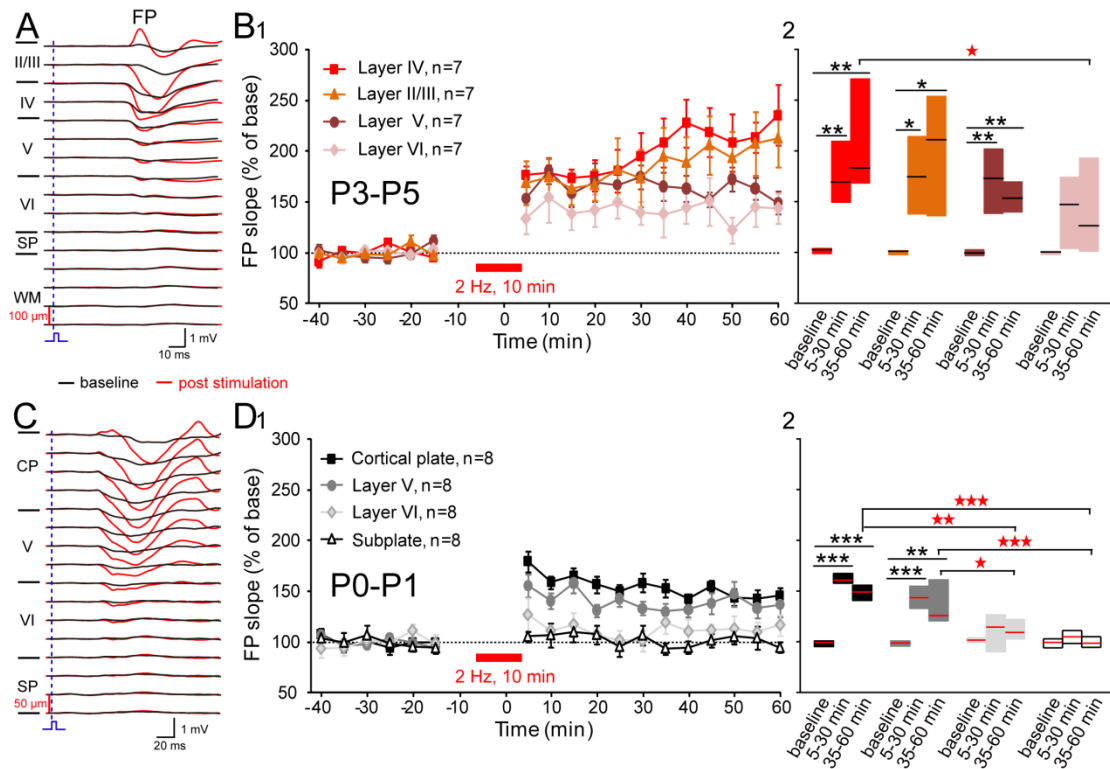
Fig. 21 Physiological whisker stimulation induces LTP in different layers.

A-C, Depth profiles of FP responses to single whisker stimulation during baseline and post LTP induction periods in a P4 *(A)* and P0 *(C)* rat. *B-D,* Relative FP recorded in various depths of the stimulated barrel in P3-P5 *(B1)* and P0-P1 *(D1)*. Data are expressed as mean ± s.e.m. Box plots of FP slopes in various depths from the centre of the stimulated barrel in P3-P5 *(B2)* and P0-P1 *(D2)* age groups with baseline, 5-30 min and 35-60 min post LTP-stimulus. In same distance groups , ***, $p < 0.001$; **, $p < 0.01$; *, $p < 0.05$ for 5-30 and 35-60 min LTP phases against baseline respectively, repeated measures ANOVA followed by multiple comparisons with Bonferroni correction. In different layers, ★★★, $p < 0.001$, ★★, $p < 0.01$，★, $p<0.05$, for relative FP slope cortical plate against layerVI and subplate, layer V against layerVI and subplate, during 35-60 min phase respectively, one-way ANOVA followed by multiple comparisons with Bonferroni correction.

4.2 Project 2

4.2.1 Voltage-Sensitive Dye Imaging Reveals Sensory Processing in the Newborn Rat Sensorimotor Cortex

The forepaw and hindpaw representations in S1 and M1 were identified in newborn rat *in vivo* by VSDI following single mechanical stimulation (**Fig. 22**). In all P3-P5 rats (n=16 pups), stimulation of the forepaw evoked reliable responses in the contralateral sensorimotor cortex with a latency of 46.19 ± 1.10 ms **(Fig. 22A-B)**. The initial sensory response was highly localized with small amplitude in contralateral S1 and then the amplitude reached maximally to 0.91 ± 0.03 % ΔF/F0 **(Fig. 22**B-D). Approximately 8 ms after the earliest response in S1 cortex, the second localized response occurred in contralateral M1 **(Fig. 22B)**. However, the evoked responses in M1 had significantly longer ($P < 0.001$) onset latency to 54.88 ± 1.58 ms **(Fig. 22D1)** and significantly smaller ($P < 0.001$) amplitude to 0.71 ± 0.03 % ΔF/F0 **(Fig. 22D2)** than the responses in S1. Moreover, the locations of these responses in S1 and M1 were mirror symmetric. These are consistent with previous studies in adult rodents, showing the sensory processing in vibrissa sensorimotor cortex (Ferezou et al., 2007), and the mirror symmetric locations of S1 and M1 (Brecht et al., 2004b;Brecht, 2011).These results demonstrate that the sensory stimulation reliably evokes the sensory processing in two separated and local regions from S1 to M1 in newborn animals.
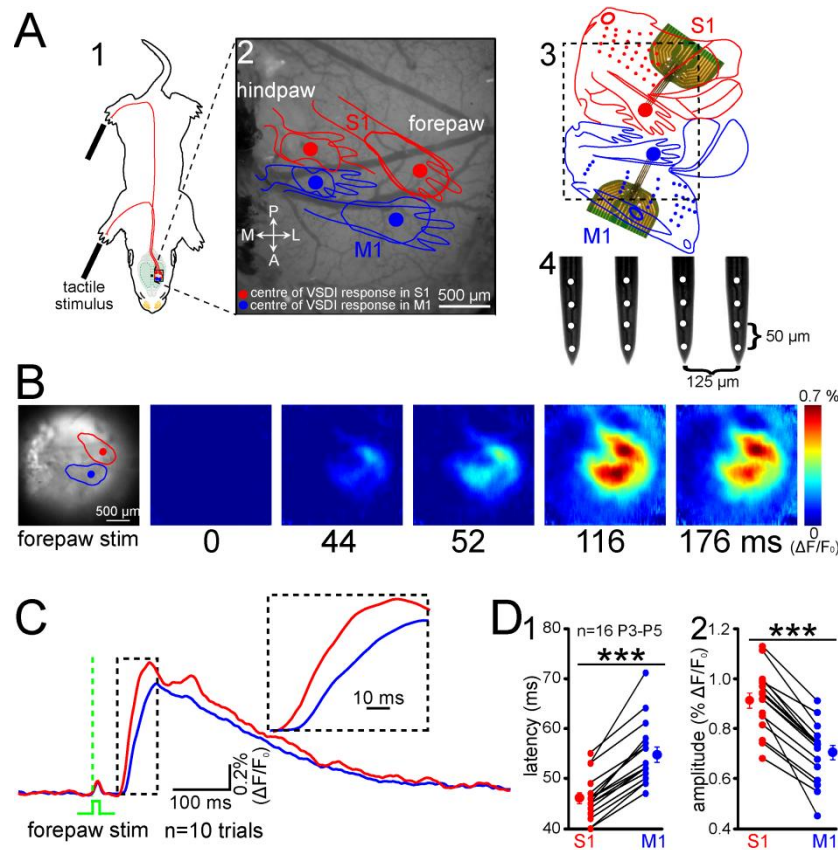
Fig. 22 A single mechanical stimulation of forepaw or hindpaw induces VSDI evoked response in both S1 and M1 of newborn rats.

(A) Schematic diagram of the experimental setup illustrating selective sensory mechanical stimulation of forepaw or hindpaw *(A1)* and simultaneous VSDI recording in S1 and M1 *(A2)*. The exposed cortex includes the forepaw and hindpaw representations in S1 (red diagram) and M1 (blue diagram). A single mechanical stimulation of the forepaw or hindpaw elicits a local VSDI response in both S1 and M1 from a P5 rat. The red line in A1 indicates for the sensory pathway. The red and blue dots indicate the centre of VSDI evoked response in S1 and M1 respectively. The red and blue circles represent the region of forepaw or hindpaw mechanical stimulation evoked VSDI responses respectively. A, anterior; L, lateral; P, posterior; M, medial. *(A3)* Flattened maps of the M1 and S1 cortices (modified from Brecht et al., 2004b). Schematic illustration marked by dash black square indicates the same area as *(A2)*. Two four-shank 16-channel electrodes are inserted into the centre of VSDI evoked response in S1 (red) and M1 (blue) respectively to record spontaneously occurring and sensory evoked activity. *(A4)* Photograph of a four-shank 16-channel Michigan electrode array shows the neighbour shanks distance of 125 μm and neighbour channels distance of 50 μm on a shank.

(B) The left image shows the same cortex as *(A2)*, but after stained with the voltage sensitive dye RH1691. From 0-176 ms VSDI evoked images were induced by the single mechanical stimulation of the right forepaw. Note that after forepaw mechanical stimulation, the local response occurred in S1 first, over about 8 milliseconds, the other localized response generated in M1.

(C) VSDI fluorescence signal traces in both S1 and M1 from the same experiment as in *(B)* induced by a single forepaw mechanical stimulation were averaged across ten trials. Representative part of example is shown at an expanded time scale (right). In this and the subsequent figures, red indicates the

data from S1 and blue indicates the data from M1. Green dash line indicates the time point of sensory stimulus. Note that after stimulation in forepaw, VSD fluorescence signal increases firstly in S1, and several milliseconds later propagates in M1.

(D) Statistical analyses of the onset latency *(D1)* and maximal amplitude *(D2)* of forepaw-evoked VSDI response obtained from 16 P3-P5 rats. Note the sensory evoked responses in neonatal M1 with a longer latency and smaller amplitude than responses in S1. The averaged data (bigger symbols) are expressed as mean ± s.e.m. Small symbols connected by black line stand for individual animal. Significant differences between S1 and M1 were tested with Mann–Whitney–Wilcoxon test. Significance levels of $p < 0.001$ (***) was identified.

4.2.2 Neonatal M1 operates in both motor and somatosensory modes

VSDI has perfect spatial resolution but not good temporal resolution, since it is unable to reflect well on the high-frequency patterns of neuronal activity (Berger et al., 2007;Ferezou et al., 2007;Yang et al., 2012;Mcvea et al., 2012). Therefore, we combined with extracellular multi-electrode recording. VSDI recording provided the locations of forepaw representations in S1 and M1 which enabled us to insert Michigan electrode into the centres of forepaw S1 and M1 (**Fig. 22**) as we did recording in the central C2 barrel in previous study (An et al., 2012).

It has been documented that the subcortical networks generate spontaneous neuronal activity to drive early motor behavior in the developing sensorimotor system (Petersson et al., 2003;Blumberg, 2010a;Tiriac et al., 2012). To study the function of M1 and the relationship between neuronal patterns in sensorimotor cortex and spontaneous motor activity during the early development of sensorimotor system, we did simultaneously recording of the cortical activity in sensorimotor cortex and the movements of forepaw (**Fig. 23A**). Interestingly, we observed three distinct relationships in P3-P5 rats. (1) Spontaneous cortical activity in M1 with the occurrence of 3.5 ± 0.3 min^{-1} drove forepaw movement and activity in S1. Gamma burst (~40 Hz) preceded forepaw movement and spindle burst in S1 (**Fig. 23B1**). (2) On the contrast, spontaneous forepaw movement triggered activity in sensorimotor cortex (with the occurrence of 5.5 ± 0.7 min^{-1}). Spontaneous forepaw movement preceded 10 Hz spindle bursts in S1 and 40 Hz gamma bursts followed by 10 Hz spindle bursts (**Fig. 23B2**). (3) Gamma and spindle bursts occurred in M1 and S1 with

the occurrence of 2 ± 0.3 min^{-1} without forepaw movement (**Fig. 23B3**). Then, we distinguished two populations of spontaneous MUA events in M1 according the time point of the forepaw movement. In P3-P5 animals, spontaneous MUA events in M1 drove forepaw movements (**Fig. 23C1**), however, most of MUA events were triggered by the movements (**Fig. 23C2**). Finally, we quantified onset latency between FP events in M1 and forepaw movements during 10 min recording from 990 events in 9 P3-P5 rats (**Fig. 23D**). 31.8% of spontaneous activities could drive the forepaw movements with the most events (1.4 ± 1.2 min^{-1}) occurring 100-150 ms earlier than the forepaw movements. In contrast, 50% of spontaneous activities were triggered by the forepaw movements with the majority of events (2.2 ± 0.5 min^{-1}) at latency of 40-60 ms following the spontaneous movements. The left 18.2% spontaneous activity happened alone not related with any paw movement.

In summary, these results indicate that M1 plays double roles. On the one hand, it works in a motor mode to drive motor outputs. On the other hand, it operates in a sensory mode to receive periphery sensory inputs.
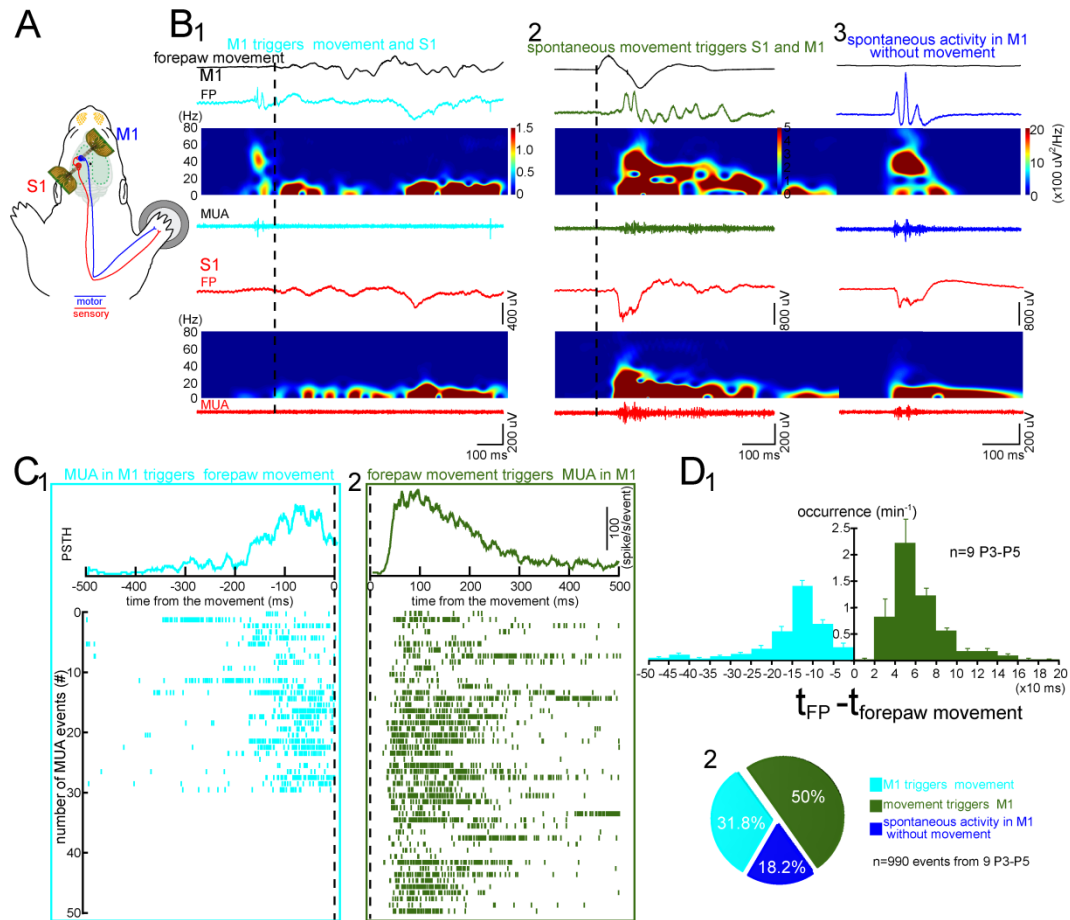
Fig. 23 Spontaneous neuronal activity in sensorimotor cortex correlates with forepaw movement.

(A) The schematic illustration of the experimental setup with two four-shank 16-channel electrodes as in **Fig 22A3-4** located in S1 (red), M1 (blue) and a movement detector attached to the contralateral forepaw. Blue line indicates the motor pathway, while red line stands for the sensory pathway.

(B) Three patterns of relationships between the cortical activity in sensorimotor cortices and forepaw movement from a P4 rat. *(B1)* Gamma burst in M1 (light blue) could trigger forepaw movement and spindle burst in S1 (red). Black dash lines indicate the time point of forepaw movements. Top black trace is the spontaneous forepaw movement detection. The middle time series spectrogram was calculated for with a time window of 100 ms and an overlapping of 99 ms from the unfiltered raw data. The bottom trace shows the MUA in a high-pass filtered (>200 Hz) trace. Light blue traces indicate activity from M1, red traces represent activity from S1. *(B2)* Spontaneous forepaw movement could trigger spindle burst in S1 (red) and gamma burst in M1 (green). *(B3)* Spontaneous activity occurred in M1 (blue) and S1 (red) during the quiet periods of forepaw.

(C1) Spontaneous MUA events in M1 (light blue) trigger forepaw movements from the same animal as in *B*. Top trace is post-stimulus time histogram (PSTH) and bottom bars represent different spontaneous MUA events in M1. Spontaneous MUA events were aligned to the onset of the forepaw movements. Black dash lines indicate the time point of forepaw movements. *(C2)* Spontaneous MUA events in M1 are triggered by forepaw movements (green) from the same recording as in *(C1)*.

(D1) Bar diagram shows the occurrences of FP events which trigger forepaw movements (light blue) and are evoked by forepaw movements (green) in 9 P3-P5 rats. Data are expressed as mean ± s.e.m. *(D2)* Pie diagram shows the percentages of three patterns of activity as in *B* from 990 events in 9 P3-P5 rats during 10 min spontaneously recording.

4.2.3 Microstimulation of layer V neurons in neonatal M1 evokes motor activity

Previous anatomical evidences have proved that, in P0 newborn mice, corticospinal motor neurons located at layer V in motor cortex have already extended the axons to spinal cords (Arlotta et al., 2005;Molyneaux et al., 2007). In adult rat motor cortex, intracellular stimulation and microstimulation of single or population of pyramidal neurons in layer V could evoke whisker movements (Brecht et al., 2004a;Brecht et al., 2004b). It is unknown that whether neuronal activity patterns (gamma ~40 Hz and spindle ~10 Hz bursts) in neonatal M1 have ability to drive early motor activity through corticospinal tracts. A direct way to address this is to check whether the different frequency stimulations through corticospinal tracts have effects on the motor activity. Therefore, we performed intracortical bipolar microstimulation of layer V neurons in M1 with Michigan electrode (**Fig. 24A**). Single pulse stimulation (150 μA, 100 μs) and bursts of twenty pulses at 10 Hz and 40 Hz stimulation were used to induce forepaw movement (**Fig. 24B**). In P3-P5 animals (**Fig 24C1**, n=8 pups), single pulse stimulation to M1 failed to evoke any reliable response, only spontaneous movement occurred randomly as the control condition without stimulation. Interestingly, burst of stimulations at 10 Hz could evoke movement with a significant increase in rate to $36.15 \pm 1.24\%$ than control condition and single pulse stimulation (p<0.001, respectively). The stimulations at 40 Hz were effective to evoke

response with the highest rate (53.55 $\pm$ 2.11 %) than the other parameters of stimulations (**Fig. 24C1**, p<0.001, for comparison against control, single stimulation and 10 Hz stimulation, respectively). Furthermore, we measured the latency of movement responses by 40 Hz burst stimulation (**Fig. 24C2**). The majority of evoked movement responses (43.26 $\pm$ 5.19 %) were induced with a latency of 100-200 ms following the stimulations, which was consistent with the latency of spontaneous movement triggered by spontaneous activity in M1 as in **Fig. 23D**. Together, these results suggest that 40 Hz gamma and 10 Hz spindle bursts of stimulations can induce the early motor activity in newborn rats.
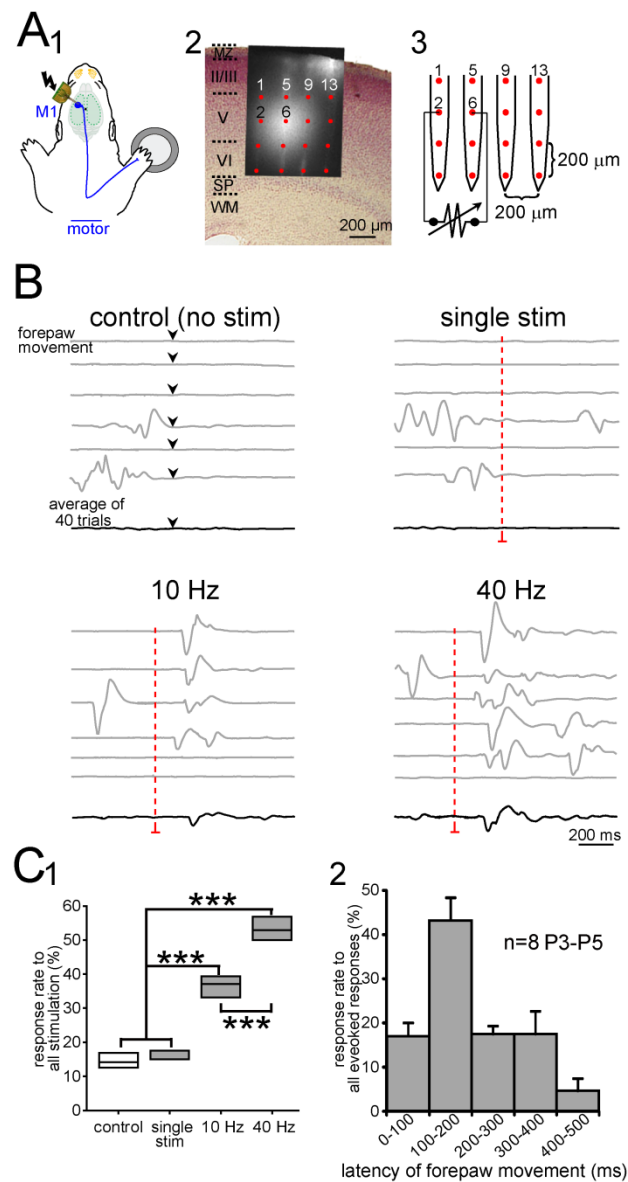
Fig. 24 Microstimulation to layer V in M1 could evoke motor movements in newborn rats.

(A1) Schematic diagram of the experimental setup illustrates microstimulation of forepaw representation in M1 using a four-shank 16-channel electrode and simultaneous detection of forepaw movements. Blue line indicates the motor pathway. *(A2)* Digital photomontage reconstructing the location of the DiI-covered electrode in coronal Nissl-stained section from a P5 rat. MZ, marginal zone; WM, white matter; SP, subplate. *(A3)* A schematic illustration of a four-shank 16-channel Michigan electrode array with neighbouring channels distance of 200 μm. Red points indicate 16 channels as in *A2*. Bipolar electrical stimulations to layer V were applied at channel 2 and 6.

(B) Forepaw motor responses elicited by different electrical microstimulations to layer V in forepaw M1. The control without stimulation only had digital input (black arrow heads) to choose the time point. Single stimulus stimulation indicates the single biphasic current pulses (150 μA, 100 μs duration) were applied to layer V. 10 Hz and 40 Hz stimulations show the forepaw evoked movement by the 20 pulses of stimulations at 10 and 40 Hz respectively. Red dash lines indicate the time point of stimulation. Black arrowheads indicate the time point of digital input. Gray traces are single trials, while the black ones are averaged traces of 40 trials.

(C1) Box plots of response rate to all stimulations were recorded in 8 P3-P5 rats with control condition and different parameters of stimulations. Note that the highest response rate was induced by 40 Hz bursts of stimulations. *(C2)* Bar diagram shows the response rate to all evoked response by 40 Hz stimulation at different latencies obtained from 8 P3-P5 rats. Note that the majority of evoked movement responses were induced with a latency of 100-200 ms. Data are expressed as mean ± s.e.m. Significant differences among different parameters of stimulations and control condition were tested with one-way ANOVA followed by multiple comparisons with Bonferroni correction. Significance levels of $p<0.001$ (***) was identified.

4.2.4 Neuronal activity in neonatal M1 contributes to part of spontaneous motor activity

Furthermore, to investigate the relative contribution of the activity in M1 to the paw movement, we completely blocked the cortical activity locally in M1 by applying the 1% lidocaine. Expectably, not all spontaneous movements were completely abolished after inactivation of M1 (**Fig. 25A**). These left movements might be

triggered by activity from brain stem, spinal cord and spontaneous muscle twitches, as reported previously (Petersson et al., 2003;Blumberg, 2010a;Tiriac et al., 2012). However, the occurrence of spontaneous forepaw movement decreased significantly (p<0.001, n= 7 P3-P5) from 12 ± 0.6 min^{-1} to 8.2 ± 0.5 min^{-1} after blockade of M1 (**Fig. 25B1**). Meanwhile, the duration of movements reduced significantly (p < 0.01, n= 7 P3-P5) from 1.6 ± 0.1 s to 0.99 ± 0.06 s (**Fig. 25B2**). These results are in agreement with (**Fig. 23D2**), suggesting that cortical activity in neonatal M1 commands ~30% of the spontaneous motor activity.
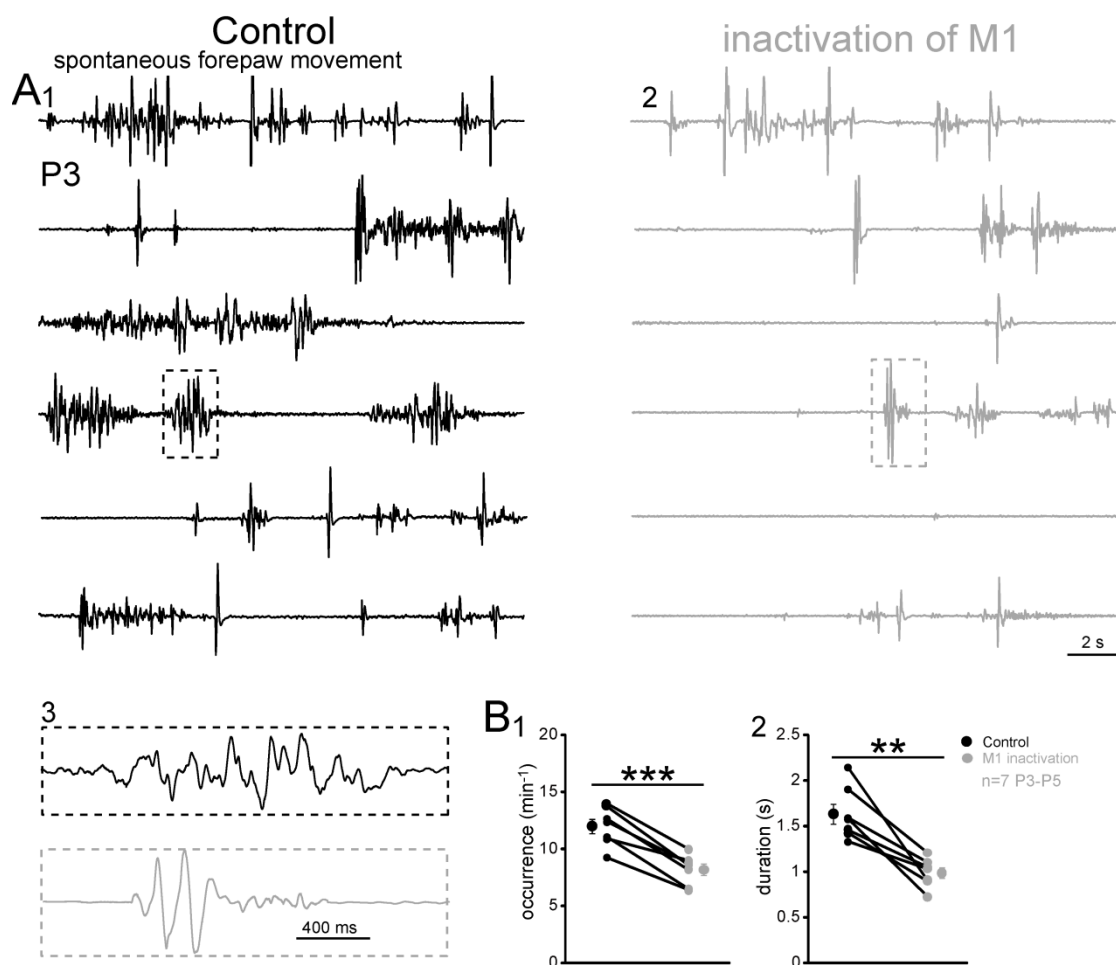
Fig. 25 Effect of the inactivation of M1 on the spontaneous forepaw movement.

(A) 2 min continuous spontaneous forepaw movement detection in a P3 rat under control conditions (*A1*, black) and 20 min after lidocaine (1% in Ringer's solution) application (*A2*, gray). Lower traces show movement traces boxed in the upper panel at higher temporal resolution.

(B) Inactivation of M1 by lidocaine application reduced the occurrence *(B1)* and duration *(B2)* of spontaneous forepaw movement. Small symbols linked by a black line stand for each individual animal. The averaged data (bigger symbols) are expressed as mean $\pm$ s.e.m. Black for control, gray for M1 inactivation. Significant differences between before and after application of lidocaine were tested with paired t-test from 7 P3-P5 pups. Significance levels of p<0.001 (***) and p<0.01 (**) were identified.

4.2.5 Self-generated gamma and spindle bursts occur in M1 in the absence of sensory inputs

Conversely, next I wondered the relative contribution of sensory inputs by spontaneous paw movement to the neuronal activity in M1. To address this question, we blocked the sensory inputs by injecting 3% lidocaine subcutaneously into forepaw. After blockade of sensory periphery, spontaneous gamma and spindle bursts still existed in M1(**Fig. 26A-B**). However, sensory stimulation could not induce any response in both M1 and S1 (**Fig. 26C**). In addition, the occurrence of spontaneous gamma and spindle bursts significantly ($p < 0.001$, n=6 P3-P5) decreased by half (**Fig. 26D**, control, 10.32 ± 1.05 min^{-1}; forepaw inactivation, 5.22 ± 0.48 min^{-1}) in M1 after inactivation of forepaw. These results are in great agreements with the percentage of spontaneous activity in M1 triggered by forepaw movement as in **Fig. 23D**. Similar phenomenon has been observed in S1 by severing the spinal cord (Khazipov et al., 2004), in barrel cortex by blocking the whisker pad (Yang et al., 2009) and in visual cortex by removing the retina (Hanganu et al., 2006). These results demonstrate that sensory periphery inputs trigger 50% of neuronal activity in M1. However, the left endogenous gamma and spindle bursts may be generated by circuits which are intrinsic to the neonatal cortex.
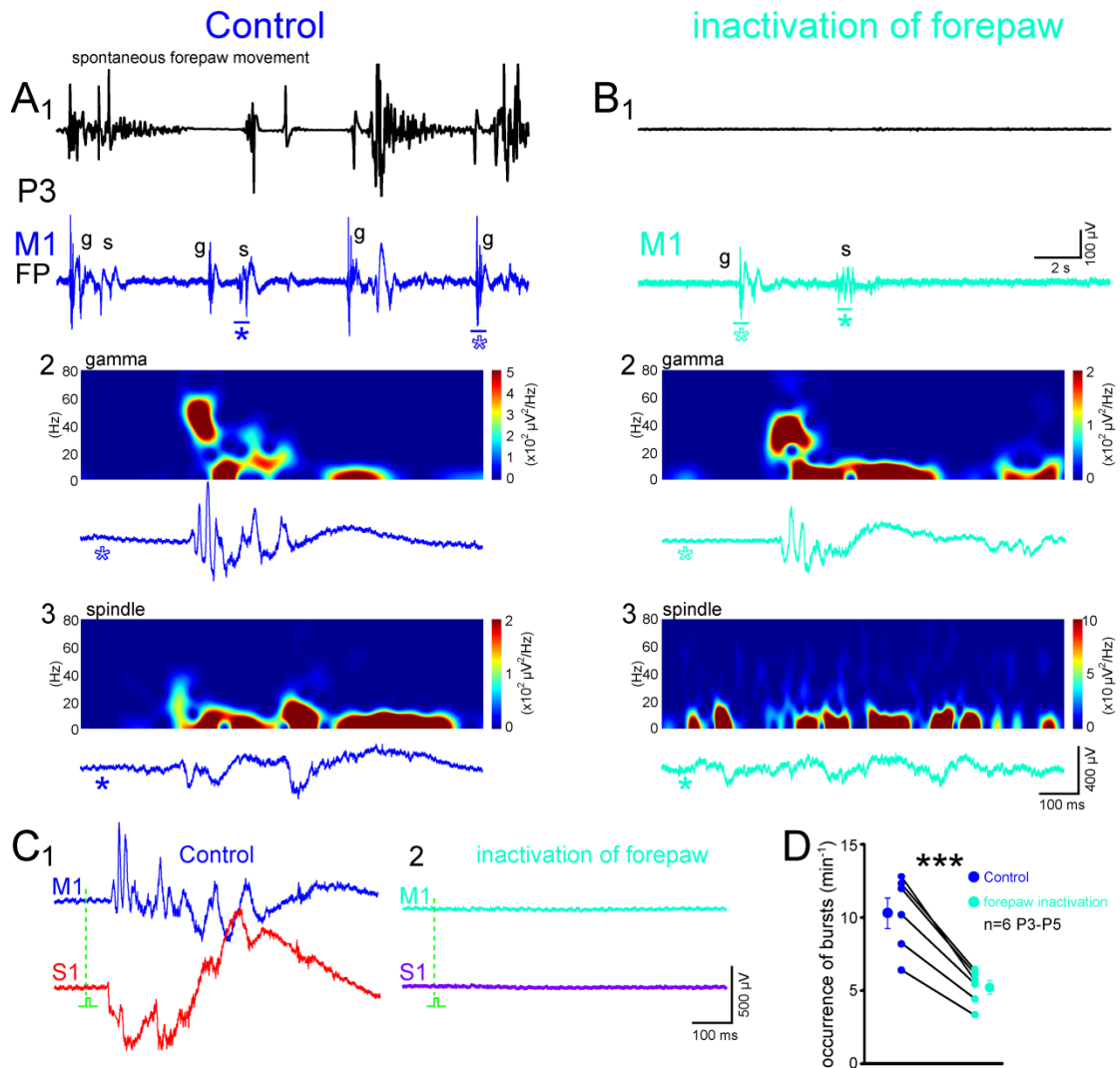
Fig. 26 Effect of blocking peripheral sensory input on the spontaneous neuronal activity in M1.

(A and *B)* 20-s-long recordings from the forepaw M1 area before (*A1*, blue color) and 20 min after (*B1*, light blue color) lidocaine injection in forepaw in a P3 pup. Top traces are the spontaneous forepaw movement detection (black). The down panel traces show the FPs in M1 from the unfiltered raw data. (*A2, 3* and *B2, 3*) Examples of gamma bursts (*A2* and *B2*) and spindle bursts (*A3* and *B3*) displayed at expanded time scale and indicated by asterisks in A1 and B1. In the upper panel, the time series spectrogram was calculated for with a time window of 100 ms and an overlapping of 99 ms from the unfiltered raw data. The bottom traces show the gamma or spindle bursts at expanded time scale before *(A2, 3)* and after *(B2, 3)* application of lidocaine. Note that less gamma (g) and spindle (s) bursts occur in M1 after inactivation of forepaw.

(C) In the same animals as *(A and B)*, sensory evoked gamma and spindle bursts could be induced in both M1 and S1 in the control condition *(C1)*, but not after inactivation of forepaw *(C2)*. Green dash line indicates the time point of sensory stimulus.

(D) Forepaw inactivation reduced the occurrence of spindle and gamma bursts in the forepaw M1 area from 6 P3–P5 pups. Each individual animal was used by small colour symbols (linked by a black line) and averaged data (big symbols) are expressed as mean ± s.e.m. (bigger symbols). Blue for control,

light blue for forepaw inactivation. Significant differences were tested with paired t-test from 6 P3-P5 pups. Significance levels of p<0.001 (***) was identified.

4.2.6 Age-dependent sensory processing in neonatal sensorimotor cortex by bilateral forepaw sensory stimulation

It has been demonstrated that sensory and motor integration is crucial for the execution of voluntary movements (Cascio and Sathian, 2001;Gamzu and Ahissar, 2001;Macaluso and Driver, 2005;Blumberg, 2010a;Koziol et al., 2011). Sensory information is used to refine motor control (Izraeli and Porter, 1995;Deschenes et al., 1998;Hoffer et al., 2003;Alloway et al., 2004). Therefore, I further investigated the sensory processing signals from S1 to M1. I did simultaneously multi-electrode recording in S1 and M1 (**Fig. 27A**) by placing the same type of electrode as in **Fig. 22A4** in the centres of forepaw representations in S1 and M1 (**Fig. 27B**). In P3–P5 rats, a single mechanical stimulation of right forepaw could elicit the earliest spindle bursts in the contralateral S1 (**Fig. 27B1**). Approximately 8 ms later, gamma followed by spindle bursts were triggered in the contralateral M1 (**Fig. 27B1**) with significantly smaller (p < 0.05, than S1) amplitude (1.92 $\pm$ 0.21 mV), longer latency (51.32 $\pm$ 1.17 ms) and shorter duration (1.03 $\pm$ 0.16 s) but without significant difference (n=12, **Fig. 27C**). These results are comparable to the evoked responses in the sensorimotor cortex by VSDI recording as in **Fig. 22D**. Similarly, left forepaw could also induce evoked responses in the ipsilateral S1 and M1. However, compared with the evoked responses in the contralateral sensorimotor cortex, these responses in ipsilateral sensorimotor cortex (**Fig. 27C**) had significantly smaller (p < 0.001, against contralateral S1 and M1, respectively) amplitude (0.40 $\pm$ 0.05 mV-ipsilateral S1, 0.41 $\pm$ 0.05 mV-ipsilateral M1), considerably longer (p < 0.001, against contralateral S1 and M1, respectively) latency (92.81 $\pm$ 4.42 ms-ipsilateral S1, 84.58 $\pm$ 4.32 ms-ipsilateral M1) and dramatically shorter (p < 0.001, p < 0.01, against contralateral S1 and M1, respectively) duration (0.19 $\pm$ 0.02 s-ipsilateral S1, 0.20 $\pm$ 0.02 s-ipsilateral M1). The similar phenomenon has been only reported in neonatal somatosensory cortex by EEG (Marcano-Reik and Blumberg, 2008) and VSDI

(Mcvea et al., 2012) recordings. These results are also in general agreement with the anatomical development of the callosal projection neurons across the corpus callosum (CC) during this age period (Molyneaux et al., 2007;Alcamo et al., 2008;Fishell and Hanashima, 2008;Sohur et al., 2012).

To address the question of whether similar evoked responses by bilateral forepaw stimulation can be also observed in younger animals, I studied sensory evoked response at P0-P1. In P0-P1 rats), forepaw stimulation could evoke the response first in the contralateral S1 (**Fig. 27B2**). Over about 11 ms, then gamma bursts were induced in the contralateral M1 (**Fig. 27B2**) cortex with significantly smaller ($p < 0.05$) amplitude (1.28 ± 0.28 mV), significantly longer ($p < 0.05$) latency (82.45 ± 11.58 ms) and significantly shorter ($p < 0.05$) duration (0.44 ± 0.03 s) compared with the response in S1 (n=6, **Fig. 27C**). However, no response could be elicited in ipsilateral S1 and M1anymore (**Fig. 27B2**).

These data demonstrate that contralateral sensorimotor cortex has the reliable cortical responses by forepaw sensory stimulation as early as P0. Furthermore, forepaw sensory stimulation can induce reliable cortical responses in ipsilateral sensorimotor cortex until P3.
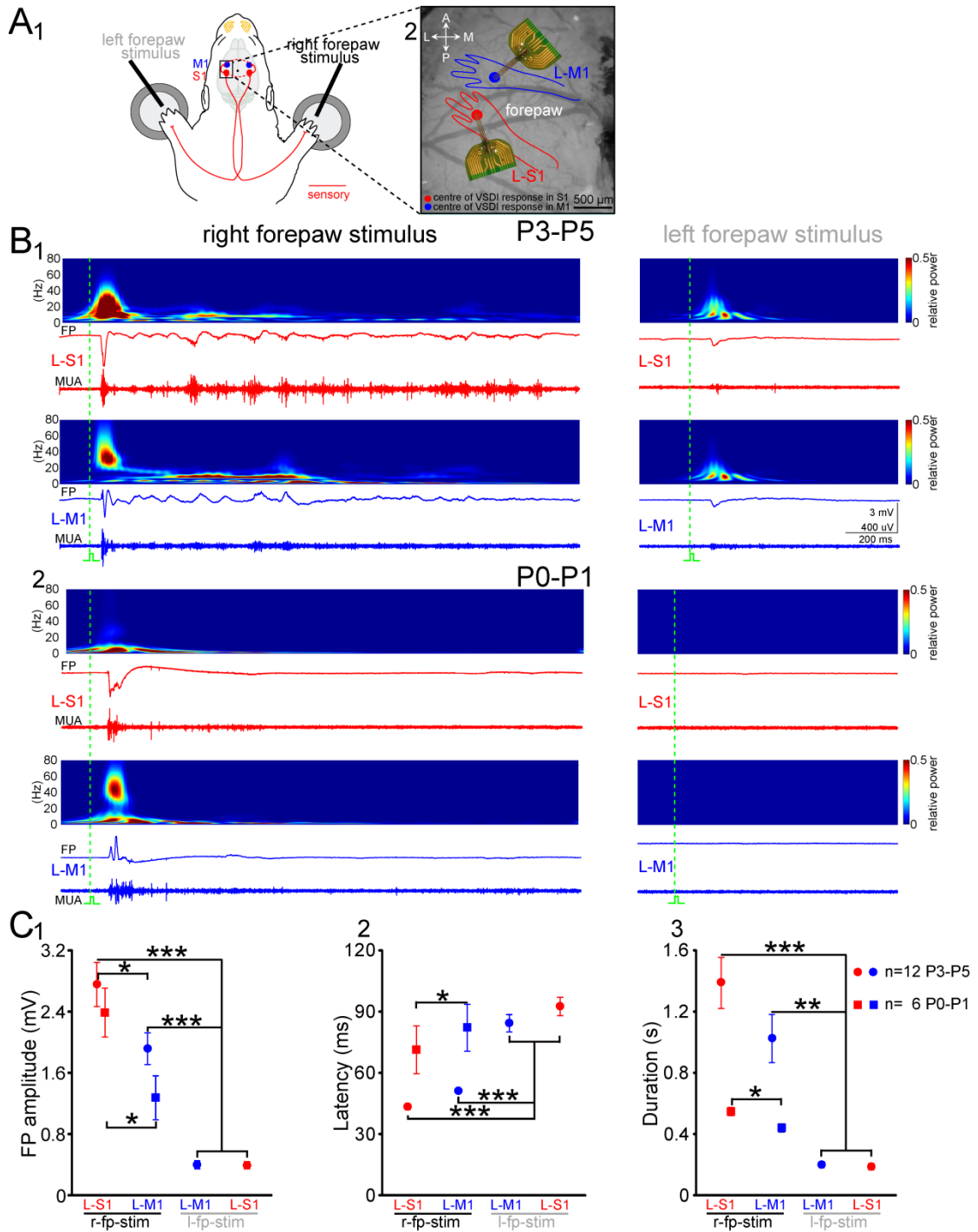
Fig. 27 Sensory evoked response in both S1 and M1 by mechanical stimulation in bilateral forepaw from newborn rats.

(A) Schematic diagram of the experimental setup illustrating selective sensory mechanical stimulation of bilateral forepaws attached to movement detectors *(A1)* and simultaneous multi-electrodes recording in S1 and M1 on the left hemisphere cortex *(A2)*. Red traces in *(A1)* stand for the sensory input pathway. *(A2)* The exposed cortex includes the S1 (red diagram) and M1 (blue diagram) cortex of

contralateral forepaw representations. The red and blue dots indicate the centre of VSDI evoked response in S1 and M1 respectively. L-S1, left-S1; L-M1, left-M1; A, anterior; L, lateral; P, posterior; M, medial.

(B1) In a P4 rat, right forepaw stimulation evoked gamma bursts in left M1and spindle burst in left S1, left forepaw stimulation also evoke responses in both left S1 and M1 but with long latency and small amplitude. The middle wavelet analysis calculated from the unfiltered raw data. The bottom traces show FP from unfiltered raw data and MUA in a high-pass filtered (>200 Hz) trace. Red traces represent activity from left S1, blue traces indicate activity from left M1. Green dash line indicates the time point of sensory mechanical stimulus. *(B2)* The similar experiment as *(B1)*, but from a P1 rat. Right forepaw stimulation evoked gamma bursts in left M1and spindle burst in left S1, while left forepaw stimulation failed to evoke any response in both left S1 and M1.

(C) Statistical analysis of peak to peak FP amplitude *(C1)*, onset latency *(C2)*, and duration *(C3)* of both right and left forepaws evoked responses in P3-P5 (dots, n=12 pups) and P0–P1 (squares, n=6 pups) rats. Red indicates data from left S1, blue indicates data from left M1. r-fp-stim, right forepaw stimulation; l-fp-stim, left forepaw stimulation. Data are expressed as mean ± s.e.m. Significant differences between S1 and M1 by bilateral forepaw stimulations at P3-P5 were tested with one-way ANOVA followed by multiple comparisons with Bonferroni correction. Significant differences between S1 and M1 at P0-P1 were performed with Mann–Whitney–Wilcoxon test. Significance levels of $p<0.001$ (***), $p<0.01$ (**) and $p<0.05$ (*) were identified.

4.2.7 Sensory processing gamma and spindle bursts in M1 depend on S1

Next, to study the relation of sensory evoked responses between S1 and M1, we compared FPs and corresponding MUA between contralateral S1 and M1 as in **Fig 27**. The FP and MUA to single forepaw stimulation recorded in newborn rat sensorimotor cortex consisted of early and late components (**Fig. 28A**), as described previously in visual cortex (Colonnese et al., 2010) and barrel cortex (Yang et al., 2012). In the early component, the autocorrelation of MUA showed peaks at ~25 ms, which indicated ~40Hz gamma band activity in M1, but not in S1 (**Fig. 28B1-2**). Moreover, the MUA in S1 preceded the MUA in M1 (**Fig. 28B3**), which was in agreement that

sensory stimulation evoked response in S1 was ~8 ms earlier than the response in M1 as in **Fig. 22D1** and **Fig. 27C2**. In the late component, the autocorrelation and crosscorrelation of MUA in both S1 and M1 showed peaks at ~100 ms, which indicated ~10Hz alpha band spindle bursts activity (**Fig. 28B4-5**). Then we quantified the spectrum of FP , MUA , coherence of FP versus MUA during early and late periods of evoked responses in both S1 and M1 (292 evoked events in 12 P3-P5 pups). During the early period, the spectrums of FP and MUA revealed a clear peak at the frequency of ~10 Hz, which was also evident in the coherence plot of the FP versus MUA (**Fig. 28C1-3**) in S1. However, in M1, the FP spectrum, MUA spectrum and coherence of FP versus MUA all showed a peak at a higher frequency of ~40 Hz (**Fig. 28D1-3**). During the late period, the spectrums of FP, MUA and coherence of FP versus MUA exhibited a peak at similar frequency of ~10 Hz in both S1 (**Fig. 28C4-6**) and M1 (**Fig. 28D4-6**). These data suggest that gamma and spindle bursts are the electrophysiological activity patterns in neonatal M1, while only spindle bursts are in S1. Gamma and spindle bursts mediate the interaction between S1 and M1 following the sensory stimulations. The sensory activity in S1 precedes the activity in M1.
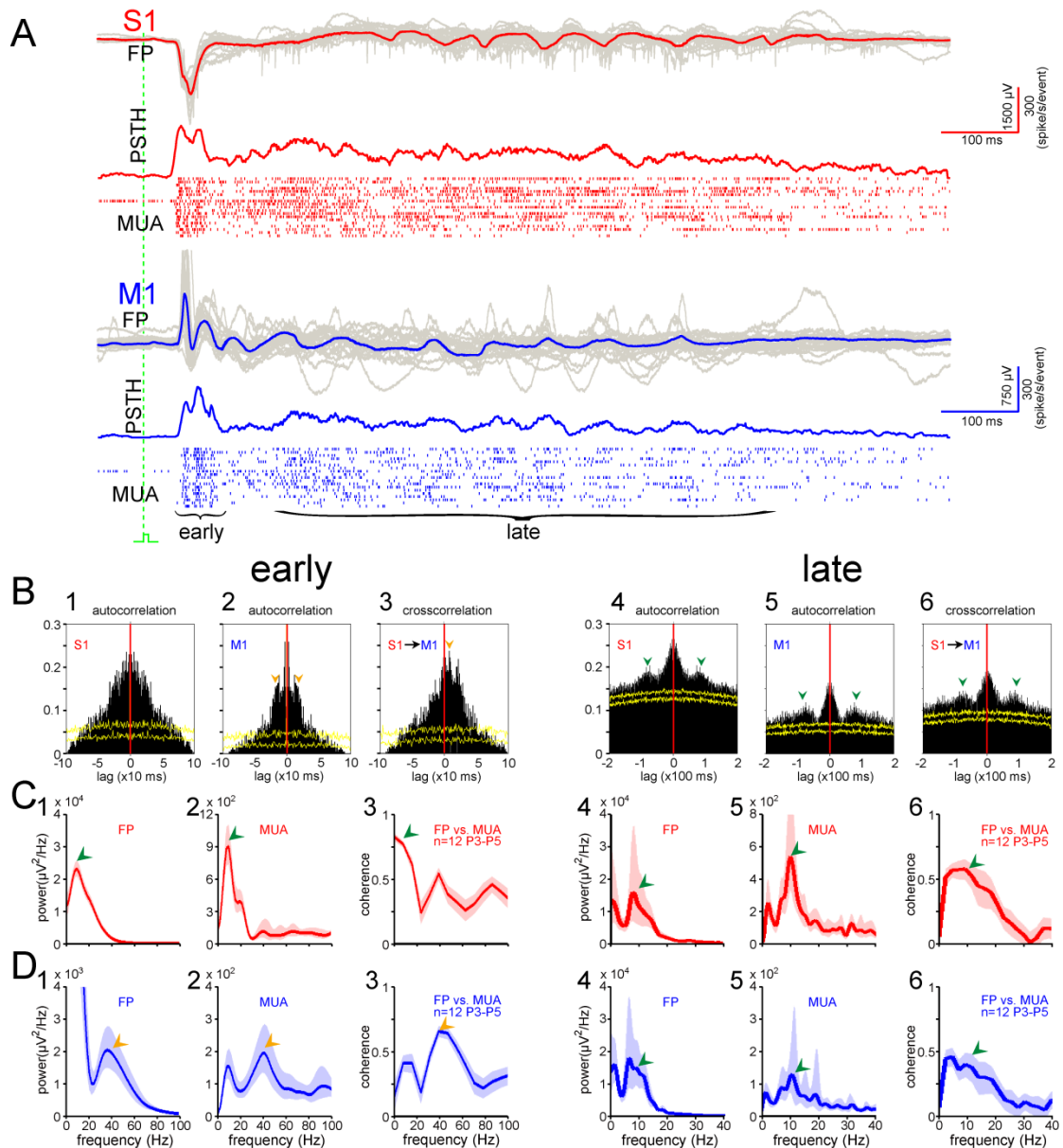
Fig. 28 Sensory processing gamma and spindle bursts mediate interactions between S1 and M1.

(A) Summarised FP (top traces), corresponding PSTH (middle traces) and multi-unit (bottom dots) recordings of forepaw sensory evoked responses simultaneously in both S1 and M1 from a P4 rat. Averaged (red and blue traces) and superimposed 20 single (gray traces) cortical FP responses of 20 succeeding forepaw stimulations. Note the presence of gamma bursts in the early response in M1 and spindle bursts in the late response in both S1 and M1 in the FP and MUA. Green dash line indicates the time point of sensory stimulus.

(B) Autocorrelation and crosscorrelation analyses of early *(B1-3)* and late *(B4-6)* MUA in S1 and M1 from data marked by curly brackets in *(A)*. In the early response, note that ~ 25 ms peaks (yellow arrowheads) exist in the autocorrelation of M1 MUA but not in S1 MUA and that the S1 MUA precedes M1 MUA (yellow arrowheads). In the late response, note ~ 10 ms peaks (green arrowheads) in both autocorrelation and crosscorrelation of S1 and M1 MUA. Yellow traces stand for predictor.

(C) Average spectrum of FP and MUA analysed of early evoked responses *(C1-2)* and late evoked response *(C4-5)* in S1 from *(A)*. Average coherence of FP versus MUA during early *(C3)* and late *(C6)* from 292 forepaw sensory evoked responses recorded in 12 P3-P5 rats. Red traces show averages, the shaded area represents the 95% CI. Note the ~ 10 Hz peaks (green arrowheads) in spectrums of FP and MUA and coherence of FP versus MUA in both early and late evoked responses.

(D) The similar analyses as in *(C)*, but from simultaneous recording in M1 (blue). Note that ~ 40 Hz peaks (yellow arrowheads) in the early evoked responses *(D1-3)* and ~ 10 Hz peak (green arrowheads) in the late evoked responses *(D4-6)* at both spectrums and coherences of FP and MUA.

Furthermore, in order to directly address the question of whether S1 plays a critical role in generating sensory evoked gamma and spindle bursts in M1, we blocked S1 by applying 1% lidocaine locally in S1. Then we analyzed the functional effects of local inactivation of S1 on the expression of sensory-evoked gamma and spindle bursts in M1 at P3-P5 (n=6 pups). In the presence of lidocaine, sensory stimulation could not evoke MUA activity in S1 anymore (**Fig. 29A-B**). Meanwhile, only weak sensory-evoked responses were induced in the M1 (**Fig. 29B**). We compared the FP and MUA responses obtained before with these after the local S1 inactivation (**Fig. 29C**). In the early component of evoked response in M1, corresponding to the gamma bursts phase, the average number of spikes and the gamma spectrum power (20-60 Hz) of FP and MUA, significantly ($P<0.01$, for spike number, FP- spectrum, MUA- spectrum, respectively) decreased from 350 ± 27 (spike number), $24.99 \pm 5.91 \times 10^3\%$ $\mu V^2/Hz$ (FP - spectrum), $2.96 \pm 0.24 \times 10^3\%$ $\mu V^2/Hz$ (MUA - spectrum) to 83 ± 17 (spike number), $6.31 \pm 2.6 \times 10^3\%$ $\mu V^2/Hz$ (FP - spectrum), $0.92 \pm 0.15 \times 10^3\%$ $\mu V^2/Hz$ (MUA - spectrum), respectively (**Fig. 29D1-3**). Similarly, In the late component of evoked response in M1, corresponding to the spindle bursts phase, the average number of spikes and the spindle spectrum (0-20 Hz) also significantly ($P<0.01$, $P<0.05$, $P<0.01$ for spike number, FP - spectrum, MUA -

spectrum, respectively) reduced from 331 ± 61 (spike number), $58.43 \pm 11.12 \times 10^3$% μV^2/Hz (FP - spectrum), $2.11 \pm 0.45 \times 10^3$% μV^2/Hz (MUA - spectrum) to 21 ± 8 (spike number), $23.61 \pm 3.2 \times 10^3$% μV^2/Hz (FP - spectrum), $0.19 \pm 0.12 \times 10^3$% μV^2/Hz (MUA - spectrum), respectively (**Fig. 29D4-6**). In summary, these results demonstrate that S1contributes dramatically to the sensory processing gamma and spindle bursts in M1.
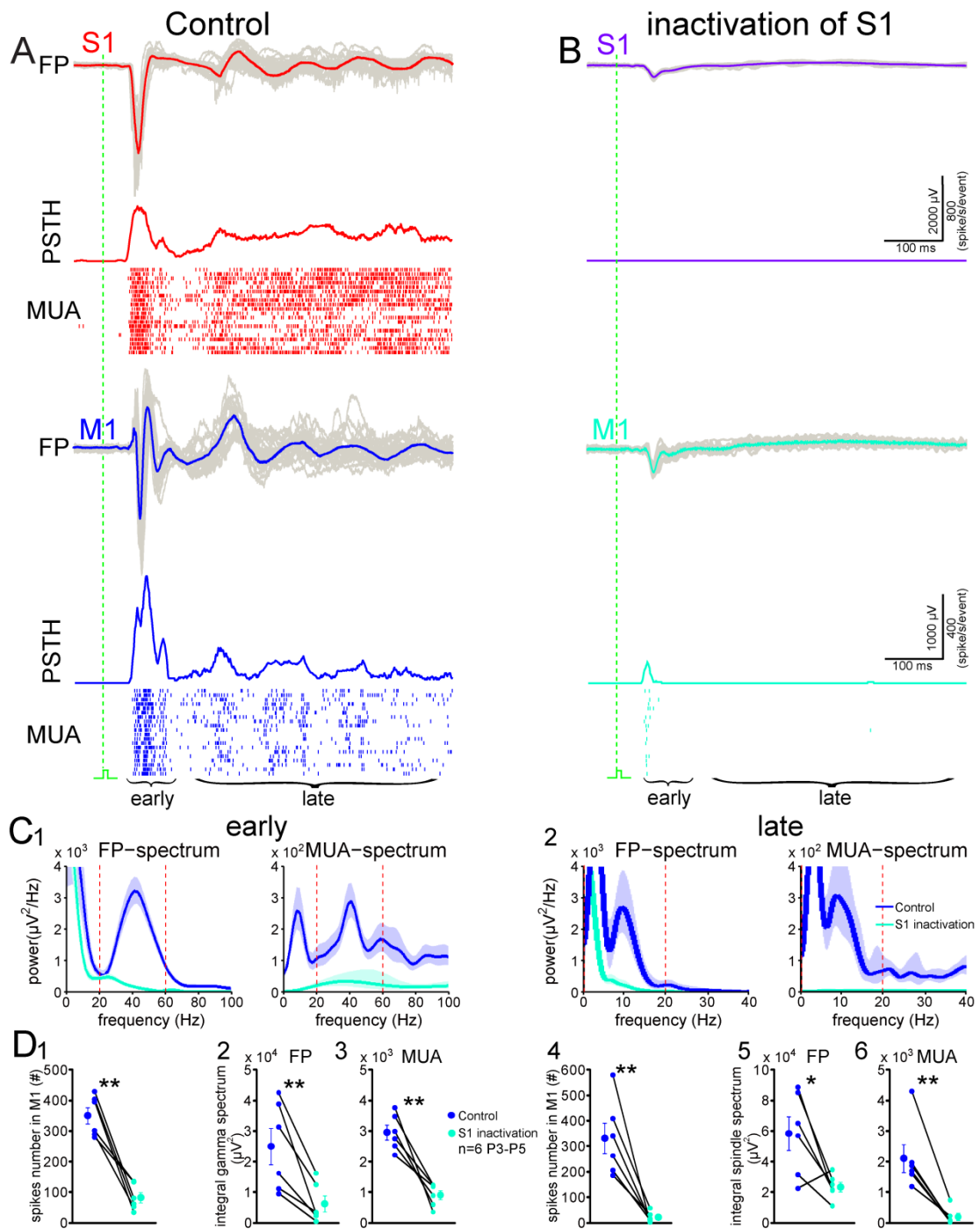
Fig. 29 Sensory processing gamma and spindle bursts in M1 depend on activity in S1.

(A) Summarised FP (top traces), corresponding PSTH (middle traces) and multi-unit (bottom dots) recordings of forepaw sensoryevoked responses in the sensorimotor cortex in control condition from a P4 rat. Averaged (red and blue traces) and superimposed 20 single (gray traces) cortical FP responses of 20 succeeding forepaw stimulations. Note the presence of gamma bursts in the early response in M1 and spindle bursts in the late response in both S1 and M1 in the FP and MUA. Green dash line indicates the time point of sensory touch stimulus.

(B) The same experiment as *(A)*, but 20 min after application of lidocaine in S1. Note that there is no MUA in S1 (purple) and that FP and MUA in M1 (light blue) decrease dramatically in both early and late response.

(C) Average FP-spectrum and MUA-spectrum analyses of early evoked responses *(C1)* and late evoked responses *(C2)* recorded in control condition (blue) and after blocked S1 (light blue) from events marked by curly brackets in *(A-B)*. Blue and light blue traces show averages, the shaded area represents the 95% CI. Note that both ~ 40 Hz gamma burst in the early response and ~ 10 Hz spindle burst in the late response was partly or completely blocked after inactivation of S1.

(D) Statics analyses of the number of spikes and integral gamma (20-60 Hz, red dash lines as in *C1*) or spindle (0-20 Hz, red dash lines as in *C2*) spectrum of FP and MUA in M1 from 6 P3-P5 pups during early (left) and late (right) periods. Note the massive decreases in the spikes number, integral gamma and spindle spectrum of FP and MUA in M1 after block S1. Data are expressed as mean ± s.e.m. Significant differences were tested with paired t-test from 6 P3-P5 pups. Significance levels of p<0.01 (**) and p<0.05 (*) were identified.

4.2.8 Spontaneous occurring gamma and spindle bursts in M1 depend on S1

Having proved that S1 contributes to sensory-evoked gamma and spindle bursts in M1, we next continued to investigate the functional role of S1 in spontaneous activity of M1. In total 448 spontaneous events both in S1 and M1 from 9 P3-P5 animals, 43.53% of them were gamma bursts (n=195) in M1 and the corresponding activity in S1, the left 56.47% events were spindle bursts (n=253) generating simultaneously both in M1 and S1 (**Fig. 30A-C**). Similar to the evoked responses, at P3-P5, the power spectrum analyses of the spontaneous gamma bursts activity in M1 also showed a prominent peak at ~ 40 Hz in FP and MUA recording (**Fig. 30D1-2**), but not in S1 (**Fig. 30E1-2**). Furthermore, the coherence plot of FP versus MUA recordings in M1, which reflects the synchronization of spikes, exhibited a clear peak at ~ 40 Hz (n=9 pups, **Fig. 30D3**), however, not in S1 (**Fig. 30E3**). In addition, the power spectrum and coherence analyses of the spontaneous spindle bursts activity exhibited a prominent peak at ~ 10 Hz not only in M1 but also in S1(**Fig. 30D4-6, E4-6**). However, the spontaneously occurring bursts activity recorded in both M1 and S1 were different from the sensory-evoked responses in other parameters. The spontaneously occurring activity in M1 had a significantly smaller amplitude (1.06 ± 0.09 mV, p < 0.001) and shorter duration (0.45 ± 0.04 s, P < 0.001) than the sensory-evoked responses (1.92 ± 0.21 mV, amplitude; 1.03 ± 0.16 s, duration;

respectively, data not shown). In S1, similarly, both the amplitude (1.13 $\pm$ 0.12 mV, p < 0.001) and duration (1.06 $\pm$ 0.09 s, P < 0.01) of the spontaneously occurring activity were significantly smaller and shorter respectively, compared with the sensory-evoked responses (2.76 $\pm$ 0.29 mV, amplitude; 1.92 $\pm$ 0.21 s, duration; respectively, data not shown). Although these differences, these results suggest that spontaneously occurring gamma and spindle bursts in M1 are closely linked to the activity patterns in S1. Moreover, the neuronal activity patterns in both S1 and M1 may mediate the interaction between them.
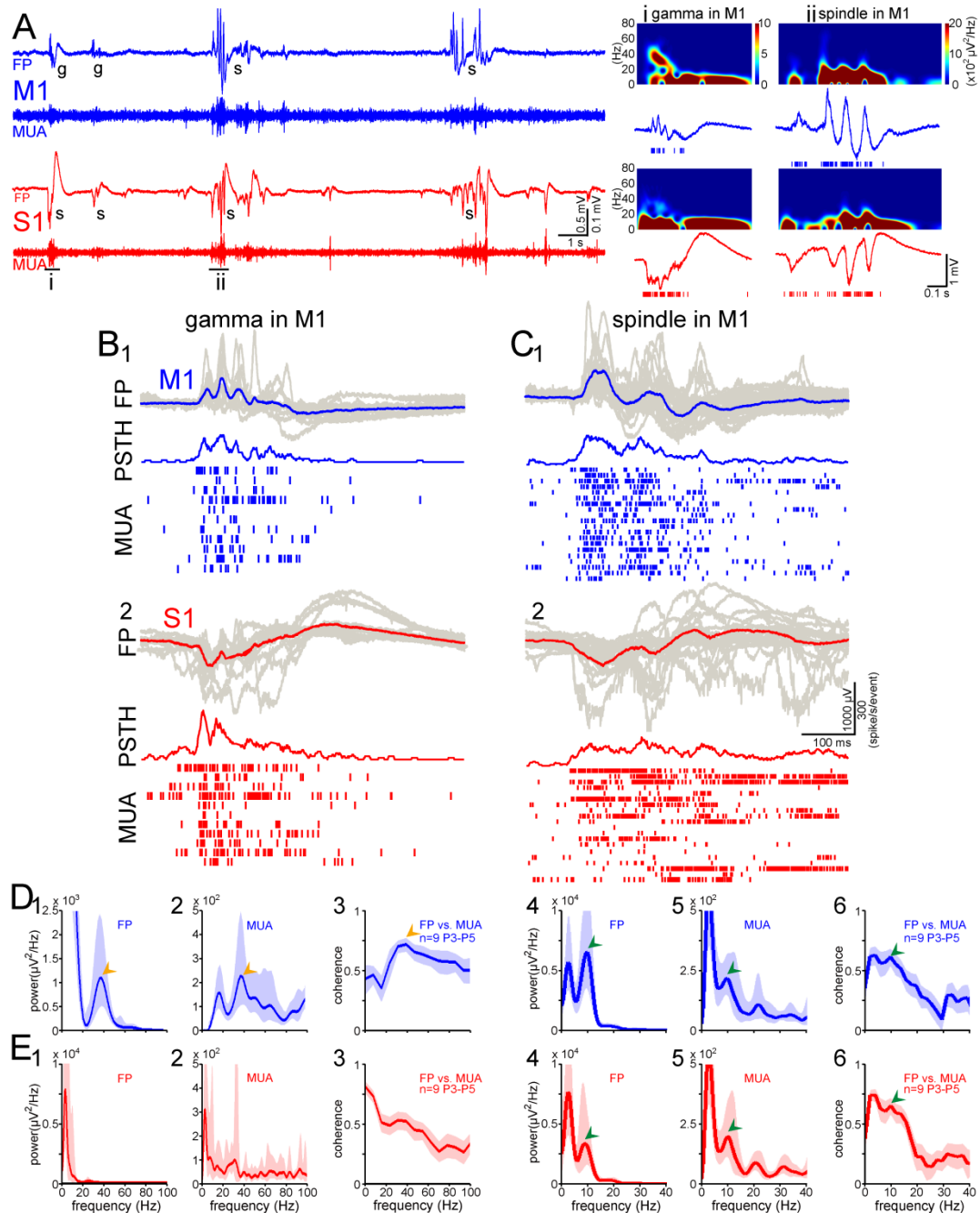
Fig. 30 Spontaneous gamma and spindle bursts mediate interaction between S1 and M1.

(A) 20 s simultaneous recording of spontaneous activity in both M1 (blue) and S1 (red) from a P3 rat. Note that most of spontaneous activities in S1 and M1 are synchronized. The events marked by i-ii on the left are shown higher resolution with corresponding spectrograms on the right. Blue and red bars at the bottom represent MUA in M1 and S1 respectively.

(B) Summarised FP (top traces), corresponding PSTH (middle traces) and multi-unit (bottom dots) recordings of spontaneous activity in M1 and S1 from the same experiment as in *(A)*. Averaged (blue trace) FP from 11 superimposed single (gray traces) spontaneous gamma bursts in M1 *(B1)* and simultaneously recording activity in S1 *(B2)*. The recordings from M1 and S1 were aligned to the onset of the M1 FP events. Note gamma bursts in M1 PF and PSTH but not in S1.

(C) The same experiment as in *(A)*, but only analyses of 20 spindle bursts in M1 and corresponding spindle bursts in S1. Note spindle bursts in both M1 and S1 FP and PSTH.

(D) Average spectrum of FP and MUA analyses of gamma *(D1, 2)* and spindle bursts *(D4, 5)* recorded in M1 (blue) from events shown in *(B1-C1)*. An averaged coherence analyses of 195 spontaneous gamma *(D3)* and 253 spindle *(D6)* bursts (FP events versus MUA) recorded in M1 from 9 P3–P5 rats. Blue traces show averages, the shaded area represents the 95% CI. Note that both ~ 40 Hz peak (yellow arrowheads) activity in the averaged gamma bursts and ~ 10 Hz peak (green arrowheads) in the averaged spindle burst response.

(E) The similar analyses as in *(D)*, but from simultaneous recording activity in S1 (red). Note that ~ 10 Hz peak (green arrowheads) in the averaged spindle burst response.

Finally, to directly address the question whether the generation of spontaneously occurring activity patterns in M1 depends on S1, we quantified the functional effects of local inactivation of the S1 on the spontaneous gamma and spindle bursts in the M1 at P3-P5 (n=6 pups). Similar to the evoked response as in **Fig 29B**, spontaneous activity in S1 were completely abolished (data not shown), while less and weak activity occurred spontaneously in M1 (**Fig. 31A, B**) after inactivation of S1. We compared the spike number, the FP and MUA spectrums in M1 before with these after the local blockade of S1 (**Fig. 31C-D**). In the gamma bursts activity, the average number of spikes and the gamma spectrum power (20-60 Hz) of both FP and MUA, significantly ($P<0.01$, $P<0.001$, $P<0.001$ for spike number, FP-spectrum, MUA-spectrum, respectively) decreased from 409 ± 61 (spike number), 9.64 ± 1.29 $\times 10^3$% μV^2/Hz (FP - spectrum), 2.51 ± 0.23 $\times 10^3$% μV^2/Hz (MUA - spectrum) to 115 ± 38 (spike number), 0.25 ± 0.09 $\times 10^3$%μV^2/Hz (FP - spectrum), 0.43 ± 0.19 $\times 10^3$% μV^2/Hz (MUA - spectrum), respectively (**Fig. 31D1-3**). Similarly, in the spindle burst activity, the average number of spikes and the spindle spectrum (0-20 Hz) also significantly ($P<0.001$, $P<0.01$, $P<0.05$ for spike number, FP - spectrum, MUA - spectrum, respectively) reduced from 647 ± 91 (spike number), 27.66 ± 6.45 $\times 10^3$% μV^2/Hz (FP - spectrum), 3.61 ± 0.87 $\times 10^3$% μV^2/Hz (MUA - spectrum) to 84 ± 29 (spike number), 7.76 ± 2.57 $\times 10^3$%μV^2/Hz (FP - spectrum), 0.44 ± 0.18 $\times 10^3$% μV^2/Hz (MUA - spectrum), respectively (**Fig. 31D4-6**). In summary, these results demonstrate that S1 played a critical role in generation of spontaneous gamma and spindle bursts in M1.
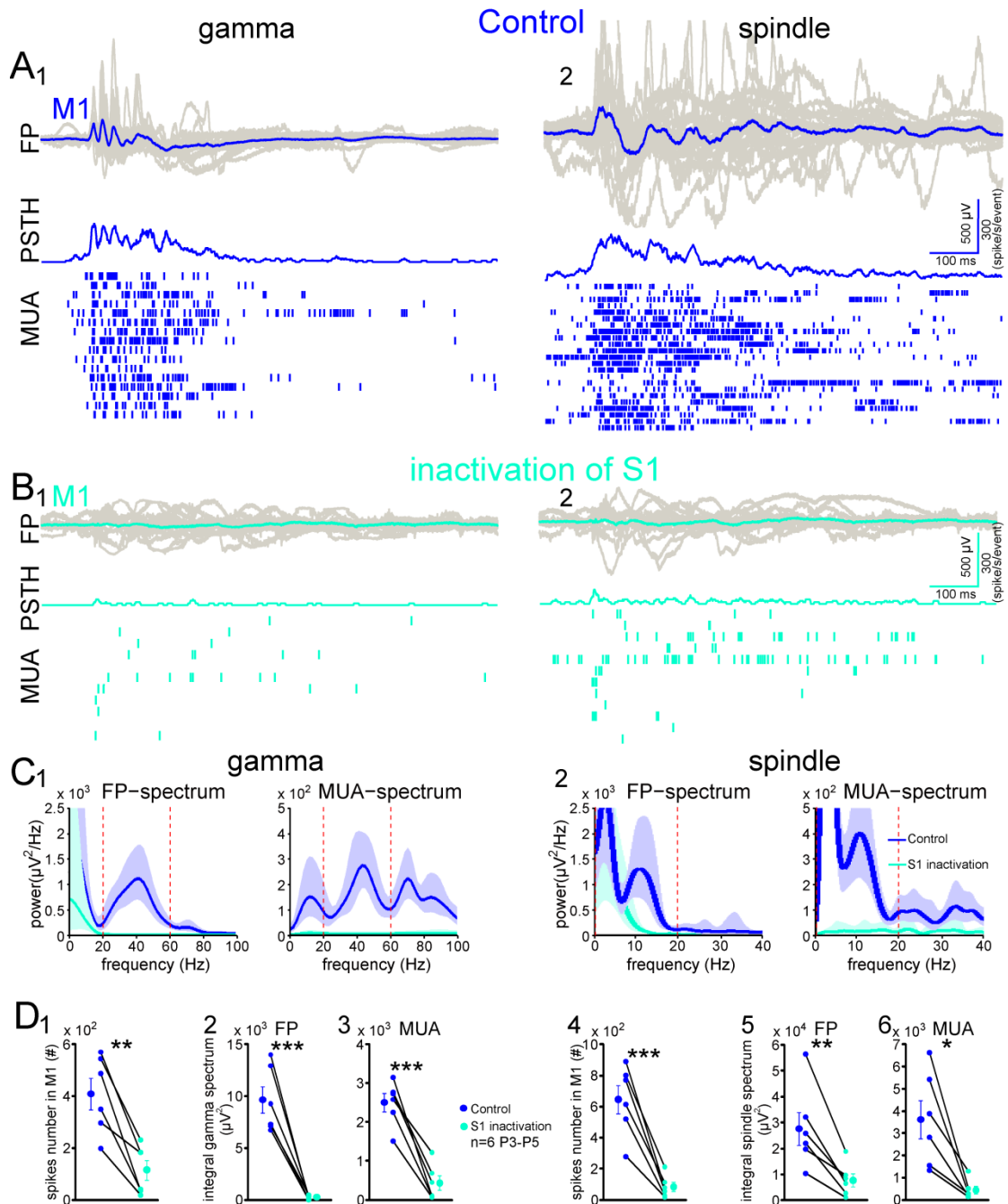
Fig. 31 Spontaneous gamma and spindle bursts in M1 depend on activity in S1.

(A) Summarised FP (top traces), corresponding PSTH (middle traces) and multi-unit (bottom dots) recordings of spontaneous activity in M1 from a P3 rat. Averaged gamma *(A1)*, spindle *(A2)* and superimposed single events (gray traces) cortical FP responses in control condition (blue).

(B) The FP and PSTH were from the same channels of the experiment as in *(A)*, but 20 min after application of 1% lidocaine in S1 (light blue). Note that gamma *(B1)* and spindle bursts *(B2)* in the FP and PSTH from M1 were completely blocked after inactivation of S1.

(C) Average FP-spectrum and MUA-spectrum analyses of gamma *(1)* and spindle bursts *(2)* recorded in control condition (blue) and after blocked S1 (light blue) from events shown in *(A-B)*. Blue and light blue traces show averages, the shaded area represents the 95% CI. Note that both ~ 40 Hz gamma burst and ~ 10 Hz spindle burst were partly or completely blocked after inactivation of S1.

(D) Statics analyses of the number of spikes and integral gamma (20-60 Hz, red dash lines as in *C1*) or spindle (0-20 Hz, red dash lines as in *C2*) spectrum of FP and MUA in M1 from 6 P3-P5 pups during early (left) and late (right) periods. Note the massive decreases in the spikes number, integral gamma and spindle spectrum of FP and MUA in M1 after block S1. Data are expressed as mean $\pm$ s.e.m. Significant differences were tested with paired t-test from 6 P3-P5 pups. Significance levels of p<0.001 (***), p<0.01 (**) and p<0.05 (*) were identified.
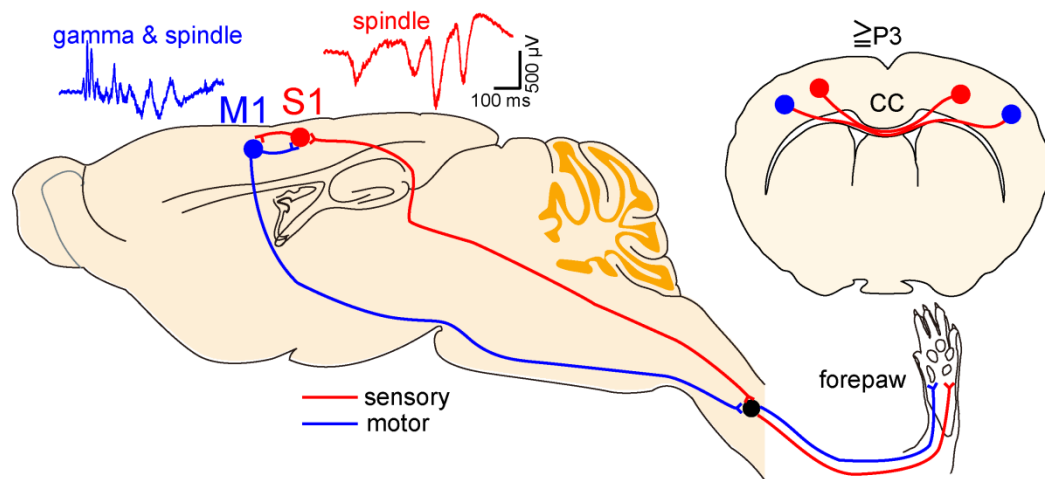
Fig. 32 Proposed sensorimotor integration model.

Schematic drawing of sensory (red) and motor (blue) pathways from the forepaw to the cortex.

5 Discussion

5.1 Project 1

We show here for the first time that physiologically relevant stimulation of the whisker to barrel cortex pathway induces in newborn rats *in vivo* a prominent LTP of the thalamocortical synaptic input. This LTP is the strongest in P3-P5 rats, weaker in P0-P1, P6-P7 animals and disappears at P8-P14. Morover, LTP is confined to the stimulated cortical barrel-related column and adjacent septa. Our observations are in good agreement with previous *in vitro* reports on the age-dependent expression of LTP in the thalamocortical slice preparations of the newborn rats (Crair and Malenka, 1995). The authors reported a gradual decrease in the magnitude of LTP from P3 to P7, while no LTP could be induced in P8-P14 animals. Furthermore our data also demonstrate that the magnitude of LTP is weaker in P0-P1 when compared to the P3-P5 age group. These results demonstrate for the first time that the whisker-to-barrel cortex pathway *in vivo* may undergo activity-dependent modifications during earliest stages of postnatal development. Our data also indicate that the *in vitro* slice preparation is a valuable model to study activity-dependent modifications in immature cortex. However, as we did not record whisker evoked synaptic responses in the trigeminal nuclei or thalamus, no conclusion about the exact site of synaptic potentiation can be drawn from these results.

5.1.1 Physiological correlations of 2 Hz whisker stimulation

Using a very similar stimulation protocol (2 Hz for 15 min) as in our study (2 Hz for 10 min), Liu et al. (Liu et al., 2004) could elicit in visual cortical slices of adolescent rats a stable LTP with a time-course comparable to our observations in newborn rat barrel cortex *in vivo*. In 3-6 months old mice, 2 or 8 Hz multi-whisker stimulation for 10 min induced in layers IV and II/III of the barrel cortex *in vivo* a stable LTP to 195% and 163%, respectively (Megevand et al., 2009), demonstrating that under this experimental condition a prominent LTP can be elicited even in adult

animals. In addition, 2 Hz is one of the dominant frequencies adult rats use for active whisking (Carvell and Simons, 1990), although active whisking is absent in early postnatal rats (for review Hanganu-Opatz, 2010). However, in preterm infants, so-called delta brush patterns during the slow activity transients (SATs) in the EEG, which consist of 1-3 Hz delta waves, play an important role in normal brain development (Khazipov and Luhmann, 2006). Therefore we propose that stimulation at 2 Hz might have some physiological correlates that are suitable to modify the synaptic plasticity in the whisker-to-barrel cortex pathway. Accordingly, we were able to potentiate this pathway with a 2 Hz single whisker stimulation already during earliest postnatal development *in vivo*.

5.1.2 Spatial and layer-specific expression of LTP

Our *in vivo* data provide strong evidence that only synaptic input to the activated barrel-related column and to a lesser extent the surrounding septal region are modified. In P3-P7 rats, it can be assumed that the thalamus-to-layer IV and lower layer II/III synapse undergoes activity-dependent changes following whisker stimulation and CSD data in the P3-P5 age group are fully compatible with this hypothesis. The situation is more complicate in P0-P1 animals since layer II/III and probably layer IV have not been formed at this early age. In somatosensory cortex of newborn rodents (Hanganu et al., 2002;Molnar et al., 2003), the thalamic input innervates the subplate (for review Luhmann et al., 2009;Kanold and Luhmann, 2010) and an activity-dependent modification of this transient synaptic connection in newborn rat *in vivo* has not been reported yet. Accordingly in P0-P1 rats a LTP was observed in both upper cortical layers and layer V (**Fig. 21E**), which corresponds to the CSD data showing prominent synaptic inputs to these layers (**Fig. 20C**).Our CSD data in P0-P1 rats provide no conclusive evidence for LTP of the thalamus-to-subplate synpase, but rather a prominent increase in the synaptic input to upper cortical layers (**Fig. 20C2**). It can be not excluded that thalamic afferents already reaching the cortical plate or a disynaptic pathway from the subplate to the cortical plate are potentiated.

5.1.3 Silent synapses may underlie age-dependent LTP

A number of *in vitro* studies have demonstrated that the developmentally regulated and activity-dependent expression of LTP in the thalamocortical synapses to the barrel cortex depend on the activation of functionally silent synapses and the insertion or stabilisation of postsynaptic AMPA receptors (for review (Feldman et al., 1999;Hanse et al., 2009). Isaac et al. (Isaac et al., 1997) have previously shown that the thalamus-to-layer IV synapses in P2-P7 rats to a large extent do not contain functional AMPA receptors and that LTP induction protocols can convert them to stabilized, AMPA-containing synapses following. In P6-P7 rats the proportion of silent synapses has decreased (Isaac et al., 1997) indicating that this synapse reveals the highest capability for activity-dependent changes between P3 and P5. Our *in vivo* data during the first postnatal week are in good agreement with these previous *in vitro* data.

In conclusion, combining VSDI and multi-channel electrode recordings, we demonstrate that single whisker deflection at 2 Hz for 10 min induces an age-dependent LTP of the whisker-to-barrel cortex pathway in the activated barrel-related column and to a lesser extent neighboring septa. These activity-dependent modifications during the critical period may play an important role in the development and refinement of the topographic map in the barrel cortex.

5.2 Project2

In the present study, we combined VSDI with extracellular multielectrode recordings to get insight into activity patterns in neonatal M1 and their functions during the first postnatal week. The findings of this study can be summarized as follow: (1) in neonatal M1, two oscillatory activity patterns (gamma and spindle bursts) can spontaneously occur or be induced by sensory stimulations *in vivo*. (2) these activity patterns enable neonatal M1 to operate as both sensory and motor roles during the early postnatal development. (3) paw sensory stimulations induce sensorimotor integration which is processed from S1 to M1. (4) both spontaneously occurring and sensory evoked activity patterns in M1 depend on the activity in S1.

5.2.1 Gamma and spindle bursts in M1

Gamma and spindle bursts are two main patterns in M1 during the early postnatal development, however, only the spindle bursts exist in S1. These activity patterns could generate spontaneously (**Fig. 23B**) or even without the periphery sensory inputs (**Fig. 26**) and be elicited by sensory stimulations (**Fig. 27-28**). Different locations of gamma and spindle bursts in sensorimotor cortex are in well agreement with spatiotemporal properties of gamma and spindle bursts in neonatal S1 as in our previous study (Yang et al., 2009). In neonatal rat S1, spindle bursts can be recorded both inside and outside of the barrel field, however, the gamma bursts are only confined to the barrel cortex. Interestingly, in human cortices, alpha band activity prevails in S1, while gamma band activity dominates in M1 by magnetoencephalographic recordings during a sensorimotor task (Tecchio et al., 2008). In addition, different neuronal activity patterns observed in S1 and M1 may result from various cellular mechanisms (for review, see Castro-Alamancos, 2013).

Furthermore, these patterns are also similar in other electrophysiological properties as gamma bursts obtained in barrel cortex (Yang et al., 2009;Minlebaev et al., 2011;Yang et al., 2012) and spindle bursts described previously in the S1

(Khazipov et al., 2004;Marcano-Reik and Blumberg, 2008), barrel cortex (Minlebaev et al., 2007;Yang et al., 2009;Minlebaev et al., 2009;Yang et al., 2012), and primary visual cortex (V1) (Hanganu et al., 2006;Colonnese et al., 2010;Colonnese and Khazipov, 2010) in newborn rats. These activity patterns have been suggested to play critical roles in cognitive operations, other biological processes, and disease (for recent review, see Buzsaki and Wang, 2012). In addition, these patterns are also essential for the generation, refinement and maturation of early neuronal cortical circuits (Khazipov and Luhmann, 2006), as further discussed below.

5.2.2 Early gamma and spindle bursts in neonatal M1 send motor commands

An important finding in our study is that gamma and spindle bursts in neonatal M1 drive paw movements. 31.8% gamma and spindle bursts of all spontaneous activity drove forepaw movements (**Fig. 23D**). Moreover, local gamma (40 Hz) and spindle (10 Hz) bursts stimulations of layer V neurons in M1 which have already extended the axons to spinal cords (Arlotta et al., 2005;Molyneaux et al., 2007) could elicit paw movements (**Fig. 24**). Furthermore, local inactivation of the M1 reduced the occurrence and duration of spontaneous paw movements by 30%-40% (**Fig. 25**). There are different hypotheses about the motor output circuits in the sensorimotor systerm. As early as 1966, Roffwarg and colleagues firstly proposed the ontogentic hypothesis. They suggested that the brainstem activity in young infants during the active sleep directs ascending activation of the cortex and desending activation of the musculature (Roffwarg et al., 1966). However, in mammals, including humans, the spinal cord has been suggested as central pattern generator, which is critical to control the locomotion movements (for reviews, see MacKay-Lyons, 2002;Dietz, 2003;Ijspeert, 2008;Guertin, 2009). In sleeping newborn rats, spontaneous muscle twitches send the tactile feedback to spinal cord and guide the organization of spinal sensorimotor circuits (Petersson et al., 2003). In adult animals, forelimb representation in M1 has been suggested to be pertaining to three different categories of movement, for example, stereotyped repetitive behaviors, complex voluntary

movements and fine motor manipulation skills (for review, see Levine et al., 2012). In newborn rats from our study, about 40% spontaneous paw movements were driven by the patterns activity in M1, the left majority of the spontaneous movements may be triggered by the spontaneous activity from brain stem, spinal cord or even muscle in paws. We put forward that during the early postnatal development, not only brainstem and spinal cord, but also M1 plays an important role in controlling the early movement behaviors. Moreover, both spontaneously occurring and sensory processing gamma and spindle bursts may be critical for formation of functional cortical spinal pathway (**Fig. 32**) and the musculotopic organization of spinal motor neurons (for review, see Levine et al., 2012).

Long latency for the forepaw movement triggered by the spontaneous activity (**Fig. 23D**) and evoked by local microstimulation (**Fig. 24**) in neonatal M1 may be due to the unmatured myelination on cortical spinal tract (Salami et al., 2003). We speculate here that, with increasing complexity for mobility tasks during the later development, the need for commands from M1 becomes more and more apparent. Martin and colleagues proved that activity- and use-dependent processes are keys to establishing the mature pattern of topographic and connectional specificity between cortical spinal axon and spinal targets (Martin et al., 2007). We propose that sensory periphery may be critical in experience-dependent plasticity in motor circuit formation for the long-term function of the system.

5.2.3 Neonatal M1 operates in somatosensory mode

Another major finding of our study is that, sensory periphery drives gamma and spindle bursts in M1. 50% gamma and spindle bursts of all spontaneous activity were triggered in M1 by the paw movements (**Fig. 23D**). In addition, gamma and spindle bursts in M1 could be also induced by paw sensory stimulations (**Fig. 27-29**). Furthermore, in the absence of forepaw movement by local lidocaine injection reduced the occurrence of gamma and spindle bursts by ~50% (**Fig. 26D**). These suggest that sensory periphery drive spontaneous occurring gamma and spindle bursts

in neonatal M1. Similarly, sensory periphery also contributes considerably to the neuronal patterns of activity in the sensory cortical areas (for review, see Hanganu-Opatz, 2010;Kilb et al., 2011). In neonatal S1, more spontaneous spindle bursts about 86% are abolished by severing the spinal cord (Khazipov et al., 2004). In the whisker system, spontaneous whisker twitches trigger patterns activity (Tiriac et al., 2012) and blockade of the whisker movements reduces the occurrence of gamma and spindle bursts by ~50% in the vibrissa S1 at P0-P7 (Yang et al., 2009). Interestingly, in the visual system, similar percentage of decrease in the occurrence of spindle bursts has been observed in V1 of P5-P6 rats after removal of retina (Hanganu et al., 2006). In addition, at P10-P11 (before eye-opening), 87% of the spontaneous cortical activity is triggered by the retina (Colonnese and Khazipov, 2010). In the developing auditory system, supporting cells in the cochlea trigger activity in auditory nerve fibers projected to primary auditory cortex (A1) before the onset of hearing (Tritsch et al., 2007;Tritsch and Bergles, 2010).

Furthermore, these patterns activity triggered by sensory periphery have been proved to be critical in the development of functional topography map of sensory perception. Somatotopic sensory cortical map has been suggested to require the spindle bursts in S1 driven by the spontaneous paws twitches (Khazipov et al., 2004). The precise topographic and functional columnar organization in barrel cortex needs the localized gamma and spindle bursts in neonatal vibrissal S1 (Yang et al., 2012) induced by the spontaneous whisker movements (Tiriac et al., 2012). The patterned spontaneous retinal waves not only contribute to   the retinotopic map refinement in the superior colliculus (McLaughlin et al., 2003;Chandrasekaran et al., 2005), but also trigger spindle bursts (Hanganu et al., 2006) required for the development of precise maps in V1 (Cang et al., 2005). Spontaneous activity in auditory nerve fibers before the onset of hearing is essential for the refinement and maintenance of tonotopic maps in the developing auditory system (Gabriele et al., 2000;Rubel and Fritzsch, 2002b;Kandler, 2004;Leake et al., 2006;Leao et al., 2006;Tritsch et al., 2007). Somatosensory topographic map in M1 which is in a mirror symmetric relationship

with the map in S1 was reported by Brecht and colleagues in rat using intracellular and extracellular stimulation (Brecht et al., 2004a;Brecht et al., 2004b). The spatial arrangement of topographic maps in M1 and S1 is characteristic for many mammalian species (for review, see Brecht, 2011). Moreover, we performed the mechanical stimulation in forepaw and found the position of localized VSDI evoked response in M1 borders the localized response in S1 as a mirror image (**Fig. 22B**). We propose that sensory periphery processing gamma and spindle bursts play an important role in the formation of functional map in neonatal M1 and the musculotopic organization of motorneurons in spinal cord (for recent review, see Levine et al., 2012).

Although anatomical data proved that the callosal projection neurons have already crossed the corpus callosum (CC) at birth (Tritsch et al., 2007;Molyneaux et al., 2007;Rouaux and Arlotta, 2012), the sensory information was transferred between both hemispheres sensorimotor cortices until P3 (**Fig. 27B**). In neonatal S1, the weak evoked responses in the ipsilateral hemisphere were observed by EEG (Marcano-Reik and Blumberg, 2008) and VSDI (Mcvea et al., 2012) recordings. Interestingly, in the visual system, the weak ipsilateral On-response could be also elicited in V1 by optic nerve stimulation from P3 onwards (Hanganu et al., 2006). In the whisker system, however, the whisker stimulation failed to evoke detectable response anymore in the ipsilateral barrel cortex in the same age newborn rats (Yang et al., 2009). In adult mice, the tactile whisker stimulation could induce the reliable VSDI evoked response in bilateral sensorimotor cortices (Ferezou et al., 2007). Our data suggest that gamma and spindle bursts in sensorimotor cortices are necessary for the normal development and maintenance of the callosal projections in the sensorimotor system.

5.2.4 Spatiotemporal dynamics of cortical sensorimotor integration is processed from S1 to M1

Approximately 8 ms following the initial sensory response in S1, the second local region of depolarization occurred in M1 at P3-P5 by both VSDI (**Fig. 22**) and Multi-electrode (**Fig, 27**) recordings. Moreover, the MUA in S1 preceded the MUA in

M1 (**Fig. 28B3**). These results are consistent with previous data in the whisker system of adult mice. A single whisker deflection induces the sensory evoked responses from S1 to M1 also with about 8 ms latency (Ferezou et al., 2007). Moreover, the evoked responses in S1 had higher amplitude and longer duration than these in M1 in both P3-P5 (**Fig. 22, 27**) and P0-P1 (**Fig. 27**) age groups. In human being, sensorimotor integration has been found in the tactile exploration with the receptors in fingertips sliding along a surface (Gamzu and Ahissar, 2001). In rodents, they can move whiskers to locate an object nearby their heads (Knutsen et al., 2006;Mehta et al., 2007;O'Connor et al., 2010). Then, the sensory input will in turn modify the whisking pattern (Mitchinson et al., 2007;O'Connor et al., 2010). It has been proved that the cortical sensorimotor integration in vibrissa sensorimotor cortex correlates strongly with behaviour in adult mice (Ferezou et al., 2007). However, we suggest that the early patterns of neuronal activity in sensorimotor cortex play a crucial role in the refinement and maturation of sensorimotor networks required for sensorimotor integration in newborn animals (Fig. 32).

5.2.5 S1 contribute to the gamma and spindle bursts in M1.

Functional inactivation of S1 significantly attenuated the spectrum powers of gamma and spindle bands for both sensory evoked (**Fig. 29**) and spontaneously occurring activity (**Fig. 31**) in M1. Unfortunately, we are not sure whether S1 were completely inactivated or just partly blocked. Not withstanding this limitation, even S1 were partly blocked, these results do demonstrate that both gamma and spindle bursts in M1 depend on the activity in S1. Furthermore, inactivation of the barrel column in vibrissa S1 by injecting CNQX and APV almost completely blocked the entire sensorimotor response (Ferezou et al., 2007). In contrast, electrical stimulation in S1 could induce the response in M1 (Farkas et al., 1999). Furthermore, anatomic data have shown that the superficial layers II/III in barrel cortex preferentially project to upper layers (LII/III, LVa) in vibrissa M1 (Ferezou et al., 2007;Mao et al., 2011).

Our data suggest that S1 contribute to the early gamma and spindle bursts in M1 in newborn rats.

In conclusion, we show that spontaneously occurring and sensory evoked gamma and spindle bursts enable neonatal M1 to operate in both motor and sensory modes. We suggest these patterns of activity in M1 may contribute to the refinement and maturation of early sensorimotor, corticospinal and callosal networks (**Fig. 32**) required for sensory perception, sensorimotor integration, coordination, motor control and associative learning.

Reference List

Alcamo EA, Chirivella L, Dautzenberg M, Dobreva G, Farinas I, Grosschedl R, McConnell SK (2008) Satb2 regulates callosal projection neuron identity in the developing cerebral cortex. Neuron 57: 364-377.

Allene C, Cossart R (2010) Early NMDA receptor-driven waves of activity in the developing neocortex: physiological or pathological network oscillations? Journal of Physiology-London 588: 83-91.

Alloway KD (2008) Information processing streams in rodent barrel cortex: The differential functions of barrel and septal circuits. Cerebral Cortex 18: 979-989.

Alloway KD, Zhang ML, Chakrabarti S (2004) Septal columns in rodent barrel cortex: Functional circuits for modulating whisking behavior. Journal of Comparative Neurology 480: 299-309.

An SM, Yang JW, Sun HY, Kilb W, Luhmann HJ (2012) Long-Term Potentiation in the Neonatal Rat Barrel Cortex In Vivo. J Neurosci 32: 9511-9516.

Antonini A, Stryker MP (1993) Development of Individual Geniculocortical Arbors in Cat Striate Cortex and Effects of Binocular Impulse Blockade. J Neurosci 13: 3549-3573.

Arlotta P, Molyneaux BJ, Chen J, Inoue J, Kominami R, Macklis JD (2005) Neuronal subtype-specific genes that control corticospinal motor neuron development in vivo. Neuron 45: 207-221.

Barnes CA (2003) Long-term potentiation and the ageing brain. Philosophical Transactions of the Royal Society of London Series B-Biological Sciences 358: 765-772.

Barth AL, Malenka RC (2001) NMDAR EPSC kinetics do not regulate the critical period for LTP at thalamocortical synapses. Nature Neuroscience 4: 235-236.

Bear MF (2003) Bidirectional synaptic plasticity: from theory to reality. Philosophical Transactions of the Royal Society of London Series B-Biological Sciences 358: 649-655.

Bear MF, Kleinschmidt A, Gu Q, Singer W (1990) Disruption of Experience-Dependent Synaptic Modifications in Striate Cortex by Infusion of An Nmda Receptor Antagonist. J Neurosci 10: 909-925.

Berger T, Borgdorff A, Crochet S, Neubauer FB, Lefort S, Fauvet B, Ferezou I, Carleton A, Luscher HR, Petersen CCH (2007) Combined voltage and calcium epifluorescence Imaging in vitro and in vivo reveals subthreshold and suprathreshold dynamics of mouse barrel cortex. Journal of Neurophysiology 97: 3751-3762.

Bliss TVP, GARDNERM.AR (1973) Long-Lasting Potentiation of Synaptic Transmission in Dentate Area of Unanesthetized Rabbit Following Stimulation of Perforant Path. Journal of Physiology-London 232: 357-374.

Bliss TVP, Lomo T (1973) Long-Lasting Potentiation of Synaptic Transmission in Dentate Area of Anesthetized Rabbit Following Stimulation of Perforant Path. Journal of Physiology-London 232: 331-356.

Blumberg MS (2010b) Beyond dreams: do sleep-related movements contribute to brain development? Front Neurol 1: 140.

Blumberg MS (2010a) Beyond dreams: do sleep-related movements contribute to brain development? Front Neurol 1: 140.

Brecht M (2011) Movement, Confusion, and Orienting in Frontal Cortices. Neuron 72: 193-196.

Brecht M, Krauss A, Muhammad S, Sinai-Esfahani L, Bellanca S, Margrie TW (2004a) Organization of rat vibrissa motor cortex and adjacent areas according to

cytoarchitectonics, microstimulation, and intracellular stimulation of identified cells. Journal of Comparative Neurology 479: 360-373.

Brecht M, Schneider M, Sakmann B, Margrie TW (2004b) Whisker movements evoked by stimulation of single pyramidal cells in rat motor cortex. Nature 427: 704-710.

Buzsaki G, Wang XJ (2012) Mechanisms of Gamma Oscillations. Annual Review of Neuroscience, Vol 35 35: 203-225.

Cang JH, Renteria RC, Kaneko M, Liu XR, Copenhagen DR, Stryker MP (2005) Development of precise maps in visual cortex requires patterned spontaneous activity in the retina. Neuron 48: 797-809.

Carvell GE, Simons DJ (1990) Biometric Analyses of Vibrissal Tactile Discrimination in the Rat. J Neurosci 10: 2638-2648.

Cascio CJ, Sathian K (2001) Temporal cues contribute to tactile perception of roughness. J Neurosci 21: 5289-5296.

Castro-Alamancos MA (2013) The motor cortex: a network tuned to 7-14 Hz. Front Neural Circuits 7: 21.

Chandrasekaran AR, Plas DT, Gonzalez E, Crair MC (2005) Evidence for an instructive role of retinal activity in retinotopic map refinement in the superior colliculus of the mouse. J Neurosci 25: 6929-6938.

Cioni G, Prechtl HFR (1990) Preterm and Early Postterm Motor Behavior in Low-Risk Premature-Infants. Early Human Development 23: 159-191.

Clarac F, Brocard F, Vinay L (2004) The maturation of locomotor networks. Brain Mechanisms for the Integration of Posture and Movement 143: 57-66.

Collingridge GL (2003) The induction of N-methyl-D-aspartate receptor-dependent long-term potentiation. Philosophical Transactions of the Royal Society of London Series B-Biological Sciences 358: 635-641.

Colonnese MT, Kaminska A, Minlebaev M, Milh M, Bloem B, Lescure S, Moriette G, Chiron C, Ben Ari Y, Khazipov R (2010) A Conserved Switch in Sensory Processing Prepares Developing Neocortex for Vision. Neuron 67: 480-498.

Colonnese MT, Khazipov R (2010) "Slow Activity Transients" in Infant Rat Visual Cortex: A Spreading Synchronous Oscillation Patterned by Retinal Waves. J Neurosci 30: 4325-4337.

Crair MC, Malenka RC (1995) A Critical Period for Long-Term Potentiation at Thalamocortical Synapses. Nature 375: 325-328.

Daw MI, Scott HL, Isaac JTR (2007) Developmental synaptic plasticity at the thalamocortical input to barrel cortex: Mechanisms and roles. Molecular and Cellular Neuroscience 34: 493-502.

Daw NW, Gordon B, Fox KD, Flavin HJ, Kirsch JD, Beaver CJ, Ji QH, Reid SNM, Czepita D (1999) Injection of MK-801 affects ocular dominance shifts more than visual activity. Journal of Neurophysiology 81: 204-215.

de Vries JI, Visser GH, Prechtl HF (1982) The emergence of fetal behaviour. I. Qualitative aspects. Early Hum Dev 7: 301-322.

Deleon R, Hodgson JA, Roy RR, Edgerton VR (1994) Extensor-Like and Flexor-Like Modulation Within Motor Pools of the Rat Hindlimb During Treadmill Locomotion and Swimming. Brain Research 654: 241-250.

Deschenes M, Veinante P, Zhang ZW (1998) The organization of corticothalamic projections: reciprocity versus parity. Brain Research Reviews 28: 286-308.

Diamond ME, Armstrongjames M, Budway MJ, Ebner FF (1992) Somatic Sensory Responses in the Rostral Sector of the Posterior Group (Pom) and in the Ventral Posterior Medial Nucleus (Vpm) of the Rat Thalamus - Dependence on the Barrel Field Cortex. Journal of Comparative Neurology 319: 66-84.

Dietz V (2003) Spinal cord pattern generators for locomotion. Clinical Neurophysiology 114: 1379-1389.

Erzurumlu RS, Jhaveri S (1990) Thalamic Axons Confer A Blueprint of the Sensory Periphery Onto the Developing Rat Somatosensory Cortex. Developmental Brain Research 56: 229-234.

Erzurumlu RS, Jhaveri S, Benowitz LI (1990) Transient Patterns of Gap-43 Expression During the Formation of Barrels in the Rat Somatosensory Cortex. Journal of Comparative Neurology 292: 443-456.

Farkas T, Kis Z, Toldi J, Wolff JR (1999) Activation of the primary motor cortex by somatosensory stimulation in adult rats is mediated mainly by associational connections from the somatosensory cortex. Neuroscience 90: 353-361.

Feldman DE, Nicoll RA, Malenka RC (1999) Synaptic plasticity at thalamocortical synapses in developing rat somatosensory cortex: LTP, LTD, and silent synapses. Journal of Neurobiology 41: 92-101.

Ferezou I, Haiss F, Gentet LJ, Aronoff R, Weber B, Petersen CCH (2007) Spatiotemporal dynamics of cortical sensorimotor integration in behaving mice. Neuron 56: 907-923.

Fishell G, Hanashima C (2008) Pyramidal neurons grow up and change their mind. Neuron 57: 333-338.

Foeller E, Feldman DE (2004) Synaptic basis for developmental plasticity in somatosensory cortex. Current Opinion in Neurobiology 14: 89-95.

Fox K (1992) A Critical Period for Experience-Dependent Synaptic Plasticity in Rat Barrel Cortex. J Neurosci 12: 1826-1838.

Fox K, Schlaggar BL, Glazewski S, Oleary DDM (1996) Glutamate receptor blockade at cortical synapses disrupts development of thalamocortical and columnar organization in somatosensory cortex. Proceedings of the National Academy of Sciences of the United States of America 93: 5584-5589.

Freeman JA, Nicholson C (1975) Experimental Optimization of Current Source-Density Technique for Anuran Cerebellum. Journal of Neurophysiology 38: 369-382.

Gabriele ML, Brunso-Bechtold JK, Henkel CK (2000) Plasticity in the development of afferent patterns in the inferior colliculus of the rat after unilateral cochlear ablation. J Neurosci 20: 6939-6949.

Galazo MJ, Martinez-Cerdeno V, Porrero C, Clasca F (2008) Embryonic and postnatal development of the layer I-directed ("Matrix") thalamocortical system in the rat. Cerebral Cortex 18: 344-363.

Gamzu E, Ahissar E (2001) Importance of temporal cues for tactile spatial-frequency discrimination. J Neurosci 21: 7416-7427.

Gramsbergen A, Schwartze P, Prechtl HF (1970) The postnatal development of behavioral states in the rat. Dev Psychobiol 3: 267-280.

Gruner JA, Altman J (1980) Swimming in the Rat - Analysis of Locomotor Performance in Comparison to Stepping. Experimental Brain Research 40: 374-382.

Guertin PA (2009) The mammalian central pattern generator for locomotion. Brain Research Reviews 62: 45-56.

Hanganu IL, Ben Ari Y, Khazipov R (2006) Retinal waves trigger spindle bursts in the neonatal rat visual cortex. J Neurosci 26: 6728-6736.

Hanganu IL, Kilb W, Luhmann HJ (2002) Functional synaptic projections onto subplate neurons in neonatal rat somatosensory cortex. J Neurosci 22: 7165-7176.

Hanganu IL, Staiger JF, Ben Ari Y, Khazipov R (2007) Cholinergic modulation of spindle bursts in the neonatal rat visual cortex in vivo. J Neurosci 27: 5694-5705.

Hanganu-Opatz IL (2010) Between molecules and experience: Role of early patterns of coordinated activity for the development of cortical maps and sensory abilities. Brain Research Reviews 64: 160-176.

Hanse E, Taira T, Lauri S, Groc L (2009) Glutamate synapse in developing brain: an integrative perspective beyond the silent state. Trends Neurosci 32: 532-537.

Harris KM, Fiala JC, Ostroff L (2003) Structural changes at dendritic spine synapses during long-term potentiation. Philosophical Transactions of the Royal Society of London Series B-Biological Sciences 358: 745-748.

Harvey MA, Bermejo R, Zeigler HP (2001) Discriminative whisking in the head-fixed rat: optoelectronic monitoring during tactile detection and discrimination tasks. Somatosensory and Motor Research 18: 211-222.

Heynen AJ, Bear MF (2001) Long-term potentiation of thalamocortical transmission in the adult visual cortex in vivo. J Neurosci 21: 9801-9813.

Hoffer ZS, Hoover JE, Alloway KD (2003) Sensorimotor corticocortical projections from rat barrel cortex have an anisotropic organization that facilitates integration of inputs from whiskers in the same row. Journal of Comparative Neurology 466: 525-544.

Ijspeert AJ (2008) Central pattern generators for locomotion control in animals and robots: A review. Neural Networks 21: 642-653.

Inan M, Crair MC (2007) Development of cortical maps: Perspectives from the barrel cortex. Neuroscientist 13: 49-61.

Isaac JTR, Crair MC, Nicoll RA, Malenka RC (1997) Silent synapses during development of thalamocortical inputs. Neuron 18: 269-280.

Izraeli R, Porter LL (1995) Vibrissal Motor Cortex in the Rat - Connections with the Barrel Field. Experimental Brain Research 104: 41-54.

Jacquin MF, Rhoades RW (1983) Central Projections of the Normal and Regenerate Infraorbital Nerve in Adult-Rats Subjected to Neonatal Unilateral Infraorbital Lesions - A Transganglionic Horseradish-Peroxidase Study. Brain Research 269: 137-144.

Jamon M, Clarac F (1998) Early walking in the neonatal rat: A kinematic study. Behavioral Neuroscience 112: 1218-1228.

Kandler K (2004) Activity-dependent organization of inhibitory circuits: lessons from the auditory system. Current Opinion in Neurobiology 14: 96-104.

Kanold PO, Luhmann HJ (2010) The Subplate and Early Cortical Circuits. Annual Review of Neuroscience, Vol 33 33: 23-48.

Khazipov R, Luhmann HJ (2006) Early patterns of electrical activity in the developing cerebral cortex of humans and rodents. Trends in Neurosciences 29: 414-418.

Khazipov R, Sirota A, Leinekugel X, Holmes GL, Ben Arf Y, Buzsaki G (2004) Early motor activity drives spindle bursts in the developing somatosensory cortex. Nature 432: 758-761.

Kilb W, Kirischuk S, Luhmann HJ (2011) Electrical activity patterns and the functional maturation of the neocortex. European Journal of Neuroscience 34: 1677-1686.

Killackey HP, Fleming K (1985) The Role of the Principal Sensory Nucleus in Central Trigeminal Pattern-Formation. Developmental Brain Research 22: 141-145.

Kirkwood A, Lee HK, Bear MF (1995) Coregulation of Long-Term Potentiation and Experience-Dependent Synaptic Plasticity in Visual-Cortex by Age and Experience. Nature 375: 328-331.

Knutsen PM, Pietr M, Ahissar E (2006) Haptic object localization in the vibrissal system: Behavior and performance. J Neurosci 26: 8451-8464.

Koziol LF, Budding DE, Chidekel D (2011) Sensory Integration, Sensory Processing, and Sensory Modulation Disorders: Putative Functional Neuroanatomic Underpinnings. Cerebellum 10: 770-792.

Krupa DJ, Brisben AJ, Nicolelis MAL (2001) A multi-channel whisker stimulator for producing spatiotemporally complex tactile stimuli. Journal of Neuroscience Methods 104: 199-208.

Kullmann DM (2003) Silent synapses: what are they telling us about long-term potentiation? Philosophical Transactions of the Royal Society B-Biological Sciences 358: 727-733.

Leake PA, Hradek GT, Chair L, Snyder RL (2006) Neonatal deafness results in degraded topographic specificity of auditory nerve projections to the cochlear nucleus in cats. Journal of Comparative Neurology 497: 13-31.

Leao RN, Sun H, Svahn K, Berntson A, Youssoufian M, Paolini AG, Fyffe REW, Walmsley B (2006) Topographic organization in the auditory brainstem of juvenile mice is disrupted in congenital deafness. Journal of Physiology-London 571: 563-578.

Levine AJ, Lewallen KA, Pfaff SL (2012) Spatial organization of cortical and spinal neurons controlling motor behavior. Current Opinion in Neurobiology 22: 812-821.

Liu HN, Kurotani T, Ren M, Yamada K, Yoshimura Y, Komatsu Y (2004) Presynaptic activity and Ca2+ entry are required for the maintenance of NMDA

receptor-independent LTP at visual cortical excitatory synapses. Journal of Neurophysiology 92: 1077-1087.

Lubke J, Feldmeyer D (2007) Excitatory signal flow and connectivity in a cortical column: focus on barrel cortex. Brain Structure & Function 212: 3-17.

Luhmann HJ, Kilb W, Hanganu-Opatz IL (2009) Subplate cells: amplifiers of neuronal activity in the developing cerebral cortex. Frontiers in Neuroanatomy 3.

Lynch G (2003) Long-term potentiation in the Eocene. Philosophical Transactions of the Royal Society of London Series B-Biological Sciences 358: 625-628.

Macaluso E, Driver J (2005) Multisensory spatial interactions: a window onto functional integration in the human brain. Trends in Neurosciences 28: 264-271.

MacKay-Lyons M (2002) Central pattern generation of locomotion: A review of the evidence. Physical Therapy 82: 69-83.

Malenka RC (2003) The long-term potential of LTP. Nat Rev Neurosci 4: 923-926.

Malenka RC, Bear MF (2004) LTP and LTD: An embarrassment of riches. Neuron 44: 5-21.

Mao TY, Kusefoglu D, Hooks BM, Huber D, Petreanu L, Svoboda K (2011) Long-Range Neuronal Circuits Underlying the Interaction between Sensory and Motor Cortex. Neuron 72: 111-123.

Marcano-Reik AJ, Blumberg MS (2008) The corpus callosum modulates spindle-burst activity within homotopic regions of somatosensory cortex in newborn rats. European Journal of Neuroscience 28: 1457-1466.

Martin JH, Friel KM, Salimi I, Chakrabarty S (2007) Activity- and use-dependent plasticity of the developing corticospinal system. Neuroscience and Biobehavioral Reviews 31: 1125-1135.

McLaughlin T, Torborg CL, Feller MB, O'Leary DDM (2003) Retinotopic map refinement requires spontaneous retinal waves during a brief critical period of development. Neuron 40: 1147-1160.

Mcvea DA, Mohajerani MH, Murphy TH (2012) Voltage-Sensitive Dye Imaging Reveals Dynamic Spatiotemporal Properties of Cortical Activity after Spontaneous Muscle Twitches in the Newborn Rat. J Neurosci 32: 10982-10994.

Megevand P, Troncoso E, Quairiaux C, Muller D, Michel CM, Kiss JZ (2009) Long-Term Plasticity in Mouse Sensorimotor Circuits after Rhythmic Whisker Stimulation. J Neurosci 29: 5326-5335.

Mehta SB, Whitmer D, Figueroa R, Williams BA, Kleinfeld D (2007) Active spatial perception in the vibrissa scanning sensorimotor system. Plos Biology 5: 309-322.

Melzer P, Champney GC, Maguire MJ, Ebner FF (2006a) Rate code and temporal code for frequency of whisker stimulation in rat primary and secondary somatic sensory cortex. Experimental Brain Research 172: 370-386.

Melzer P, Sachdev RNS, Jenkinson N, Ebner FF (2006b) Stimulus frequency processing in awake rat barrel cortex. J Neurosci 26: 12198-12205.

Minlebaev M, Ben Ari Y, Khazipov R (2007) Network mechanisms of spindle-burst oscillations in the neonatal rat barrel cortex in vivo. Journal of Neurophysiology 97: 692-700.

Minlebaev M, Ben Ari Y, Khazipov R (2009) NMDA Receptors Pattern Early Activity in the Developing Barrel Cortex In Vivo. Cerebral Cortex 19: 688-696.

Minlebaev M, Colonnese M, Tsintsadze T, Sirota A, Khazipov R (2011) Early Gamma Oscillations Synchronize Developing Thalamus and Cortex. Science 334: 226-229.

Mitchinson B, Martin CJ, Grant RA, Prescott TJ (2007) Feedback control in active sensing: rat exploratory whisking is modulated by environmental contact. Proceedings of the Royal Society B-Biological Sciences 274: 1035-1041.

Mitzdorf U (1985) Current Source-Density Method and Application in Cat Cerebral-Cortex - Investigation of Evoked-Potentials and Eeg Phenomena. Physiological Reviews 65: 37-100.

Molnar Z, Adams R, Blakemore C (1998) Mechanisms underlying the early establishment of thalamocortical connections in the rat. J Neurosci 18: 5723-5745.

Molnar Z, Kurotani T, Higashi S, Yamamoto N, Toyama K (2003) Development of functional thalamocortical synapses studied with current source-density analysis in whole forebrain slices in the rat. Brain Research Bulletin 60: 355-371.

Molyneaux BJ, Arlotta P, Hirata T, Hibi M, Macklis JD (2005) Fezl is required for the birth and specification of corticospinal motor neurons. Neuron 47: 817-831.

Molyneaux BJ, Arlotta P, Menezes JRL, Macklis JD (2007) Neuronal subtype specification in the cerebral cortex. Nature Reviews Neuroscience 8: 427-437.

Morris RGM (2003) Long-term potentiation and memory. Philosophical Transactions of the Royal Society of London Series B-Biological Sciences 358: 643-647.

Nicoll RA (2003) Expression mechanisms underlying long-term potentiation: a postsynaptic view. Philosophical Transactions of the Royal Society of London Series B-Biological Sciences 358: 721-726.

Nugent FS, Niehaus JL, Kauer JA (2009) PKG and PKA Signaling in LTP at GABAergic Synapses. Neuropsychopharmacology 34: 1829-1842.

O'Connor DH, Clack NG, Huber D, Komiyama T, Myers EW, Svoboda K (2010) Vibrissa-Based Object Localization in Head-Fixed Mice. J Neurosci 30: 1947-1967.

Petersson P, Waldenstrom A, Fahraeus C, Schouenborg J (2003) Spontaneous muscle twitches during sleep guide spinal self-organization. Nature 424: 72-75.

Pinon MC, Jethwa A, Jacobs E, Campagnoni A, Molnar Z (2009) Dynamic integration of subplate neurons into the cortical barrel field circuitry during postnatal development in the Golli-tau-eGFP (GTE) mouse. Journal of Physiology-London 587: 1903-1915.

Pittenger C, Kandel ER (2003) In search of general mechanisms for long-lasting plasticity: Aplysia and the hippocampus. Philosophical Transactions of the Royal Society of London Series B-Biological Sciences 358: 757-763.

Polleux F (2005) Genetic mechanisms specifying cortical connectivity: Let's make some projections together. Neuron 46: 395-400.

Price DJ, Kennedy H, Dehay C, Zhou LB, Mercier M, Jossin Y, Goffinet AM, Tissir F, Blakey D, Molnar Z (2006) The development of cortical connections. European Journal of Neuroscience 23: 910-920.

Ratzlaff EH, Grinvald A (1991) A Tandem-Lens Epifluorescence Macroscope - Hundred-Fold Brightness Advantage for Wide-Field Imaging. Journal of Neuroscience Methods 36: 127-137.

Roffwarg HP, Muzio JN, Dement WC (1966) Ontogenetic development of the human sleep-dream cycle. Science 152: 604-619.

Rouaux C, Arlotta P (2012) Direct lineage reprogramming of post-mitotic callosal neurons into corticofugal neurons in vivo. Nat Cell Biol 15: 214-221.

Rowan MJ, Klyubin I, Cullen WK, Anwyl R (2003) Synaptic plasticity in animal models of early Alzheimer's disease. Philosophical Transactions of the Royal Society of London Series B-Biological Sciences 358: 821-828.

Rubel EW, Fritzsch B (2002a) Auditory system development: Primary auditory neurons and their targets. Annual Review of Neuroscience 25: 51-101.

Rubel EW, Fritzsch B (2002b) Auditory system development: Primary auditory neurons and their targets. Annual Review of Neuroscience 25: 51-101.

Salami M, Itami C, Tsumoto T, Kimura F (2003) Change of conduction velocity by regional myelination yields constant latency irrespective of distance between thalamus and cortex. Proceedings of the National Academy of Sciences of the United States of America 100: 6174-6179.

Schlaggar BL, Fox K, Oleary DDM (1993) Postsynaptic Control of Plasticity in Developing Somatosensory Cortex. Nature 364: 623-626.

Schlaggar BL, Oleary DDM (1994) Early Development of the Somatotopic Map and Barrel Patterning in Rat Somatosensory Cortex. Journal of Comparative Neurology 346: 80-96.

Shuler MG, Krupa DJ, Nicolelis MAL (2002) Integration of bilateral whisker stimuli in rats: Role of the whisker barrel cortices. Cerebral Cortex 12: 86-97.

Sohur US, Arlotta P, Macklis JD (2012) Developmental Controls are Re-Expressed during Induction of Neurogenesis in the Neocortex of Young Adult Mice. Front Neurosci 6: 12.

Tecchio F, Zappasodi F, Porcaro C, Barbati G, Assenza G, Salustri C, Rossini PM (2008) High-gamma band activity of primary hand cortical areas: A sensorimotor feedback efficiency index. Neuroimage 40: 256-264.

Tiriac A, Uitermarkt BD, Fanning AS, Sokoloff G, Blumberg MS (2012) Rapid Whisker Movements in Sleeping Newborn Rats. Current Biology 22: 2075-2080.

Tritsch NX, Bergles DE (2010) Developmental Regulation of Spontaneous Activity in the Mammalian Cochlea. J Neurosci 30: 1539-1550.

Tritsch NX, Yi EY, Gale JE, Glowatzki E, Bergles DE (2007) The origin of spontaneous activity in the developing auditory system. Nature 450: 50-+.

Vanderloos H (1976) Barreloids in Mouse Somatosensory Thalamus. Neuroscience Letters 2: 1-6.

Yang JW, An S, Sun JJ, Reyes-Puerta V, Kindler J, Berger T, Kilb W, Luhmann HJ (2012) Thalamic Network Oscillations Synchronize Ontogenetic Columns in the Newborn Rat Barrel Cortex. Cereb Cortex.

Yang JW, Hanganu-Opatz IL, Sun JJ, Luhmann HJ (2009) Three Patterns of Oscillatory Activity Differentially Synchronize Developing Neocortical Networks In Vivo. J Neurosci 29: 9011-9025.

Acknowledgments

I would like to express my first and sincerest gratitude to my supervisor for giving me the opportunity to work in his lab.

I am very grateful to all supervisors and professors for reviewing my PhD defense.

Thanks to those who helped me on this manuscript.

Thanks to all colleagues of the lab for all the kinds of help.